Pattern Selection in a Liquid Crystal Flow

A thesis submitted to the University of Manchester
for the degree of Doctor of Philosophy
in the Faculty of Science and Engineering

2004

By

Selin Hekimoglu

Department of Physics and Astronomy

Contents

Abstract **11**

Legal Notices **12**

The Author **14**

Acknowledgements **15**

1 Introduction **18**

1.1 Nematic Liquid Crystals 20

1.1.1 The optical and electrical properties 22

1.2 Freedericksz Transition and Electroconvection 25

1.3 Bifurcations 31

1.4 Previous Studies 33

1.5 Preview of Chapters 43

2 Apparatus and Experimental Techniques **45**

2.1 The Apparatus 45

2.2 The Liquid Crystal Cell 47

2.3 Electrical Equipment 55

2.4 Experimental Techniques 59

3 General Observations **61**

3.1 Large and Small Aspect Ratios 61

3.2 Primary States of Various Aspect Ratios 65

3.3 Observations in Aspect Ratio Two 74

3.4 Conclusions 82

4 Priority Exchange of Four and Six-Roll States **83**

4.1 Neigbouring states 85

4.2 Benjamin's Theory 90

4.3 Experimental Method 94

4.4 Results 95

4.5 Discussion 99

4.6 Conclusions 100

5 Priority Exchange of Freedericksz Transition and Electroconvection **102**

5.1 Experimental Method 104

5.2 Results 105

5.3 Discussion 108

5.4 Conclusions 115

6 Conclusions **116**

Appendix **119**

A Unfolding of a pitchfork bifurcation **119**

B Nematic TX2A **123**

B.1 Dielectric Anisotropy of TX2A 123

List of Figures

1.1 A schematic illustration of the nematic phase of liquid crystals. . 21

1.2 The propagation of unpolarised light through crossed polarisers (i) without a liquid crystal sample, (ii) with a liquid crystal sample placed between the polarisers. The direction of the polarisers are represented by the black lines. The red arrows give the polarisation direction of the light, which propagates in a direction indicated by the blue arrows. 24

1.3 Alignment of nematic liquid crystal molecules according to the sign of dielectric anisotropy, $\Delta\epsilon$, when a field $\mathbf{E}$ is applied on the molecules. Part (i) represents the effect on a sample with a positive $\Delta\epsilon$ and (ii) negative. 26

1.4 Freedericksz transition observed through polarising microscope. The image seen in part (i) was taken when no field was applied to the nematic sample TX2A. In part (ii) the colour change due to the realignment of the molecules under the effect of non-zero electric field is shown. 27

1.5 Rolls observed in a nematic liquid crystal (TX2A) with negative $\Delta\epsilon$. 29

1.6 An illustration of the Carr-Helrich model for EHC. The thick black lines represent the electrodes that apply an external electric field, E_{ex}, to the molecules. Local variations in the director field are symbolised by cigar-like shapes. The plus and minus signs indicate the segregation of impurity ions that give rise to an internal electric field, E_{in}. The circles denote the onset of convection where each roll rotates in a counter direction to its nearest neighbours. 29
1.7 An illustration of the buckling of an elastic strut under the compression of an applied load P. 31
1.8 Bifurcation diagram for a transcritical bifurcation 33
1.9 Alignment of nematic LC molecules according to the sign of dielectric anisotropy, $\Delta\epsilon$ [2]. 37
1.10 Examples of patterns in EHC: (i) Oblique-roll, (ii) zig-zag, (iii) skew-varicose, (iv) grid patterns [28]. 38
1.11 Taylor rolls are shown in part (i). The cross-section view of the same rolls are given in part (ii) [17]. 40

2.1 The apparatus used in the experiments. 46
2.2 The LC cell placed on the hotstage. 47
2.3 A schematic illustration of a liquid crystal cell. The spacers inside the cell provide even spacing at the ends. The electric field is effective over the active area created by the crossing of the transparent electrodes. This is denoted by the colour pattern. As before the $\boldsymbol{n}$ vector represents the director. 48
2.4 The active area of a liquid crystal cell and the dimensions that define the aspect ratio $(l : w : t)$. 49

2.5 An illustration of the mask used for the small aspect ratio cells. The electrode widths from top to bottom were 20, 10, 7, 5, 3, 2μm. Distance between each electrode was 100μm. 50

2.6 The final state of the cell. Solid lines indicate the electrodes on the top glass and the ones on the bottom glass are shown as dashed lines. Freedericksz Transition or electroconvection is expected to evolve only within the active area marked with a cross. 52

2.7 Convection rolls created in aspect ratio $2.0 \pm 0.2 : 2.0 \pm 0.2 : 1.0$. The black solid line indicates 20μm. The crossings of different size electrodes creating a range of different aspect ratios can also be partially seen. The response to electric field is only in the active area of the connected electrodes and in its neighbourhood where the fringing fields existed. The picture was taken with a 10X objective and numerical aperture (NA) = 0.25. 53

2.8 The stability graph of the amplifier and the multimeter. The data was collected and sent to the computer by the multimeter after the signal was amplified. 57

2.9 The stability graph of the temperature controller. On the vertical axis $0.1V$ corresponds to $\sim 0.008^oC$. 58

3.1 EHC created in nematic TX2A in a large aspect ratio (2000:2000:1) cell near the threshold voltage. Different patterns are seen in various sections of the cell. The black solid line indicates 5μm. 63

3.2 Patterns created in nematic TX2A in a large aspect ratio (2000:2000:1) cell above the threshold voltage for the primary state. As before different patterns coexist. The black solid line indicates 5μm. . . . 64

3.3 The results of numerical calculations giving the threshold voltages as a function of aspect ratio, r [45]. The solid lines give the loci of parameters where the primary states emerge from no-flow state. The number of rolls in each primary state is given on the associated curve. The dashed lines are indicate the secondary bifurcations. . 66

3.4 A pattern suggesting a single roll observed in active area with an aspect ratio 0.31 : 0.52 : 1. The black solid line indicates $3\mu m$ and white lines give the borders of the electrodes. The picture was taken at voltage and frequency values $29.60V_{rms}$ and $30.10kHz$ respectively, with 80X objective and N.A. number of 0.75. 68

3.5 The image in the background is a LC cell with $200\mu m$. A piece of human hair is focused in the photograph [40]. It should be noted that the largest electrode width in the LC cell used in this study was $20\mu m$ which is approximately one quarter of the diameter of a human hair. 69

3.6 Two rolls observed in the active area with an aspect ratio 1.03 : 1.03 : 1. The black solid line indicates $5\mu m$ and the white lines show the borders of the electrodes. The picture was taken at voltage and frequency values $23.04V_{rms}$ and $30.10kHz$ respectively, with 80X objective and N.A. number of 0.75. 71

3.7 Four rolls created in an aspect ratio 2 : 2 : 1. The black solid line indicates $5\mu m$ and the borders of the electrodes are given by the white lines. The picture was taken at voltage and frequency values $20.60V_{rms}$ and $30.10kHz$ respectively, with 80X objective and N.A. number of 0.75. 73

3.8 A Freedericksz Transition (FT) observed in aspect ratio 2 : 2 : 1. The black solid line indicates $5\mu m$ and the white lines show the borders of the electrodes. The picture was taken at voltage and frequency values $7.42V_{rms}$ and $20kHz$ respectively, with 20X objective and N.A. number of 0.40. 76

3.9 A Freedericksz Transition (FT) observed in aspect ratio 2 : 2 : 1. The black solid line indicates $5\mu m$ and the borders of the electrodes are imposed on the photograph by the white lines. The picture was taken at voltage and frequency values $37.50V_{rms}$ and $20kHz$ respectively, with 20X objective and N.A. number of 0.40. 77

3.10 A Freedericksz Transition observed in a large aspect ratio cell filled with a nematic LC [3]. The bright lines are transient patterns are observed prior to complete Freedericksz transition due to competition between the applied and elastic forces. 78

3.11 Six rolls created in an aspect ratio 2 : 2 : 1. The black solid line indicates $5\mu m$ and the white lines denote the borders of the electrodes. The picture was taken at voltage and frequency values $22.60V_{rms}$ and $32.10kHz$ respectively, with 80X objective and N.A. number of 0.75. 79

3.12 Periodic motion of the end rolls observed in an aspect ratio 2 : 2 : 1. The black solid line indicates $5\mu m$ the white lines give the borders of the electrodes. The picture was taken at voltage and frequency values $30.00V_{rms}$ and $32.10kHz$ respectively, with 80X objective and N.A. number of 0.75. 80

3.13 Disordered state in an aspect ratio 2 : 2 : 1. The black solid line indicates $5\mu m$ and the white lines show the borders of the electrodes. The picture was taken at voltage and frequency values $37.50V_{rms}$ and $32.10kHz$ respectively, with 80X objective and N.A. number of 0.75. 81

4.1 Loci of bifurcations are shown in part (i). The effect of varying A for $B = p$, $B = r$ and $B = q$ are given in parts (ii), (iii) and (iv) respectively. 86

4.2 Bifurcation diagram including imperfections are shown in blue whereas the black branches indicate the perfect case. 88

4.3 Branches framed in the red box possess a counter sense of symmetry to the ones outside the frame. Due to large separation of the enclosed branches they are not observed in EHC and will be omitted. 89

4.4 The neighbouring states N and K. The primary state N evolves smoothly while the nearby secondary state K stays disconnected. 89

4.5 The limit points of equation 4.1 and a series of bifurcations predicted by Benjamin's theory for the stability exchange of two neighbouring states. 91

4.6 The set of limit points found for the stability exchange between the primary (4- and 6-rolls) states in EHC of nematic TX2A. The red circles and blue squares indicate the upper and lower limit points of the 4-roll state whereas the black triangles are the limit points of the 6-roll state. The associated bifurcation diagrams for each set of limit points are given in subfigures (i)-(iv). The arrows have the same meaning as in figure 4.5. 96

4.7 The section of the parameter space where the experiment was done and the paths taken on the parameter space. 97

5.1 The set of limit points found for the stability exchange between the EHC and FT. The limit points between B and E indicate the loci at which FT lost stability to EHC. The rest of the data denote limit points where EHC jumped/collapsed suddenly to FT. However, the limit points between A and D and C and A were found by taking a different route on the parameter space than the one followed to find the open triangles. The plot is divided into six sections by dashed lines where each line corresponds to a bifurcation diagram in figure 5.2 and is numbered accordingly. 106
5.2 The bifurcation sequence suggested for the exchange mechanism of FT and EHC. 109
5.3 An illustration of a dual cusp. In the top figure the shaded region indicates a stable state whereas the upper and lower layers are unstable. The bottom surface demonstrates the parameter space comprised by frequency and voltage. In the experiment the limit points were determined by following the paths represented by the solid lines with arrows in the upper figure. Thus, a dual cusp is the projection of the folded surface on the parameter space. . . . 111
5.4 Limit points of 3 and 5-roll states in a Taylor-Couette system with asymmetric end conditions [85]. 113

A.1 Bifurcation diagram for an ideal pitchfork bifurcation. 120
A.2 Pitchfork bifurcation diagram after the imperfection β term is included. 121
A.3 The cusp formed by the limit points of equation A.2. 121
A.4 An illustration of the limit points of equation A.3. 122

B.1 Dielectric anisotropy as a function of frequency of the AC field. . 124

Abstract

We present results from an experimental study which is concerned with the priority exchange of patterns in a dual-frequency nematic liquid crystal under the effect of an applied sinusoidal electric field. The aim of the work was to investigate an intrinsic mechanism for the exchange processes.

A device with microscopic electrodes was initially constructed in order to contain the liquid crystal and apply an electric field to a specified portion of it. The geometry of the device was such that electrodes of different sizes overlapped at thirty-six separate locations to give a distinct small aspect ratio at each crossing. The flow pattern resulting from the electric field effect was then examined as a function of aspect ratios and frequency of the applied field.

The first experiment concerning the priority exchange of patterns was performed for two convective flow states. In this case, the patterns of interest comprised of four or six convection rolls. Our results confirm that the priority exchange of these states follow the general mechanism proposed by Benjamin. Specifically, unfolding of a transcritical bifurcation takes place during the exchange process.

The second experiment was conducted to study the competition between a convective flow and a static re-alignment state of the liquid crystal molecules known as a Freedericksz transition. The results of this experiment revealed a complex bifurcation sequence including evidence for a dual cusp.

Declaration

No portion of the work referred to in this thesis has been submitted in support of an application for another degree or qualification of this or any other university or other institution of learning.

Copyright

The Author

Selin Hekimoglu was born in Ankara, Turkey in 1977 and attended Ankara Atatürk Anatolian High School. She studied for her undergraduate degree at the University of Manchester, where she was awarded a 1^{st} class MPhys(Hons) in Physics.

Acknowledgements

First and foremost, I would like to thank my supervisor, Prof. Tom Mullin, FRSE. He guided me all along my PhD with great amount of patience, taught me how to do research, how to write scientific work and shared his enormous amount of knowledge in nonlinear dynamics with great generosity. How much of that I have managed to learn is limited merely by my capacity.

The members of Nonlinear Dynamics and Liquid Crystals group in Manchester witnessed every stage of this work and gave me immense support at times of frustration. I am grateful to Dr. Nick Roberts, Julie Conn, Dr. Winnie Wang, Dr. Piers Treacher, Dr. Carlos del Pino, Prof. Helen Gleeson, Dr. Ingo Dierking, Dr. Pablo Moresco, Dr. Jorge Peixinho, Paul Archer and Dr. Pedro M. Reis for their help, support and friendship.

During the tragicomical times of my experimental work, the great team of the electronics workshop, Jim Allen, Jonathan Hird and Paul Spiteri fixed everything I managed to blow up and Paul Tipler from the mechanical workshop helped me always with speed. Thank you all for your help.

I am truly indebted to Dr. Tim Wilkinson for building the liquid crystal cell used in our experiments, which cost him a lot of time and effort. Yet he helped us in numerous occasions. I would also like to express my gratitude to Allan Fenwick from QinetiQ and Hulme Hall Trust Fund for their financial support.

My life has been blessed outside the lab, as well as inside, with very special people who honoured me with their friendship: Elena Barabantseva, Dr.

David Butler, Dr. Pedro M. Reis, Yan Lim, Jia Hwei Koh, Riccardo Orlandi, Simone Babuin, Susannah Tresilian, Maida Hrnic, Bilkay Gülaçti, Burçak Alp, Doru & Simona Davidescu and Nadia Lisovskaya ...and from a land far away: Ayça Ö. Karakuş, P. Ayşe Eren, Melike Bezgin, Sanem Y. Gülbaş, Zeynep T. Ultav, Gülhan Koçak and Bengi Ünsay; the support you gave me to achieve my goals is unforgettable. I do not know how to express my love and gratitude. *Candostlarim! Tebessümleriniz en büyük mutluluğumdur...*

Finally, I would like to thank my beloved family who taught me the most precious thing in life by giving me unconditional love and inspired me endlessly throughout my studies with their dedication to knowledge and learning. I would consider myself successful only if I can become the daughter/granddaughter/sister they deserve. *Herşeyim, canim ailem! Size layik olabilirsem kendimi başarili addedeceğim.*

Canim Annem ve Babam,

Nesrin & Kadri Hekimoğlu'na...

Chapter 1

Introduction

Solids, liquids and gases are generally accepted as the three main phases of matter. However, between 1850 and 1888, experiments related to studies of biological specimens, crystallization and compounds synthesized from cholesterol led to the discovery of a new phase [1]. It was observed to exist between the isotropic liquid and crystalline solid states and was thus named the *liquid crystal phase*. Hence, materials that exhibit this phase are called liquid crystals.

Since their discovery, liquid crystals have been a fertile subject in scientific research. Along with various studies done on their material properties and technological applications, liquid crystals have also been of interest in the field of nonlinear dynamics due to interesting pattern formations they exhibit [2, 3]. In particular, the unique optical and electrical properties of liquid crystals provided practical advantages to conduct fruitful experiments regarding the flow patterns that arise from electrohydrodynamic instabilities.

The work presented in this thesis is concerned with investigations of the underlying bifurcation structure of electrohydrodynamic flows. Specifically, the experimental studies on the priority exchange between flow patterns and the corresponding bifurcation sequences are presented.

In this chapter, firstly, nematic liquid crystals and their optical and electrical

properties are introduced. The dynamical effects observed in accordance with these properties, which build the foundation of our studies, are then explained. The chapter continues with a summary of previous works done on pattern formation in nematic liquid crystals under the effect of an electric field, pattern competition in various nonlinear systems and concludes with an outline of the thesis.

1.1 Nematic Liquid Crystals

As the name suggests, liquid crystals possess some properties of both the crystalline solid and the isotropic fluid states. A liquid crystal material shows some degree of fluidity, yet its molecules are spatially ordered, as with solids. A material may pass through one or more liquid crystal phases, known as mesophases, of varying degrees of orientational and positional order, before it becomes an isotropic fluid. Transitions to these phases may be via purely thermal processes or by changing the concentration ratio of a solvent that is added to a material.

In order for a material to display liquid crystal phases its molecules must be geometrically anisotropic. A strongly elongated rod-like (calamitic) shape is a common form of liquid crystal molecules. For a collection of such molecules, the structure resulting from the simplest orientational order is known as the *nematic* phase [4] and is schematically illustrated in figure 1.1. As shown in the figure, the position of nematic liquid crystal molecules are not fixed as in the case of the solid phase, but on average they are aligned in a single direction and therefore possess a certain degree of order. The preferred direction of the molecules is along the long axis and is defined by a unit vector called the *director*, which is denoted by $\boldsymbol{n}$. The order of molecules in a nematic liquid crystal depends on temperature. Hence, it can be destroyed at a temperature called the *clearing point*, which is specific to each nematic material, and become isotropic.

The equations that describe the dynamics of isotropic fluids, namely the Navier-Stokes equations, are not sufficient to model the hydrodynamics of nematic materials. The main difference between nematic liquid crystals and isotropic fluids is that in nematic liquid crystals the translational motion of the molecules is coupled to their orientation. A model developed by Ericksen [5], Leslie [6] and Parodi [7] (ELP theory) contains the coupling between the flow and the orientation of molecules. This is achieved by using a macroscopic approach based on the

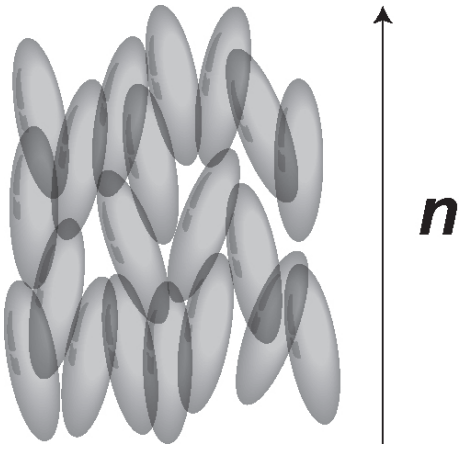

Figure 1.1: A schematic illustration of the nematic phase of liquid crystals.

approximation of classical mechanics. It considers deformations of the structure without taking into account the details at the molecular scale and is therefore a continuum model [8]. The equations that describe the dynamics of nematic liquid crystals in terms of the velocity field, $v(x,t)$, and the director field, $n(x,t)$, according to ELP theory are as follows:

$$\nabla_i v_i = 0 \tag{1.1}$$

$$\rho(\frac{\partial}{\partial t} + v_j \nabla_j) v_i = \rho F_i + \nabla_j \sigma_{ij} \tag{1.2}$$

$$\rho K_i + \epsilon_{ijk} \sigma_{kj} + \nabla_j l_{ij} = 0 \tag{1.3}$$

where ρ is the density, $\boldsymbol{F}$ is an external body force per unit mass, σ is non-Newtonian stress tensor, $\boldsymbol{K}$ is an external body torque per unit mass and l is a couple stress tensor. The non-Newtonian stress tensor and couple stress tensor are sources of nonlinearities as they include fourth order terms in $\boldsymbol{n}$, the director.

The anisotropic nature of liquid crystals, which is contained in the set of equations given above, is also present in the way molecules interact with light and

electric fields. As a result, liquid crystals possess unique electrical and optical properties, which are used widely in scientific studies as well as in technological applications. An introduction to these properties is given next.

1.1.1 The optical and electrical properties

Optical anisotropy, known as *birefringence*, is a phenomenon commonly seen in nature. Materials that exhibit birefringence, such as liquid crystals, possess two refractive indices since their optical properties vary in different directions within a sample. The measure of optical anisotropy for these materials is the difference of their refractive indices and is denoted by Δn. Accordingly, Δn in a liquid crystal is defined by [9]:

$$\Delta n = n_{\parallel} - n_{\perp} \tag{1.4}$$

where $n_{\parallel}$ and $n_{\perp}$ indicate the refractive indices parallel and perpendicular to the director respectively.

The most important and practical outcome of optical anisotropy of liquid crystals is obtained when white, unpolarised light propagates through a liquid crystal sample that is placed between crossed linear polarisers. Normally, white light cannot pass through perpendicularly positioned linear polarisers [10]. This situation is illustrated in figure 1.2(i), where the red arrows indicate the polarisation direction of light that travels in the direction represented by the blue arrow and the black stripes indicate the direction of polarisers. As schematically shown in figure 1.2(i), the unpolarised light first passes through polariser 1 and becomes linearly polarised along the direction of polariser 1. However, this direction is perpendicular to polariser 2 and therefore, no light can pass through the crossed polarisers.

When a liquid crystal sample is placed between crossed linear polarisers, the

effect that occurs is somewhat different. This is illustrated in figure 1.2(ii) where the symbols and the colour codes have the same meanings as before. Similar to the case explained in part (i), as the unpolarised light passes through polariser 1, it becomes linearly polarised in a direction parallel to the polariser. However, this polarised light experiences a phase shift as it goes through the liquid crystal molecules, due to their anisotropy[1]. Consequently, the polarisation direction of light becomes altered. Therefore, when the polarised light reaches polariser 2, they do not meet at 90^o to each other and the component of light that is parallel to polariser 2 passes through.

The phase shift, $(d\Delta n)$, experienced by the polarised light as it travels through the liquid crystal sample is given in equation 1.5 [10]:

$$d\Delta n = (m + \frac{1}{2})\lambda \tag{1.5}$$

where d is the thickness of the liquid crystal sample, as shown in figure 1.2(ii), Δn is the optical anisotropy, m is an integer and λ is the wavelength of the polarised light when it reaches polariser 2.

An important consequence of equation 1.5 is that if the molecules change their orientation, then the optical anisotropy acquires a different value and according to equation 1.5 a different wavelength is then allowed to pass from the second polariser. Therefore, the colour corresponding to the wavelength of this outcoming light gives an indication of the alignment of liquid crystal molecules. A new orientation appears as a different colour when viewed from crossed linear polarisers. This advantageous property makes liquid crystals a beneficial tool in experimental studies [1].

The electrical properties of liquid crystals also arise from the anisotropic nature of the molecules. These properties are exploited widely in research and

[1]The details of this process can be found in reference [10].

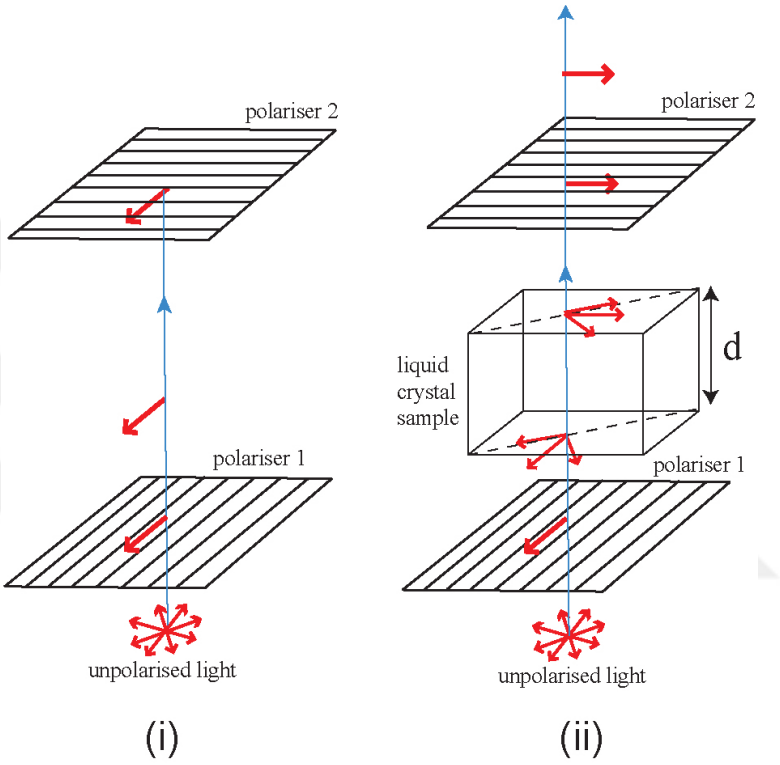

Figure 1.2: The propagation of unpolarised light through crossed polarisers (i) without a liquid crystal sample, (ii) with a liquid crystal sample placed between the polarisers. The direction of the polarisers are represented by the black lines. The red arrows give the polarisation direction of the light, which propagates in a direction indicated by the blue arrows.

applications since an electric field can alter the director alignment or induce a flow in a sample, which can then be detected using the optical properties of liquid crystals. Thus, the interaction of the molecules with an applied electric field provides an easy and effective method to probe the material or dynamical properties of liquid crystals. The response of the molecules to an applied electric field is determined by the following terms [9]:

$$\Delta\epsilon = \epsilon_{\parallel} - \epsilon_{\perp} \tag{1.6}$$

where $\epsilon_{\parallel}$ is the dielectric constant measured along the director (i.e. along the long axis of the molecules) and $\epsilon_{\perp}$ perpendicular to the director (i.e. along the short axis of the molecules). Their difference, $\Delta\epsilon$, is called the *dielectric anisotropy*.

Another related term is the *conductivity anisotropy*, $\Delta\sigma$, and is given by [9]:

$$\Delta\sigma = \sigma_{\parallel} - \sigma_{\perp} \tag{1.7}$$

where $\sigma_{\parallel}$ is the conductivity measured parallel to the director and $\sigma_{\perp}$ perpendicular to it.

Next, we will discuss two of the main dynamical effects that can be observed when an electric field is applied to a nematic liquid crystal, in relation to the terms given above. These dynamical effects comprise the foundation of the studies presented in this thesis.

1.2 Freedericksz Transition and Electroconvection

The main criteria that determine the response of a nematic liquid crystal to an electric field ($\mathbf{E}$) is the sign of the dielectric anisotropy. This is schematically

illustrated in figure 1.3 where the subfigure (i) represents the effect of **E** on materials with positive $\Delta\epsilon$ and (ii) on samples with negative $\Delta\epsilon$. In both cases the orientation of the long axis of the molecules is assumed to be horizontal in the absence of a field.

For positive $\Delta\epsilon$ the free energy is minimised when the molecules align in the direction of the electric field applied [1, 9]. This reorientation is called *Freedericksz transition*(FT) after its discoverer [11]. The photographs presented in figure 1.4 show how FT appeared when a sample was observed through a polarising microscope. The image seen in figure 1.4(i) was taken when no field was applied to the sample. By increasing the field strength, the orientation of the molecules was altered and this was indicated as a change in colour, for the reasons explained in the previous section. The modified colour observed from the polarising microscope is presented in figure 1.4(ii).

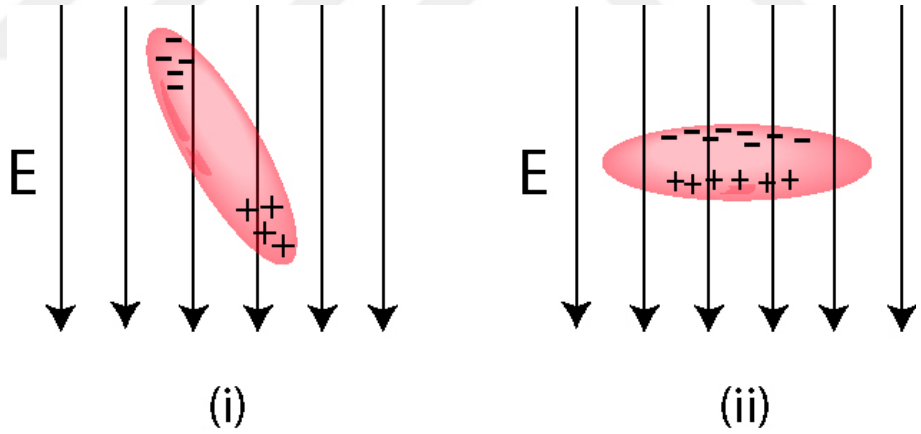

Figure 1.3: Alignment of nematic liquid crystal molecules according to the sign of dielectric anisotropy, $\Delta\epsilon$, when a field **E** is applied on the molecules. Part (i) represents the effect on a sample with a positive $\Delta\epsilon$ and (ii) negative.

In cases where an alternating (AC) electric field is applied to a nematic liquid crystal with positive $\Delta\epsilon$, the response of the molecules can also have a dependency on the frequency of the field applied. The response time of nematic liquid

(i)

(ii)

Figure 1.4: Freedericksz transition observed through polarising microscope. The image seen in part (i) was taken when no field was applied to the nematic sample TX2A. In part (ii) the colour change due to the realignment of the molecules under the effect of non-zero electric field is shown.

crystals to external fields is generally given as a few hundred milliseconds [1]. Consequently, if the frequency of an AC field is low in comparison to the response time of a specific material, then the molecules can follow the field direction. In other words, they can change their orientation as the field direction changes. For AC fields with high frequency values[2], the response of the molecules is proportional to the magnitude of the square of the field. Therefore, the effect of the field will not differ from that of a DC field.

Alternatively, when an electric field is applied to a liquid crystal sample with negative $\Delta\epsilon$ the preferred alignment of the molecules is perpendicular to the direction of the field [12] as illustrated in figure 1.3(ii), i.e. they remain in their original alignment. However, above a threshold value, the molecules rearrange so that a pattern of rolls emerge. An example of such a domain of pattern is given in figure 1.5. This effect is called *electrohydrodynamic convection*(EHC) or *electroconvection* and was first observed by Williams in 1963 [13]. Six years later Carr [12] and Helfrich [14] proposed the following explanation for the phenomena which is schematically shown in figure 1.6.

When $\Delta\sigma$ is positive in a nematic material, in addition to negative $\Delta\epsilon$, the effect of electric field, E_{ex}, is to segregate the impurity ions, which are always present in a material. These impurity ions originate from the synthetic roots of the materials and their segregation is caused mainly by the alignment fluctuations of the molecules. Rigorous theoretical descriptions of this segregation process can be found in [3, 12, 14, 15]. According to the Carr-Helfrich model, the segregated charges flow due to the applied electric field and create shear as they drag the fluid with them. This exerts a torque on the molecules, which is referred to as shear induced torque. Simultaneously, an internal electric field, E_{in}, is created between the separated charges. This internal field creates another type of torque

[2]compared to the response time of the molecules

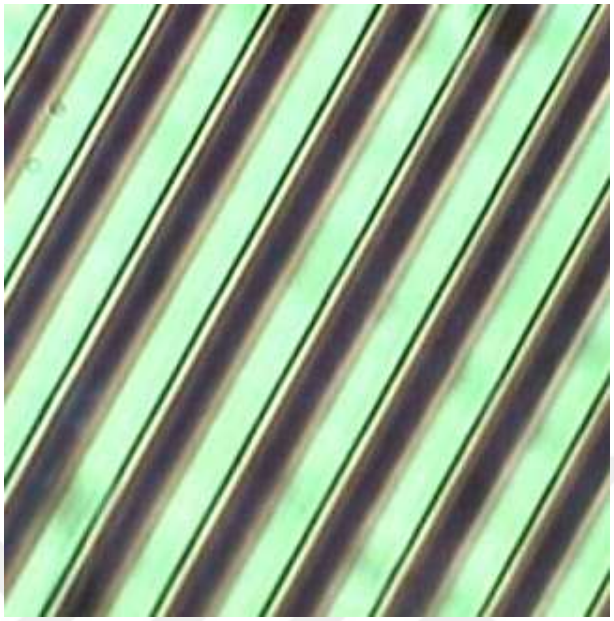

Figure 1.5: Rolls observed in a nematic liquid crystal (TX2A) with negative $\Delta\epsilon$.

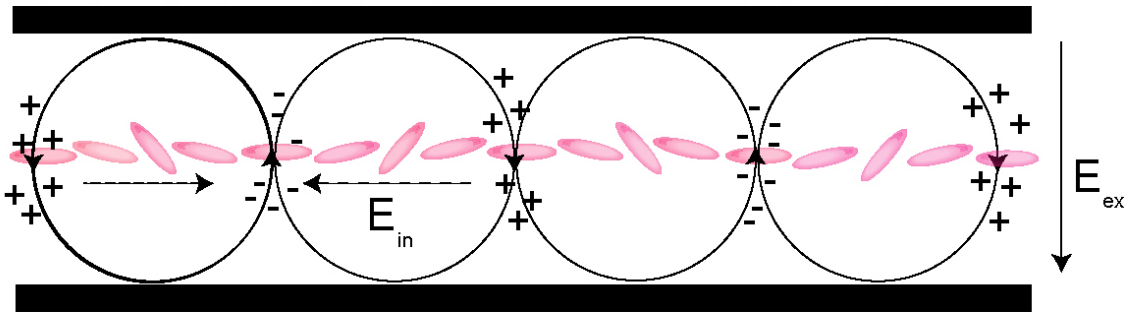

Figure 1.6: An illustration of the Carr-Helrich model for EHC. The thick black lines represent the electrodes that apply an external electric field, E_{ex}, to the molecules. Local variations in the director field are symbolised by cigar-like shapes. The plus and minus signs indicate the segregation of impurity ions that give rise to an internal electric field, E_{in}. The circles denote the onset of convection where each roll rotates in a counter direction to its nearest neighbours.

on the molecules, called conductivity induced torque. Both types of torques act as destabilising forces and compete with the visco-elastic forces that seek to maintain the molecules in their original alignment. However, above a critical value, the destabilising effects dominate and the system undergoes cellular convection. It should be noted that in addition to Leslie-Ericksen equations (equations 1.1, 1.2, 1.3), a charge continuity equation is included in the Carr-Helfrich model in order to account for the impurity ions, introduced above, which are crucial for the onset of EHC in the model [14]:

$$(\frac{\partial}{\partial t} + v_i \nabla_i)\rho_d + \nabla_i J_i = 0 \tag{1.8}$$

where ρ_d is the space charge density and J is the current density.

The appearance of EHC under a polarising microscope is in accord with the spatial arrangement of the director field, illustrated in figure 1.6. Since the optical anisotropy, Δn, depends on the director orientation, the spatially periodic director field gives rise to a periodically varying Δn. The effect of this is equivalent to a range of diverging and converging lenses that alternate with the same periodicity of the director field. Consequently, a set of spatially periodic bright and dark lines, as seen in figure 1.5, appear where the out-coming light converges and diverges respectively.

As clearly demonstrated, EHC can be viewed easily through a polarising microscope and furthermore, modest electric field strengths (of the order of Volts) are sufficient for its onset. These characteristics make EHC a practical system to study pattern formation, which makes up an important branch of nonlinear science. The fundamental ideas used for nonlinear dynamical systems, such as the concept of bifurcations, can be applied to pattern forming systems to examine the emergence and stability of the patterns. A rigorous mathematical description of bifurcations can be found in reference [16], however, a brief introduction is

given in the next section.

1.3 Bifurcations

Here we will firstly refer to a well known example, the Euler strut, in order to demonstrate a qualitative change that can occur in the state of a nonlinear system as a control parameter is varied. In this particular problem, an elastic strut is compressed under a load P as schematically shown in figure 1.7.

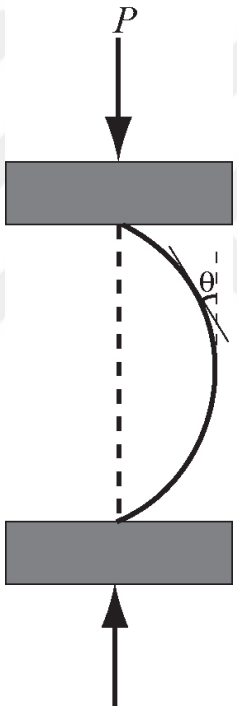

Figure 1.7: An illustration of the buckling of an elastic strut under the compression of an applied load P.

The equilibrium equation for such a strut of length l is as follows [17]:

$$B\frac{d^2\theta}{dx^2} + P\sin\theta = 0 \tag{1.9}$$

where B is the elastic bending stiffness, θ is the deflection angle as shown in figure 1.7 and P is the applied load, which is the control parameter of the

problem. For small values of θ, equation 1.9 can be linearised by replacing the $\sin\theta$ term by θ and hence, exact solutions to the equation can be found. One of these solutions is zero deflection angle and it is commonly called the *trivial state*.

However, as P is increased further, the trivial state becomes unstable at a critical value of P. Consequently, the strut buckles either to the left or right above this critical value and each of the bucklings correspond to a new stable state. Then, the trivial state of the strut is said to have *bifurcated* to new solutions. The type of bifurcation that is described here is an example of a symmetry-breaking or *pitchfork bifurcation* since the buckled states break the left/right symmetry of the trivial state.

There are two types of bifurcations, which we will frequently refer to in this work. These are *pitchfork* and *transcritical* bifurcations. A simple demonstration of a pitchfork bifurcation has already been explained, however, a mathematical description and further details on unfolding of a pitchfork bifurcation are given in Appendix A. Therefore, we will introduce a transcritical bifurcation, which is described locally by the following equation[3]:

$$\frac{dx}{dt} = \lambda x - x^2 \tag{1.10}$$

where x is a dynamical variable, which defines an equilibrium state, $\frac{dx}{dt}$ gives the evolution of an equilibrium state and λ is a control parameter. The equilibrium states as a function of λ are shown in figure 1.8 where solid lines denote the stable states and the dotted lines indicate the unstable solutions.

A significant difference to emphasize between a transcritical and a pitchfork bifurcation is that a pitchfork bifurcation occurs in systems with perfect symmetry whereas this is not the case for a transcritical bifurcation. A consequence of

[3]Note that the term *local* in this context indicates that equation 1.10 is valid for the values of λ and x near the bifurcation point

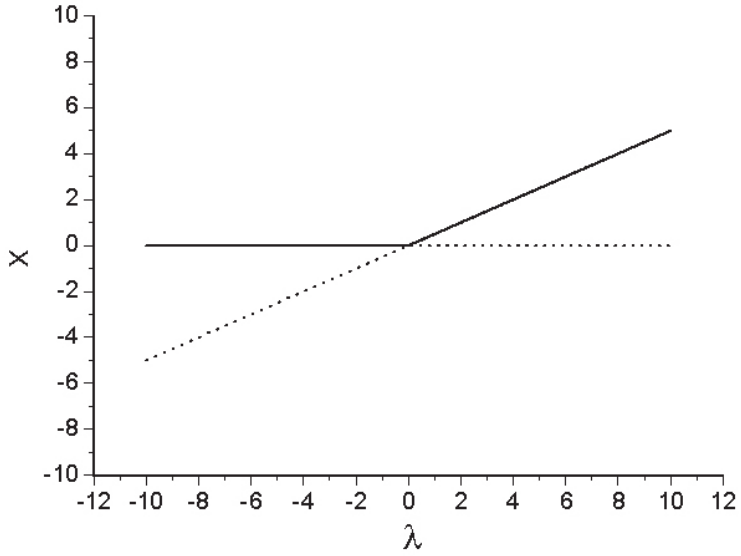

Figure 1.8: Bifurcation diagram for a transcritical bifurcation

this difference determines the role transcritical bifurcations play in the interaction of neighbouring states in real systems. A detailed discussion of this topic is given in Chapter 4 and Appendix A.

As noted in section 1.2, concepts of bifurcations can be applied to systems that exhibit pattern formation. In such systems, a pattern that is realisable in an experiment corresponds to a stable solution in the parameter space. Consequently, the emergence of a pattern can be explained by a suitable type of bifurcation. As a result, FT and to somewhat greater extend EHC, have been studied intensively as cases of pattern formation in nematic liquid crystals. An overview of the work done in this field, in addition to pattern competition studies in other systems, are given in the next section.

1.4 Previous Studies

We will consider the past studies on FT prior to those on EHC in accordance with the chronological order of their discoveries. FT was first observed in 1934 [11] in

an experiment where magnetic field was applied to a nematic liquid crystal. The phenomenon was studied theoretically in the following years by Saupe [18] and Dafermos [19], who developed an integral expression that describes the free energy of a nematic sample. Consistent with the original experiment of Freedericksz, they carried out the calculations considering the application of a magnetic field on the nematic material. When the condition of a minimum was imposed on the integral expression giving the free energy, they found a threshold field strength above which FT takes place [15]:

$$H_o = \frac{\pi}{d}(\frac{K}{\Delta\chi})^{1/2} \tag{1.11}$$

where H_o is the threshold field strength and d is the thickness of the liquid crystal cell, which is the device containing the nematic material. K is the elastic constant of the liquid crystal and $\Delta\chi$ is the diamagnetic anisotropy of it, which is defined as $\chi_{\parallel} - \chi_{\perp}$. Similar to dielectric anisotropy described in section 1.1.1, subscripts indicate the values of diamagnetic constant measured in the direction parallel and perpendicular to the long axis of the molecules respectively.

In 1970, Leslie [20] carried out theoretical calculations for the solutions of equations based on continuum theory for a sample of liquid crystal under the effect of a magnetic field. Two separate configurations were considered for the geometry of the liquid crystal cell. In the first one, the material was assumed to be deposited in an annular gap created between two concentric cylinders. Thus, the alignment of the molecules were tangential to the surface of the cylinders and a radial field was applied on the molecules. In the second case, the nematic material was in a wedge shape container, so that the director alignment and the field could be reversed compared to the previous case, i.e. the molecules were aligned radially to the surface of the container and the field applied was tangential. The threshold field determined from these theoretical calculations

agrees with the results found by Saupe and Dafermos.

Another theoretical study, following on the findings explained thus far was done by Derfel [21] where he examined nematic liquid crystal molecules confined between parallel plates with their alignment set to be parallel to the surface of the plates. By considering a magnetic field that is applied perpendicular to the director he studied the resulting orientation of the molecules from the perspective of Catastrophe Theory. He showed that the threshold field strength corresponds to the bifurcation point at which the trivial state[4] bifurcates into two states defined by the sign of the angle the director makes with the surface of the plates after the field is applied. Moreover, he reported that the transition between the states has a dependency on the history of the field application.

The Freedericksz transition arising from the application of an electric field was also investigated by researchers. Deuling [22], as well as Gruler et al. [23], confirmed theoretically and experimentally that the onset of FT induced by electric fields was similar to that created by magnetic fields. Explicitly, they found a critical field strength above which the molecules re-aligned in a configuration to give a minimised free energy. In addition, Gruler et al. calculated the angle deviation of the director as a function of the field strength. The experimental results of Gruler et al, however, showed discrepancies from the theoretical results at large field strengths. The explanation proposed for this observation was the imperfections in the uniformity of the field applied, which was approximated accurately for the small values of the field.

The study of FT as a bifurcation problem was revisited by Blake et al. in 1999 [24]. The numerical calculations they performed were for a nematic liquid crystal placed between parallel plates and both electrical and magnetic field effects were studied. The original alignment of the molecules in the absence of the field

[4]i.e. the theoretical rest state that exists in the absence of a field

was considered to be parallel to the plate surfaces. The bifurcation diagram they produced for the idealised case, i.e. without imperfections, gave a well defined threshold field strength. This threshold value acted as a bifurcation point giving rise to a pitchfork bifurcation as the field strength was increased further. When the imperfections were included either in the applied field or in the director orientation near the boundaries, one of the branches of the pitchfork bifurcation was disconnected whereas the other branch became a smoothly evolving one from the trivial state. The locus of the limit points[5] of the disconnected branch was examined and hysteretic behaviour was found. Consequently, loci of limit points of the disconnected branch formed a cusp. Blake et al. also investigated the effects of fields in a two-dimensional version of the problem. They set the ratio of the length of the plates to the thickness of the gap between them to small values and successfully revealed the charge density, the director angle and the electric potential as a function of distance from the mid-plane of the gap in the vertical direction.

The second main electro-dynamical effect of interest in this thesis, EHC, was discovered by Williams [13] in 1963 as noted in section 1.2. Following the development of the model explained above by Carr and Helfrich, the next important contribution to the explanation of the phenomenon was made by the Orsay group [25], who extended the theory for alternating (AC) fields. The experimental studies of EHC are mostly carried out with AC fields to minimise possible charge injection from the electrodes on the glass plates of the liquid crystal cell, i.e. the device in which the nematic material is contained. The Orsay group found that two types of convective instabilities arise depending on the frequency of the applied field. The regimes of the parameter space where these instabilities occur are seperated by a critical frequency. In the region with frequency values lower

[5]A detailed discussion of limit points is given in Chapter 4.

than the critical frequency, called the *conduction regime*, the space charge density, ρ_d, oscillates in phase with the field and the director distortions are static. For frequency values higher than the critical frequency, that is, in the *dielectric regime*, director distortions follow the field applied whilst ρ_d stays static. The photograph presented in figure 1.9 is a so called chevron pattern observed only in the dielectric regime of the parameter space [2]. This pattern is created by the periodic structure of defects that form due to the director motions determined by the field and hence, is a trademark of the dielectric regime. In 1972, the models developed by Helfrich and the Orsay group were detailed further by Penz and Ford [26] who took into account the upper and lower boundaries and extended the model to two-dimensions.

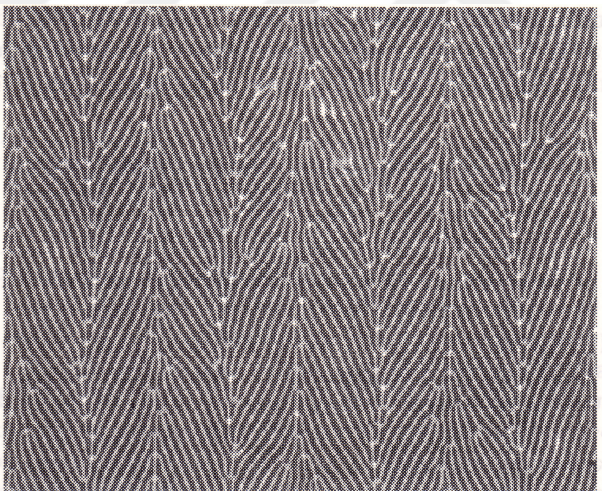

Figure 1.9: Alignment of nematic LC molecules according to the sign of dielectric anisotropy, $\Delta\epsilon$ [2].

Investigations of pattern formations in EHC were initiated by Kai and Hirakawa [27] and were carried forward by Joets and Ribotta [28, 29]. They reported that the onset of EHC was followed by oblique-roll, zig-zag, skew-varicose and grid patterns subsequently as the voltage was increased. Photographs of these patterns are presented in figure 1.10. The criteria for acquiring some of

these patterns, such as oblique-rolls, were studied by Bodenschatz et al [30] who carried out a three dimensional linear stability analysis of the trivial state. The same group also considered competition between various instabilities by describing secondary instability mechanisms with amplitude equations[6].

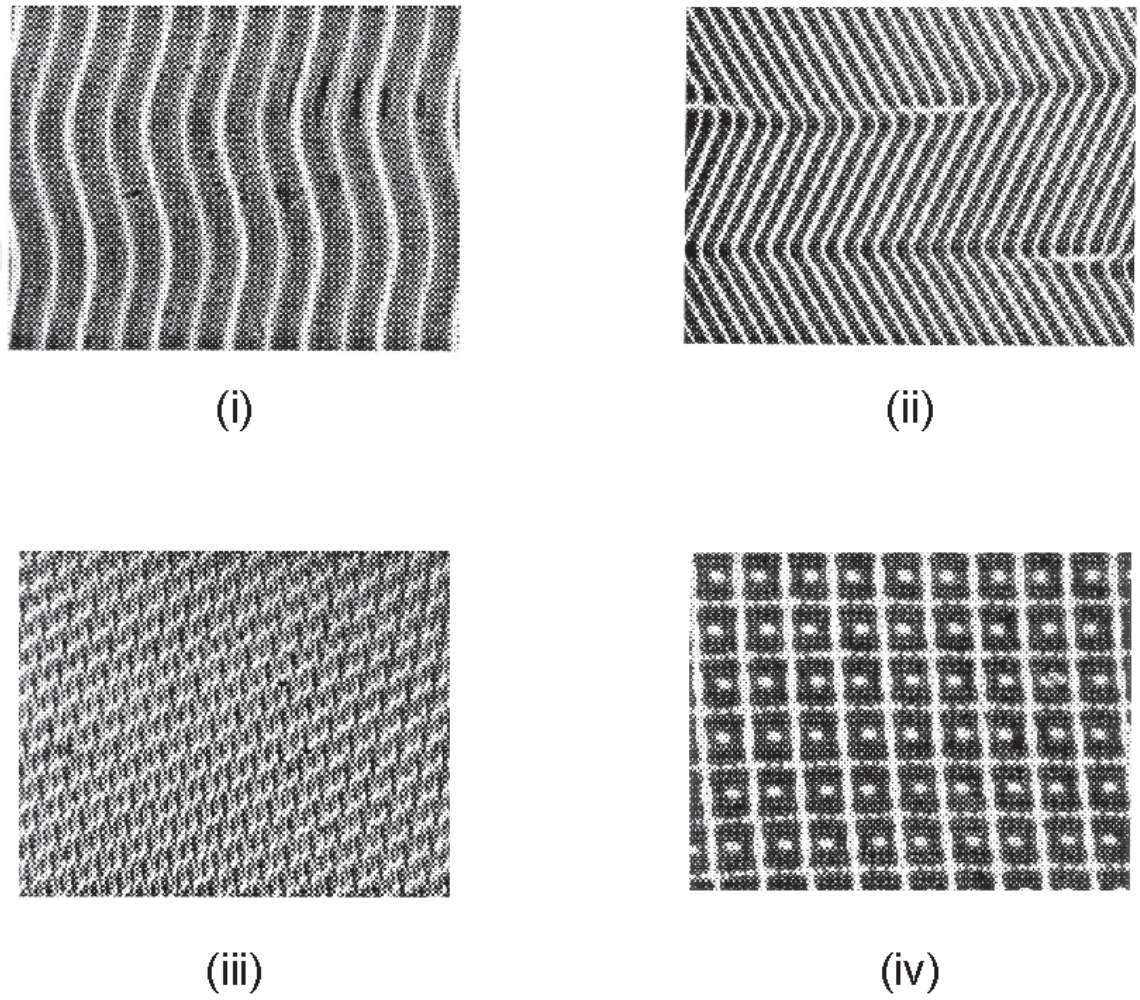

Figure 1.10: Examples of patterns in EHC: (i) Oblique-roll, (ii) zig-zag, (iii) skew-varicose, (iv) grid patterns [28].

The studies on EHC discussed thus far were carried out for systems where the liquid crystal cell had large aspect ratios. The concept of aspect ratio is discussed in detail in Chapter 3. Briefly, it is the ratio of the length and width

[6]see Section 3.1 for an explanation of amplitude equations

to the thickness of the three-dimensional section of the device where the fluid is confined and the experiments are conducted. The reason for the preference of large aspect ratio liquid crystal cells is to approach the approximation of infinitely large experimental setups and hence to consider periodic boundary conditions. A difficulty of this approach in practice is that the solution set can be very large i.e. many different states can coexist at a given point in parameter space.

Nevertheless, some studies in other fluid mechanical systems with small aspect ratios provide interesting results since in this case the solutions in the parameter space are well separated and the multiplicity of states in the fluid system is decreased. In addition, better experimental control can be achieved in such systems. Thus, ideas related to finite-dimensional dynamics could be adapted for the interpretation of the fluid motion [31].

An example of such studies is the work of Libchaber and Maurer [32] who found a period doubling cascade to chaos in a small aspect ratio model of Rayleigh-Bénard flow. In this system, convection is set in a fluid confined between two parallel plates, by creating a thermal gradient across the fluid. Another fluid system that revealed low dimensional dynamics was the Taylor-Couette system [33, 34] where a fluid is placed in a gap between concentric cylinders. Then, by rotating one of the cylinders while keeping the other one stationary, a shear is created across the fluid layer [17]. When the Reynolds number of the fluid reaches a critical value a banded flow structure, shown in figure 1.11(i), arises. A cross-sectional view of the cylinders (figure 1.11(ii)) reveal that the bands, in fact, are a range of cellular flows placed on top of each other and every cell rotates in a counter direction to its nearest neighbours. At higher values of the Reynolds number the cells can leave their place to further hydrodynamic instabilities and ultimately turbulent flow can form in the system. Mullin and Price [35], who carried out an experimental study regarding the global dynamics of this system,

reported mechanisms for the origins of chaos of the Šil'nikov type[7]. A review of low dimensional dynamics investigations in Taylor-Couette systems can be found in reference [36].

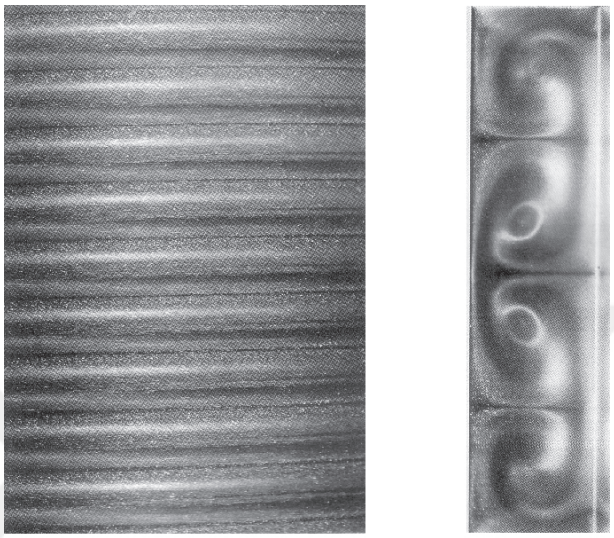

Figure 1.11: Taylor rolls are shown in part (i). The cross-section view of the same rolls are given in part (ii) [17].

Consequently, these studies gave motivation for the investigation of EHC in small aspect ratio systems, where only few number of convection rolls are accommodated in the liquid crystal cell. The first one of such studies was carried out by Yang et al. [37], who studied oscillations of the convection rolls and found consistency with Hopf bifurcation[8]. Later, Hidaka et al. [38] showed evidence for quasi-periodicity in transition to chaos in EHC of nematic liquid crystals. Another observation regarding the complex behaviour of oscillating 6 and 10-roll states of EHC was reported by Binks [39]. Following his work, Peacock [8] reported two qualitatively different forms of oscillatory flow in EHC that arise via a Hopf bifurcation and the existence of random bursting in their time series. The

[7]see [8] for an introduction to Silnikov Dynamics

[8]see [16] for Hopf bifurcation

cause of bursting was believed to be the thermal noise in the system, which gave rise to Brownian fluctuations of the director. Furthermore, a detailed study of low-dimensional dynamics in EHC was also done by Peacock et al. [8, 40, 41, 42] where he found a so called codimension-2 point, which leads to homoclinic bifurcations and acts as an organizing centre for the dynamics.

As the number of studies with small aspect ratio liquid crystal cells increased and observations concentrated on the dynamics of few convection rolls, a problem related to the symmetry of roll patterns was realised. Explicitly, the rotation of the outer-most convection rolls in EHC is persistent in only one direction, namely downwards [8, 39, 43]. This observation is considered to be peculiar on the following basis. The onset of EHC is considered as a pitchfork (symmetry breaking) bifurcation by Kramer and Pesch [44]. Accordingly, each branch of the pitchfork corresponds to one of the two possible rotation directions of the outer-most convection rolls. Since experimental observations show that the outer rolls form prior to the inner ones [8] and every roll rotates in a counter direction to its nearest neighbours, the rotation direction of the inner rolls are determined by the outer ones. Therefore, the observations made demonstrate only one of the branches and to date, the attempts to find the second branch of the pitchfork have not succeeded [43, 45]. This important result cannot be interpreted as separation of the branches due to experimental imperfections since the second branch could not be observed at nearby values in the parameter space. The problem was investigated numerically by Tavener et al. in [45]. They, in particular, studied the effect of fringing electrical fields and the possibility of a large separation of the branches as a result of them. However, they found that the separation of the branches in such a case is small and therefore, both states ought to be realisable in an experiment. Hence, this fundamental problem remains unsolved to date. A similar situation also exists for Taylor-Couette flows, where the cellular

structures always prefer the same rotation direction. However, in this case, the large separation of the branches representing the two possible rotation direction of the Taylor cells is related to the type of symmetry that is broken with the onset of Taylor cells. This is a translational symmetry that cannot be achieved in a physical system. A more detailed explanation on Taylor-Couette flows can be found in reference [17].

Another convective system that is modelled as an example of a pitchfork bifurcation is Rayleigh-Bénard convection [46]. Contrary to EHC, the existence of both branches are confirmed experimentally [47, 48] for this system. The reason for this is the validity of the Boussinesq approximation in Rayleigh-Bénard systems, which introduces a symmetry between upward and downward motion and thus, allows the existence of both flow directions of the convection rolls [46]. This is unlike the situation with EHC where the symmetry that exists in the system is believed to be a translational one, akin to the case of Taylor-Couette problem.

As a result of the studies in various nonlinear systems explained above, a qualitative similarity between EHC and Taylor-Couette flows was recognised. This led to further investigation of the two systems and enabled comparisons between them. An important one of these investigations was carried out by Binks et al. [39, 49], who showed that the priority competition between two flow patterns in EHC followed the exchange mechanism proposed by Benjamin [50]. According to this mechanism, two flow states exchange priority via a transcritical bifurcation and hysteresis is involved in the process. The same exchange mechanism was demonstrated for 2 and 4-cell Taylor-Couette flows by the experimental results presented by Benjamin and Mullin [51, 52, 53]. Also, the numerical calculations by Cliffe [54], Bolstad and Keller [55], Furukawa et al. [56] agree with the experimental observations. The ideas were then applied to a connected system of

Euler struts under compression by Tavener et al [57] and to flows in horizontal and curved ducts by Nandakumar et al [58, 59].

The experimental results of Benjamin [51] on a Taylor-Couette system were studied further by Schaeffer [60, 61], Hall [62, 63] and Cliffe [54]. In his work, Schaeffer applied the methods of Singularity Theory to investigate the effects of boundaries. His analysis, which produced qualitative agreement with the results presented by Benjamin [51], was done for exchange processes between $2k$ and $2k+2$ rolls where $k \geq 2$. The model includes cubic nonlinearities, whereas for $k = 1$ quadratic terms are also required. Later, Hall, [63] who studied Schaeffer's model further by using perturbation methods with no slip boundary conditions reported that the degeneracy stemming from the quadratic terms ought to play a significant role in the experimental results of Benjamin. Subsequently, Cliffe showed that the hysteresis observed in Taylor-Couette experiments is highly suppressed for the priority exchange of 2 and 4-cell states.

The work presented in this thesis was concerned with taking the experimental investigations on pattern selection further by using a unique liquid crystal material, which allowed us to generate both FT and EHC in the same device. As explained above, the emergence of a FT state is modelled in general as a pitchfork bifurcation. On the contrary, describing the onset of EHC with a pitchfork bifurcation is inappropriate due to large separation of the branches. Thus, the studies presented here were an investigation of the pattern selection between two effects that are different in origin. A preview of these studies is given next.

1.5 Preview of Chapters

In Chapter 2 the apparatus and experimental technique are described. Following this, the details of the liquid crystal cell constructed for our studies is given in Chapter 3 and the role of aspect ratio on flow patterns is discussed furthermore.

The general observations made in both FT and EHC systems are also presented in the same chapter.

The first of the sets of experimental results that constitutes the main focus of our investigation is the subject of Chapter 4. Specifically, the chapter is concerned with the study of the priority exchange of two neighbouring EHC states. The theoretical background required for the interpretation of the experimental results is given in the beginning of the chapter. This is followed by the details of the experiment, and the results are compared with those obtained from similar systems.

The results of a second experimental investigation are presented in Chapter 5, where the pattern selection occurs between the primary flow state of EHC and a FT state. As a result, an experimental evidence for the existence of a dual cusp in a liquid crystal flow is presented. Finally, the conclusions of our studies are given in Chapter 6.

Chapter 2

Apparatus and Experimental Techniques

In this chapter the apparatus and experimental procedures used to study the pattern selection in a nematic liquid crystal flow are introduced. The accuracy and the control of the equipment is detailed with an emphasis on the geometry and manufacture of the liquid crystal cell. Finally, the rationale behind the design of the experiments is discussed.

2.1 The Apparatus

A photograph of the apparatus used in the experiments is shown in figure 2.1. The nematic liquid crystal was enclosed between two glass plates to form the *liquid crystal cell* (LC cell) which was placed on the *hotstage*. A close-up image of the LC cell is given in figure 2.2. During the experiments a thermally insulating lid was mounted on the hotstage in order to minimise the heat transport between the cell and the room. The temperature of the hotstage and consequently of the LC cell was controlled and kept constant to within $\pm 0.01^{o}C$ by a temperature controller[1].

[1]Linkam Temperature Controller TMS 93

In all experiments a sinusodial alternating (AC) electric field generated by the function generator[2] was amplified[3] and applied to the LC cell. The final amplitude of the field was read from the multimeter[4] in units of Volts(V_{rms}). The effect of the AC field on the nematic LC was then observed from a polarising microscope[5].

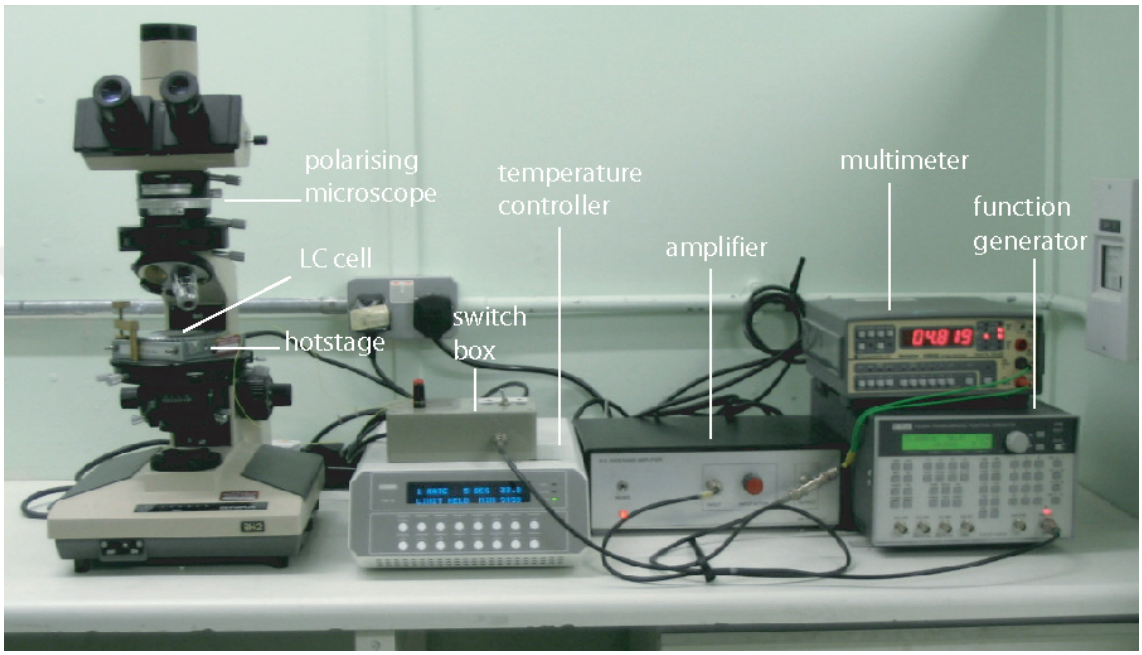

Figure 2.1: The apparatus used in the experiments.

Pictures of the images observed through the microscope were taken by adapting a digital camera[6] fitted to the polarising microscope. These were then transferred and stored on a computer.

[2]Thunder and Thurlby, *TTi* TG1304 Programmable Function Generator

[3]High Voltage Wide Band Amplifier Serial code EW1896/PA41. Made in the electronics workshop of the University of Manchester, Department of Physics

[4]Black Star 4503 Intelligent Multimeter

[5]Olympus BH2

[6]JVC Digital Camera KY-F1030

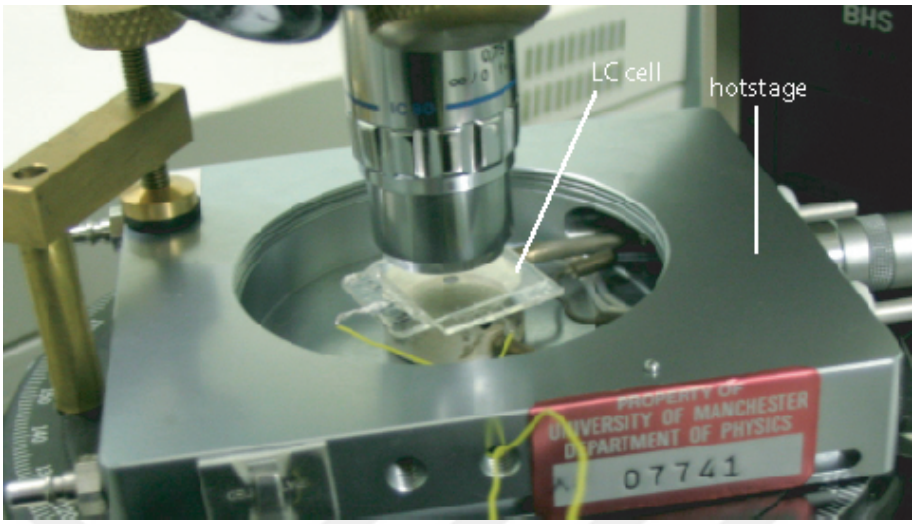

Figure 2.2: The LC cell placed on the hotstage.

2.2 The Liquid Crystal Cell

The central part of the experimental system was the LC cell itself. Careful consideration was given to the design and construction of the cell since its geometry defined the boundary conditions of the experiments. The local structure of the three dimensional rectangular cell selected for our LC studies is shown schematically in figure 2.3.

The manufacture of the cell used was carried out in Cambridge University clean rooms by Dr. Timothy Wilkinson. In essence, the LC cell was constructed from two pieces of glass, with dimensions $(25.60 \pm 0.01)mm$ by $(19.11 \pm 0.01)mm$ and thickness of $(1.31 \pm 0.01)mm$, placed on top of each other. The size of the gap between the glass slides was $(9.7 \pm 0.1)\mu m$ and set with polyethylene terephthalate (PET) film *spacers*, which acted like pillars inside the cell. In order to apply the electric field across the cell, transparent electrodes were etched onto the inner surface of the glass using a series of special procedures, which will be discussed shortly.

The cell was assembled such that the electrodes were perpendicular to each

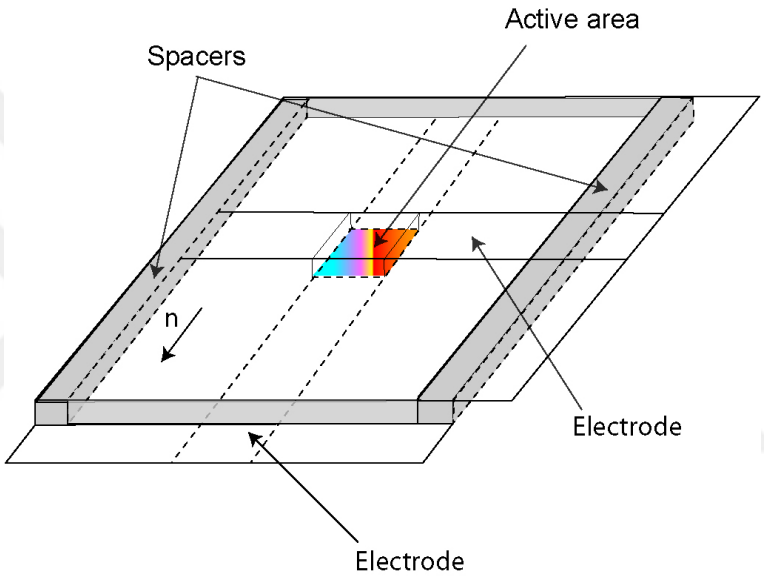

Figure 2.3: A schematic illustration of a liquid crystal cell. The spacers inside the cell provide even spacing at the ends. The electric field is effective over the active area created by the crossing of the transparent electrodes. This is denoted by the colour pattern. As before the $\boldsymbol{n}$ vector represents the director.

other. Therefore, when an AC field was applied to a LC cell it acted over a region where the transparent electrodes crossed. This region is referred to as the *active area*. A sketch of the active area is given in figure 2.4. The relation between the dimensions of the active area and the thickness of the cell, i.e. (length:width:thickness), is called the *aspect ratio* and it is the defining geometric parameter for the LC cell. The significance of the effect of aspect ratio on dynamical systems and their experimental studies is discussed in further detail in Chapter 3.

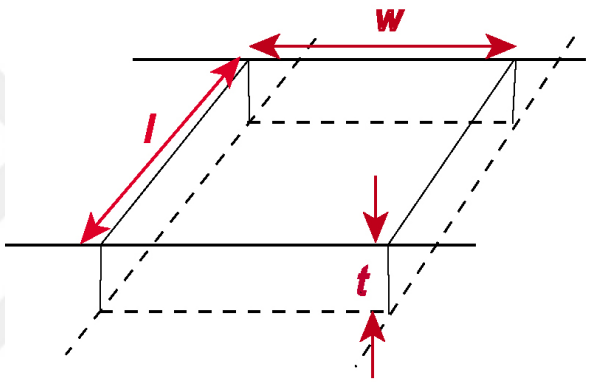

Figure 2.4: The active area of a liquid crystal cell and the dimensions that define the aspect ratio $(l : w : t)$.

The electrode patterns were deposited on the glass using lithography. Briefly, the method of lithography is as follows: The glass was first covered with photoresist and then exposed to ultraviolet light with a *mask* on top. After the development, the photoresist under the mask remained. Then Indium-Tin-Oxide (ITO) was etched in acid and remains of the photoresist cleaned. Hence, the pattern of the mask was used to define the location of the transparent electrodes on the glass.

The geometry of the mask designed for the cell we used is illustrated in figure 2.5. The electrodes etched on the top and bottom glass plates had the pattern

of the black lines shown in figure 2.5. The electrode widths were 20, 10, 7, 5, 3, $2\mu m$ from top to bottom respectively with $\pm 1\mu m$ accuracy. A distance of $100\mu m$ was set between each electrode.

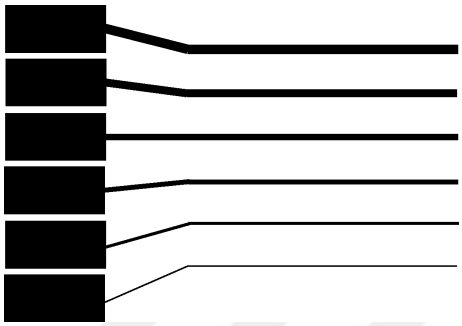

Figure 2.5: An illustration of the mask used for the small aspect ratio cells. The electrode widths from top to bottom were 20, 10, 7, 5, 3, 2μm. Distance between each electrode was $100\mu m$.

After the etching of the electrodes, another layer was prepared on the same side of the glasses by spinning polyimide AM4276 for 20 seconds at $3000rpm$. The glass plates were then hard baked (at 220^oC for 2 hours) and buffed with a roller to make microgrooves which mechanically align the molecules closest to the surface. A discussion of the alignment of LC using surface preparation can be found in [64, 65]. In short, when the polymer surface is rubbed a shear is generated and the near-surface polymer chains undergo shear induced configurational rearrangements [66]. Hence, the surface geometry created aligns the bulk liquid crystal [67]. It is also known that near the surface the alignment induces a tilt of $1 - 5^o$ in the molecules [9]. Therefore, the upper and lower glasses were rubbed in antiparallel directions in order to minimise this effect and create an approximately constant alignment. Such type of alignment, where the molecules are parallel to the surface of the glass plates, is called *planar alignment*[7]. Thus

[7]When the molecules are aligned perpendicular to the surface the alignment is said to be *homeotropic*.

the director $\boldsymbol{n}$, introduced in Chapter 1, was defined.

When the construction of the cell was completed, nematic TX2A was filled into it by the vacuum created in the void between the glasses and spacers. The edges of the cell were sealed with epoxy resin to prevent any leakage or contamination. The nematic TX2A, whose properties are detailed in Appendix B, is a so called *dual frequency* LC. In dual frequency materials the dielectric anisotropy[8] varies as a function of the frequency of the AC field applied to it and changes its sign at a well defined frequency called the *crossover frequency*. The results of the dielectric anisotropy measurements done for the nematic TX2A as a function of frequency are given in Appendix B.1. Since the response of a LC to electric fields depends on the sign of the dielectric anisotropy, we were able to observe both EHC and FT in this material.

Finally, wires were soldered onto the electrodes with indium so that an electric field could be applied to the LC cell. A schematic diagram of the cell in its final state is given in figure 2.6. The red cross indicates the active area of the connected electrodes and a matrix of different aspect ratios embedded within the same device can be clearly seen.

The electrodes and their crossings were tested to check whether there was any residue of photoresist or ITO which would create a short circuit when an AC field was applied. No such cross connections between the neighbouring electrodes was found. An example is shown in figure 2.7 where the rolls formed only at the active area of the connected electrodes, with an aspect ratio $2.0 \pm 0.2 : 2.0 \pm 0.2 : 1.0$.

An important point to consider, when applying electric fields to a LC cell with small electrode widths and cell thickness, such as the one explained above, is the existence of fringing fields at the edge of the electrodes. To date, two main studies have been done on fringing fields. The first one of these was carried out by Cas-

[8]see Chapter 1 for a definition

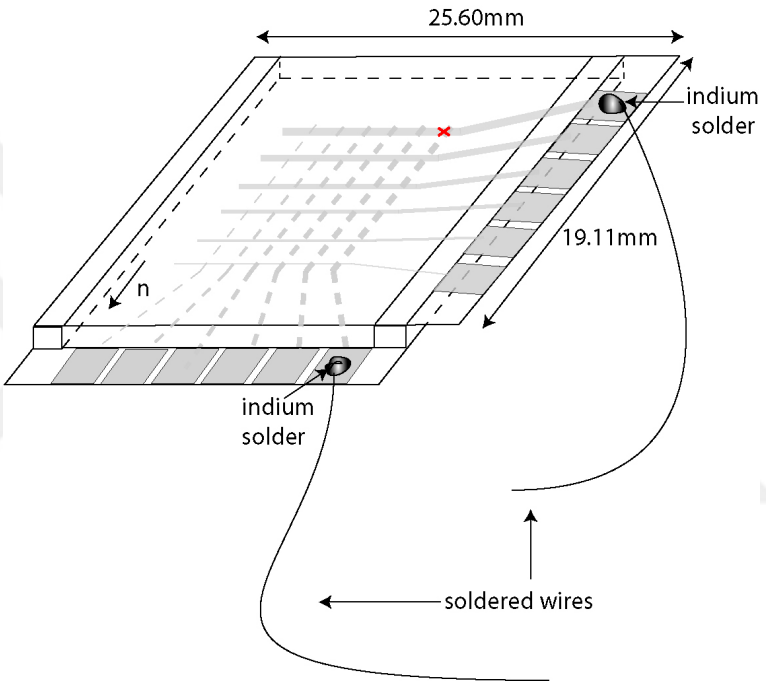

Figure 2.6: The final state of the cell. Solid lines indicate the electrodes on the top glass and the ones on the bottom glass are shown as dashed lines. Freedericksz Transition or electroconvection is expected to evolve only within the active area marked with a cross.

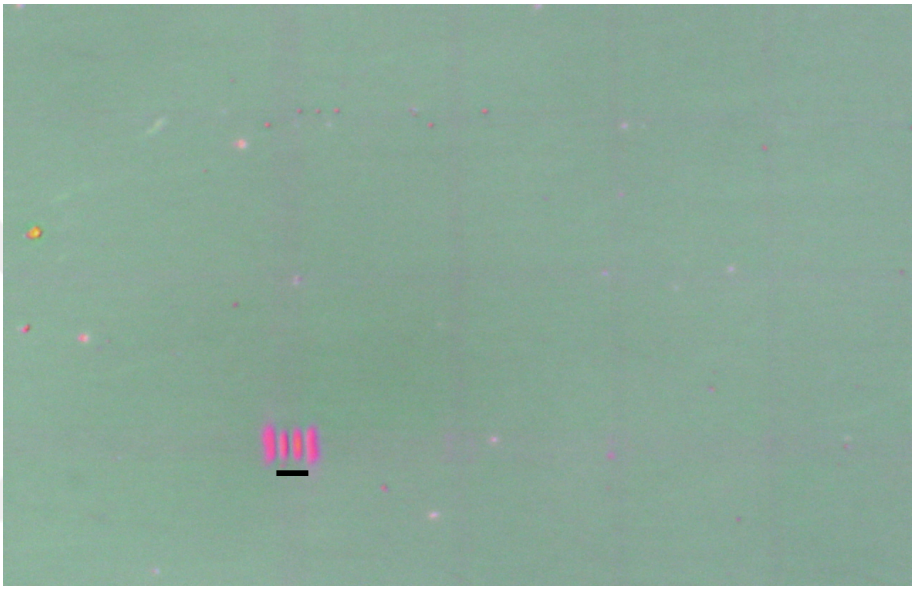

Figure 2.7: Convection rolls created in aspect ratio $2.0 \pm 0.2 : 2.0 \pm 0.2 : 1.0$. The black solid line indicates $20\mu m$. The crossings of different size electrodes creating a range of different aspect ratios can also be partially seen. The response to electric field is only in the active area of the connected electrodes and in its neighbourhood where the fringing fields existed. The picture was taken with a 10X objective and numerical aperture (NA) = 0.25.

sarly and Young [68] where they modelled the effects of fringing fields on optical properties of a nematic LC and gave predictions for the extension of electric fields at electrode edges. Their predictions were tested experimentally by Storrow et al. [69] who used liquid crystal devices to create a phase difference between two laser beams and then combined the beams to examine the resulting interference patterns. Their experimental setup consisted of a Michelson interferometer with two planarly aligned LC cells, each adjusted on one of the arms of the interferometer. The LC cells were filled with the same nematic material[9] and a laser beam was directed towards each cell after it was split by a beam splitter. Meanwhile, an electric field was applied to one of these cells (the retarding cell) whose effect was to re-align the liquid crystal molecules in a way explained in Chapter 1 for materials with positive dielectric anisotropy. Thus, the refractive indices of the material were altered due to the birefringent nature of liquid crystals and the phase of the laser beam experienced a shift as it passed through cell.

Similarly, an electric field was applied to the second liquid crystal cell (the test cell), however, the values of the field amplitude were chosen specifically to orient the molecules to produce phase shifts of 0, $\pi/2$ and π relative to the first beam. By combining the beams after they passed through the LC cells at set voltage values, three different interference patterns were obtained. The intensity of patterns were examined for quantitative information regarding the phase shift a wavefront experienced at any point on the retarding cell[10]. In principle, no phase shift was expected outside the electrodes since, in these regions, the molecules were assumed to be in the planar orientation they retain in the absence of electric field. Nevertheless, Storrow et al. observed phase variations generated by the molecules whose orientations were disturbed by the fringing fields which extended beyond

[9]The nematic E49. This material has positive dielectric anisotropy [70].

[10]The technique explained here is called phase-stepping interferometry (PSI) and further information about it can be found in reference [69].

the electrode edges by 18%. This value was two orders of magnitude greater than the theoretical predictions of Cassarly and Young.

Subsequently, Binks [39] and Peacock [8] observed that for a cell with thickness of $50\mu m$ and electrode widths of $200\mu m$, the fringing fields are not large at moderate voltages and the flow patterns are confined within the active area only. However, given that the actual dimensions of the active areas in the LC cell we manufactured were significantly smaller than the values of the cell used by Binks and Peacock, the effects of fringing fields were evident and examples of their effects are given in the next chapter.

2.3 Electrical Equipment

The quality of the electrical equipment used in the experiments was checked with computer codes written in LabView measurement and automation software. Specifically, the long term stability of the function generator, the amplifier, the multimeter and the temperature controller were examined.

According to the manufacturer's quote, the accuracy of the function generator in frequency is equal to that of the amplitude for the range of values applied in our experiments and is given as $\pm 0.01\%$ for both parameters. In order to test if this level of accuracy can be maintained in frequency and amplitude of the AC field applied to the LC cell in our experiments, firstly, the function generator was set to produce a selected sinusoidal AC signal. Then, the amplitude of this test signal was modified by the amplifier to a typical value applied in the experiments whilst the frequency was kept at its original value, which was also within the range applied in our experiments. Afterwards, the root-mean-square(rms) value of the amplified AC signal was measured by the multimeter whose accuracy given by the manufacturer is $\pm 0.01\%$ for measuring values with three significant digits. Finally, the frequency and the modified amplitude values of the AC signal were

sampled by a computer every 15 minutes for 5 hours by the signal generator and the multimeter respectively through separate GPIB (General Purpose Interface Bus) ports.

The results shown in figure 2.8 are the *rms* voltage readings sent to the computer from the multimeter, after the original signal was amplified. As such, the accuracy of the function generator, the amplifier and the multimeter are included in the data presented. The standard deviation of the mean, shown as the error bars, is $\pm 0.0014 V_{rms}$ which corresponds to a percentage error of $\pm 0.01\%$. Hence, the precision of the measurements was in agreement with the values quoted by the manufacturers of the multimeter and the signal generator. The results also indicate that the fluctuations in the amplifier were less than or equal to $\pm 0.01\%$. No variation could be detected in the value from the measurements of the frequency of the AC signal sampled by the computer from the function generator with the sampling rate specified above. Therefore, the value quoted by the manufacturer was accepted as the accuracy of the function generator in frequency. Conclusively, the parameter values in the experiments could be maintained to within this level of accuracy, explicitly $\pm 0.01\%$.

Thermal stability was considered and examined with great care. According to Rehberg et al [71] random Brownian-like fluctuations, which can result from thermal fluctuations, have a significant effect near the onset of EHC. Furthermore, Peacock [8] reported that thermal fluctuations can give rise to bursts near the onset of the oscillatory motion observed in nematic BDH-1786. Therefore, a special temperature monitor was designed to test for fluctuations for the temperature controller shown in figure 2.1 whose stability specified by the manufacturer is 0.1^oC (relative temperature). For our test, firstly, the temperature controller was set to increase the temperature of the hotstage from room temperature to 33^oC, which was considered to be a suitable temperature to conduct the exper-

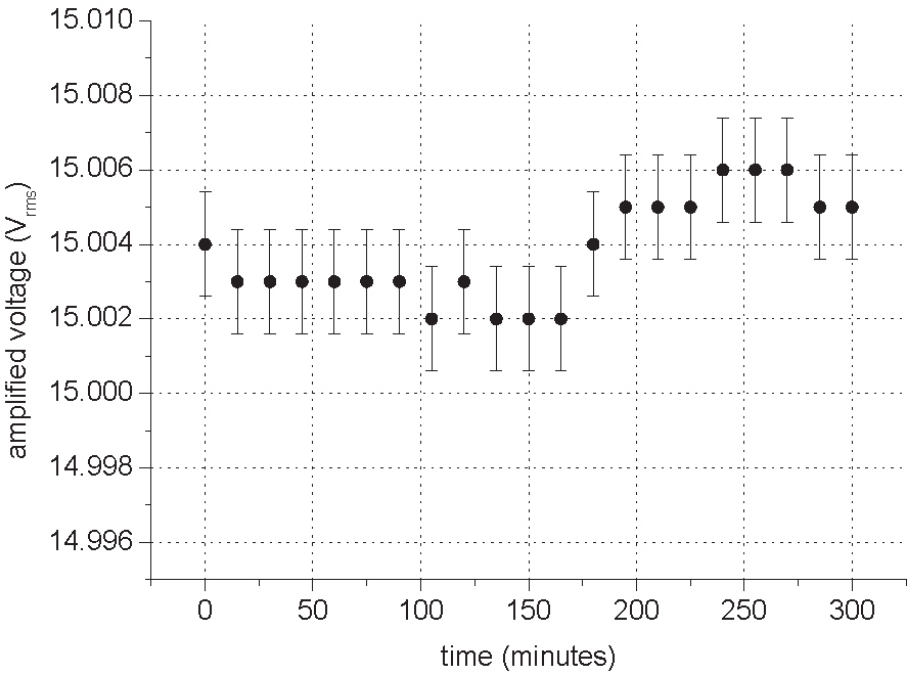

Figure 2.8: The stability graph of the amplifier and the multimeter. The data was collected and sent to the computer by the multimeter after the signal was amplified.

iments for the reasons which are given below. Furthermore, a lid was mounted on the hotstage to isolate it thermally from the room temperature. It should be emphasized that here, the aim was to check for the fluctuations in temperature rather than its absolute value. Therefore, the hotstage and the temperature monitor were connected to each other and the offset of the monitor was calibrated for the temperature of the hotstage after the display of the temperature controller confirmed that it has reached 33^oC. Finally, the temperature of the hotstage was measured every minute for more than 16hours and the difference between the calibrated and the measured temperature values were converted to a DC signal such that $12V$ corresponded to 1^oC. The results were recorded by a computer and are shown in figure 2.9, which confirms that the temperature fluctuations were approximately 0.01^oC.

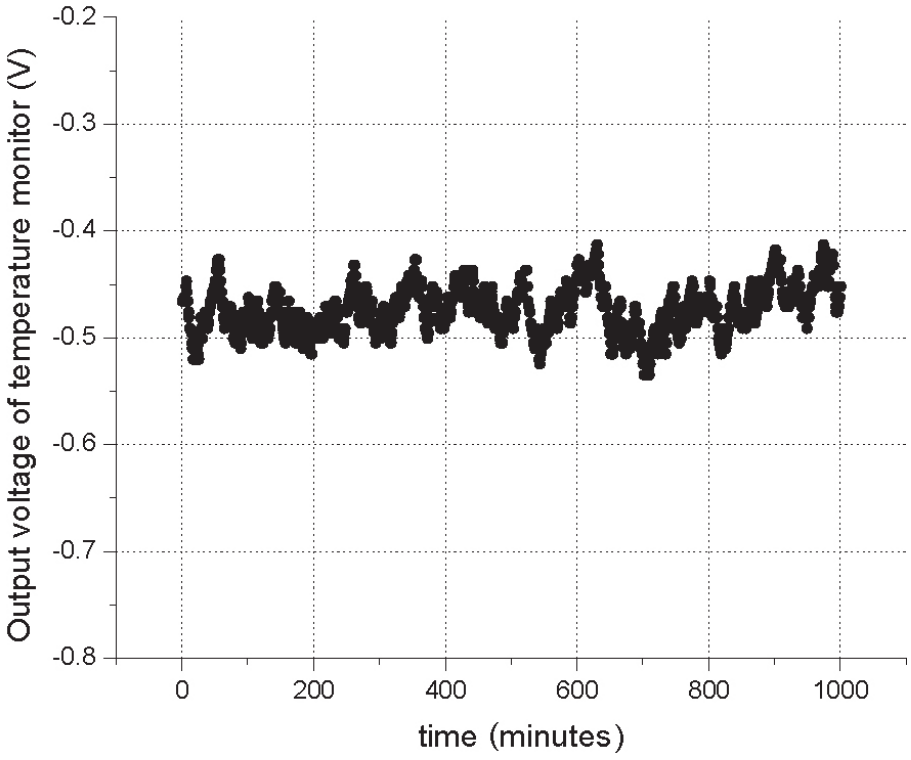

Figure 2.9: The stability graph of the temperature controller. On the vertical axis $0.1V$ corresponds to $\sim 0.008^oC$.

2.4 Experimental Techniques

In investigating the priority exchange between different phenomena and patterns observed in nematic TX2A, experimental methods outlined below were used. The details of specific experiments are given in the related sections of Chapters 4 and 5.

The first effect to be considered in the experiments was the drift in the conductivity of LC, which arises from contamination by impurity ions. It is believed that the electrodes slowly corrode and contaminate the liquid crystal with time [9]. The amount of drift changes on a day to day basis and thus produces a quantitative shift in the value of the limit points[11] measured in the experiments. This problem has also been an issue in previous investigations [8, 39]. All the bifurcations were steady and the technique used by Binks [39], of nondimensionalising the results by a well defined critical point, was adopted. Specifically, a limit point was chosen to provide a reference value and was measured at regular intervals. Relative values of the voltage were obtained by dividing the absolute value by the reference value as shown in equation 2.1:

$$V_{rel} = V_{abs}/V_{ref} \tag{2.1}$$

where V_{rel} is the relative voltage, V_{abs} is the absolute voltage (the rms value found as the result of a measurement) and V_{ref} is the reference value explained above. The same technique was applied also to frequency measurements for the experiment discussed in Chapter 5.

The increments/decrements on the control parameters were made in steps of

[11]The concept of *limit points* is introduced and its role in the experiments is described in detail in Chapter 4.

$0.01kHz$[12] and $0.03V_{rms}$[13] for frequency and amplitude respectively. The waiting time between the steps was determined by considering typical response time of nematic LC's to electric fields. This value is usually of the order of one hundred milliseconds [1]. Therefore the waiting time of the order of seconds between the increments/decrements was regarded sufficient. However, the specific value for the waiting time and justification for its choice is given in Chapter 4.

The temperature of the LC cell was kept constant at $(33.00 \pm 0.01)^oC$ throughout the experiments. The first reason for choosing this value was that it is well below the clearing point[14] of TX2A (101^oC). Therefore, the possible effects resulting from a nearby phase transition, such as increased orientational fluctuation of the molecules, can be neglected. Further detail on phase transitions from nematic to isotropic phase can be found in reference [72]. Another reason for choosing this temperature value was to minimise possible fluctuations of the temperature controller in case of a thermal leakage. In such a situation, if the temperature set for the hotstage is close to the room temperature, the heat flow between the hotstage and the environment will be from and to the hotstage, due to thermal fluctuations of the room temperature. Hence, the temperature controller will operate both heating and cooling processes in order to maintain the required temperature. On the contrary, if the set temperature is well above the room temperature, the temperature controller can operate more steadily since its single practice will be heating.

[12] corresponding to 0.4% and 0.7% in the experimental range specified in Chapters 4 and 5 respectively

[13] corresponding to 0.7% in the experimental range specified in Chapters 4 and 5

[14] see section 1.1 for the definition of *clearing point*

Chapter 3

General Observations

In this chapter the significance of the aspect ratio of the active area on the observed flow patterns will be examined. Firstly, the advantages and disadvantages of large and small aspect ratios in studies of fluid systems driven from equilibrium will be compared. Following this, the primary flow patterns in various aspect ratios will be discussed leading to the justifications of the aspect ratio used in the experiments. Finally, general observations of flows in this aspect ratio will be summarised.

3.1 Large and Small Aspect Ratios

For studies of flow problems in EHC, large aspect ratio cells are commonly selected [73]. The motivation for this preference is to attempt to approach the abstraction of an infinite experimental setup so that the results can be compared with those obtained from mathematical models where periodic boundary conditions are used. The advantage of periodic boundary conditions is that they allow the flow to be decomposed into its Fourier modes and thus, permit the derivation of *amplitude equations* which are applicable just above the onset of finite wavelength instabilities. Amplitude equations, especially near stationary bifurcations,

give the slow modulation in space and time of the finite wavelength pattern [74]. Therefore, the assumption of periodic boundary conditions is a favored tool in pattern formation studies carried out in EHC as well as in other nonequilibrium systems [75, 76, 77].

However, there is another outcome of periodic boundary conditions that requires attention. Specifically, in very large systems where such boundary conditions are applicable a continuum of flow states exist in the solution space. If the system were an ideal one, i.e. with no experimental imperfections, a single flow pattern from a continuum would be selected as a stable state. Nonetheless, a large number of others will exist nearby, that is, with small variations in the values of control parameters a different flow pattern can become stable.

This is an important consequence of periodic boundary conditions that should be taken into consideration when evaluating the experimental appropriateness of large aspect ratio cells in practice. By definition, in large aspect ratio cells the active area is significantly greater than the thickness of the cell[1]. Therefore, the imperfections on the glass surfaces and the bending of the glass due to its own weight cause unavoidable variations in the cell thickness, which in turn will mean that different flow patterns will be selected in various parts of the LC cell. Photographs presented in figures 3.1 and 3.2, where the colours are natural, display such a case in EHC. The image in figure 3.1 was taken near the threshold voltage for the onset of convection. On the upper left and lower right sections of the photograph oblique roll pattern is seen where the rolls undulate. Straight rolls dominate the rest of the picture but dislocation points are also present. The photograph in figure 3.2 was taken at a value far from the threshold. As seen in the figure, different patterns coexist in well separated domains in this case and small regions of disordered flow or dislocations can also be noticed. Moreover,

[1]A typical value for the electrode widths in a large aspect ratio cell can be $\sim 1cm$ whereas the cell thickness can be down to $5\mu m$.

it is possible that the patches of different patterns shown in figures 3.1 and 3.2 can interact with each other, since liquid crystals are non-compressible fluids. Rasenat et al. [78] show in their studies, regarding the defect dynamics in EHC, that the coherence length of perturbations in a LC cell is of the order of the cell thickness. As clearly demonstrated by these photographs large aspect ratio cells cannot provide a well defined experimental system in practice and therefore are not suitable for studies on pattern competition.

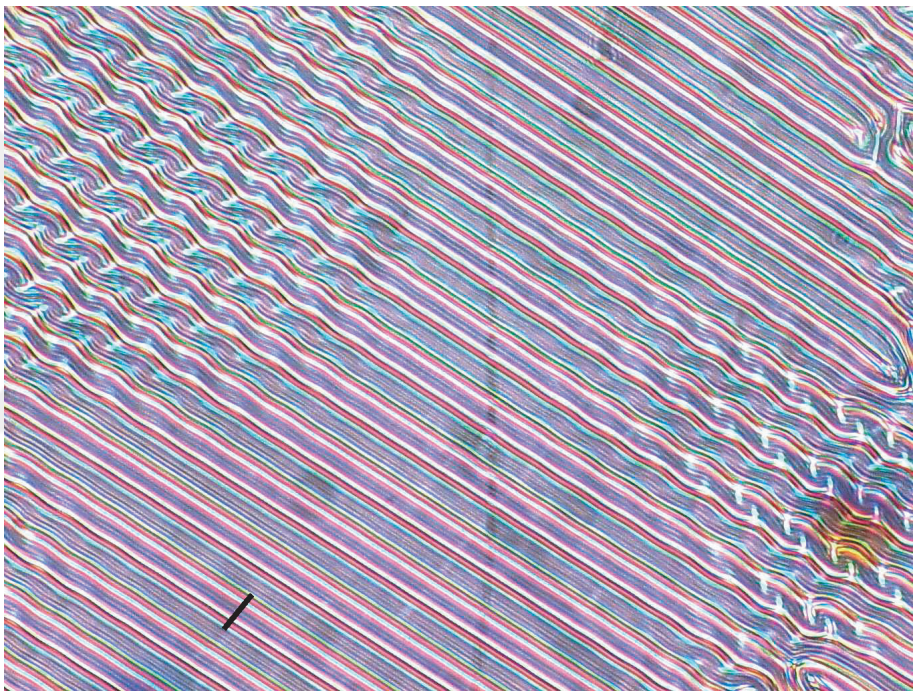

Figure 3.1: EHC created in nematic TX2A in a large aspect ratio (2000:2000:1) cell near the threshold voltage. Different patterns are seen in various sections of the cell. The black solid line indicates $5\mu m$.

On the other hand, small aspect ratio systems have proved to be advantageous for detailed studies of nonlinear systems, including the competition between initial neighbouring solutions [49, 52]. The effect of using small scales is to reduce the multiplicity of flows [53, 79] by restricting the number of fixed points in the solution space [31]. Furthermore, better experimental control can be obtained

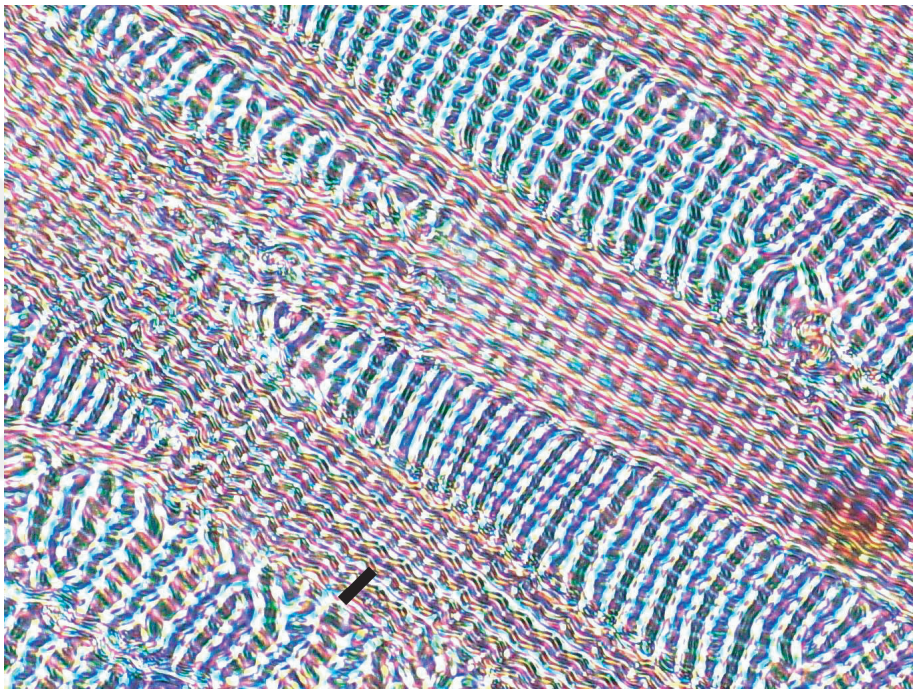

Figure 3.2: Patterns created in nematic TX2A in a large aspect ratio (2000:2000:1) cell above the threshold voltage for the primary state. As before different patterns coexist. The black solid line indicates $5\mu m$.

when the actual size of the active areas are decreased. In that case, physical imperfections, such as the thickness variations on the glass surfaces of the cell will be minimised. Also, it should be considered that the alignment of nematic liquid crystal molecules cannot be well defined for cell thicknesses greater than $100\mu m$ [15]. Hence, in small scale aspect ratios, the well separated steady states can uniquely be identified and their dynamics can be investigated. The studies regarding low-dimensional dynamics in EHC experiments, explained in Chapter 1, are also conducted in small aspect ratio cells for the same reasons. Therefore, following the discussions given above, a small aspect ratio cell with actual electrode width and cell thickness sizes of the order a few microns, was decided to be the best and only option for our experiments on how the basic flow states interact. However, before detailing these studies, we will now present the observations regarding the primary roll numbers in relation to various aspect ratio values.

3.2 Primary States of Various Aspect Ratios

The main purpose of constructing the cell explained in the previous chapter as a matrix of aspect ratios was to study experimentally the predictions made in the numerical work of Tavener et al [45] concerning the roll number of primary states[2] for various aspect ratios. The associated results they presented in [45] are shown in figure 3.3.

In figure 3.3, the vertical axis gives the electric field strength applied to a nematic liquid crystal[3] in volts and the aspect ratio, r, is given along the horizontal axis. In the calculations, r is defined as w/t, where w and t indicate the

[2]i.e., the state that emerges continuously from no-flow state as one of the control parameters in the experiment is varied (electric field strength in this case) whilst the other parameters are kept fixed. A more detailed definition is given in Chapter 4.

[3]with negative dielectric anisotropy

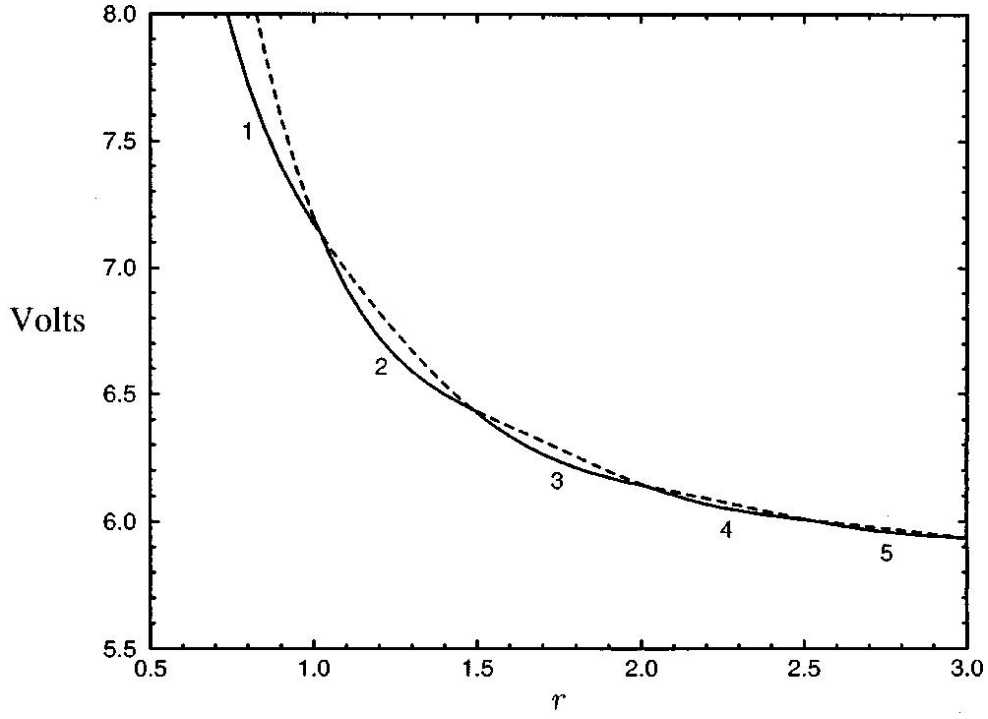

Figure 3.3: The results of numerical calculations giving the threshold voltages as a function of aspect ratio, r [45]. The solid lines give the loci of parameters where the primary states emerge from no-flow state. The number of rolls in each primary state is given on the associated curve. The dashed lines are indicate the secondary bifurcations.

width and the thickness of the active area respectively, as illustrated in figure 2.4. This two dimensional definition of r is considered to be suitable to investigate the roll number of the primary state that evolves in the system, since the width of convection rolls are determined by t [2] and the number of rolls that can be accommodated within the active area depends on w. The role of the third dimension, i.e. l shown in figure 2.4, is to determine the length of the convection rolls. However, the effect of l on the roll number of the primary state is negligible compared to that of w or t.

In figure 3.3, for a fixed value of r, the no-flow state, which exists in the absence of electric field, remains stable for voltage values below the solid lines. When the voltage is increased to a value on the solid lines the no-flow state loses stability to an EHC state (primary state) for the corresponding value of r. The predicted number of convection rolls that form in the EHC state is indicated on each curve and the dashed lines represent the secondary bifurcations[4]. Here, we are particularly interested in comparing our results to those shown in figure 3.3 with reference to the number of rolls in primary state for fixed values of the aspect ratio. The absolute values of the threshold voltages can not be compared since the numerical calculations in [45] were carried out for nematic material MBBA, and not TX2A. Consequently, the threshold voltages for the primary states of the two will differ due to differences in their material properties. Moreover, in experimental systems, the primary state forms continuously and therefore, well defined critical points, such as those in the numerical calculations presented in figure 3.3, cannot be realised in practice.

As illustrated in figure 2.6, the cell constructed for our experiments included thirty-six different aspect ratios. However, this range of aspect ratios can be divided into three categories, namely, those less than 1, approximately/equal to 1

[4]The concept and the necessity of secondary bifurcations is given in Chapter 4.

and greater than 1. An example representing the primary pattern from each group is given below and as before, the colours are natural in all figures. Within the categories the roll numbers of the primary states stayed the same but the width of the convection rolls varied according to the actual width of the electrodes.

The first example displayed in figure 3.4 is for aspect ratios less than 1. The actual width of the horizontal electrode in the picture was $3\mu m$. This length is nearly 30 times smaller than an average size of a human hair ($90\mu m$). For comparison, a picture of a LC cell with $200\mu m$ electrode width is presented next to a human hair in reference [40] by Peacock et al and is shown in figure 3.5.

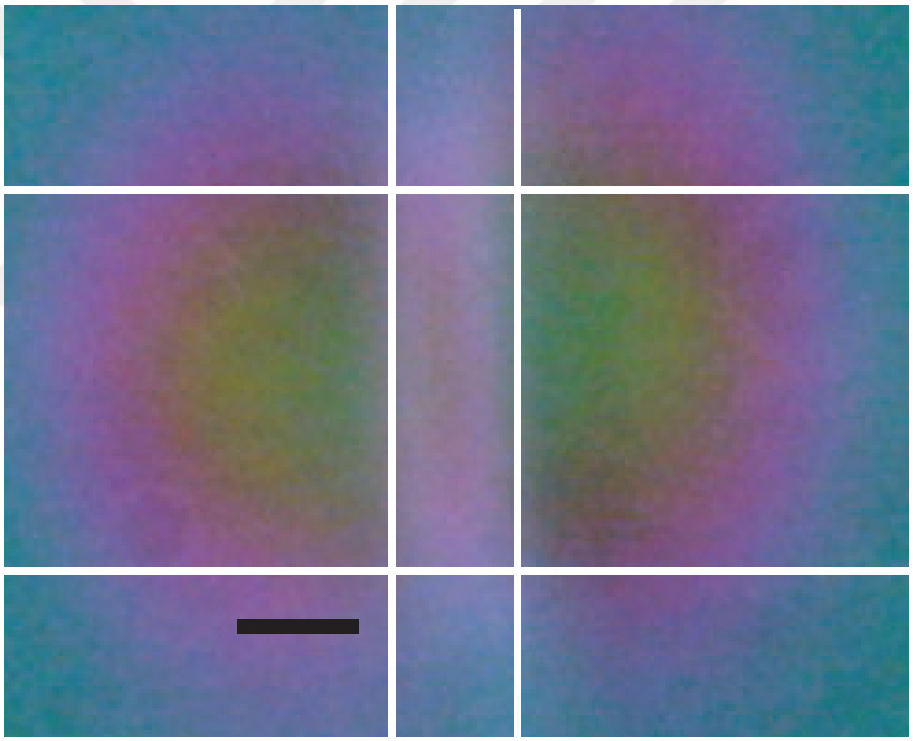

Figure 3.4: A pattern suggesting a single roll observed in active area with an aspect ratio 0.31 : 0.52 : 1. The black solid line indicates $3\mu m$ and white lines give the borders of the electrodes. The picture was taken at voltage and frequency values $29.60V_{rms}$ and $30.10kHz$ respectively, with 80X objective and N.A. number of 0.75.

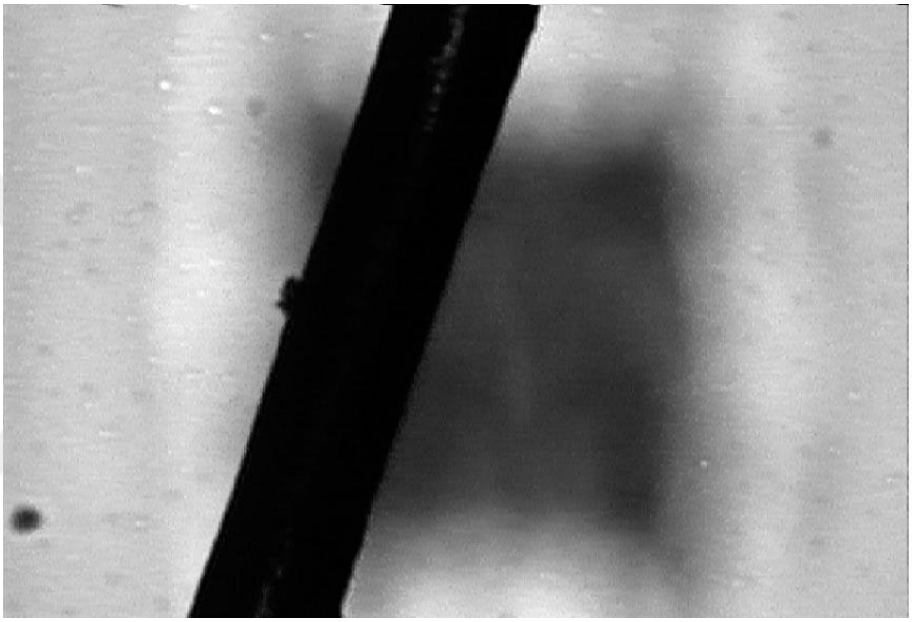

Figure 3.5: The image in the background is a LC cell with $200\mu m$. A piece of human hair is focused in the photograph [40]. It should be noted that the largest electrode width in the LC cell used in this study was $20\mu m$ which is approximately one quarter of the diameter of a human hair.

The pattern seen at the centre of figure 3.4 suggests a single roll in accordance with the prediction presented in figure 3.3. It is believed that this may be the first observation of a single roll in an EHC system to date and is of importance for the following reason. When an even number of rolls form in EHC, translational symmetry is broken. In that case, as explained in Chapter 1 with comparisons to Taylor-Couette and Rayleigh-Benard systems, EHC cannot be modelled as a pitchfork bifurcation since experimental investigations to observe both rotation directions of the convection rolls have failed [45]. This problem is stressed again in the discussion given below for the 4-roll state observed in aspect ratio 2:2:1. However, a possible single roll presented in figure 3.3 will break not translational but the left/right symmetry and thus, the state with counter rotating direction may exist at control parameter values close to the one given for the pattern presented in the figure. The details of the pattern shown in the photograph could not be resolved due to the small width of the electrodes and the effect of fringing fields, introduced in the previous chapter, which is revealed as a distribution of molecular orientation near the electrode edges. Nevertheless, it is a novel observation which warrants further investigation in the future.

In figure 3.6 the initial flow pattern formed in an aspect ratio $1.03 : 1.03 : 1$ is presented. The width of the electrodes for this image were $10\mu m$. The purple regions contrasting with the green background suggest that two rolls exist in the picture. Since the neutral curves for the states with two rolls begin near the aspect ratio value of 1.0 in figure 3.3, the image presented in figure 3.6 is consistent with numerical predictions.

A photograph of a typical flow field for aspect ratios greater than 1 is shown in figure 3.7. Aspect ratio $2 : 2 : 1$ revealed four rolls, as shown in figure 3.7, which is once again in agreement with the numerical results given in figure 3.3. The actual size of the electrodes in this case were $20\mu m$. While acquiring this

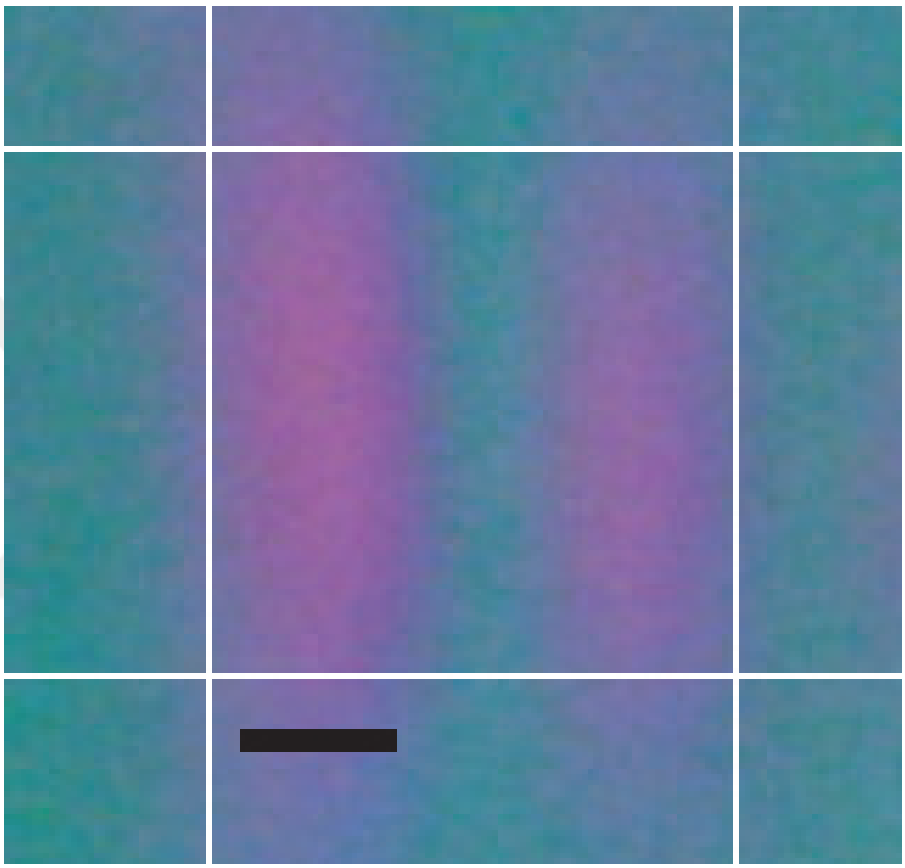

Figure 3.6: Two rolls observed in the active area with an aspect ratio 1.03 : 1.03 : 1. The black solid line indicates $5\mu m$ and the white lines show the borders of the electrodes. The picture was taken at voltage and frequency values $23.04V_{rms}$ and $30.10kHz$ respectively, with 80X objective and N.A. number of 0.75.

picture, the focal plane of the microscope was adjusted so that it matched with the plane of the upper glass of the LC cell. This contrasts with the other pictures presented thus far, where the focal plane was adjusted to coincide with the mid-plane between the two glasses. As a consequence, the bright pink lines in figure 3.7 are in focus. These indicate upward flow of the rolls. Hence, consistent with the flow structures suggested by Hirata and Tako in [43], the rolls flowed downwards at the ends of the active area. Also, akin to the observations of Binks[39] and Peacock[8], the rolls did not display a counter rotation direction throughout our study. An explanation for the absence of such symmetric flows was proposed by Hirato and Tako [43]. According to their argument, the free ions in a LC material have a single sign and the impurities that localize near the electrode edges force a downward flow direction in these regions. Tavener et al. [45] also addressed this problem numerically by investigating the effect of fringing electric fields on the bifurcation structure of EHC. However, they found that fringing fields disconnect off the branches but the two solutions exist near each other. Consequently, the absence of counter rotation direction of the rolls still remains as one of the fundamental questions related to EHC.

The active area with aspect ratio $2 : 2 : 1$, which revealed the flow pattern shown in figure 3.7, was used extensively in our experiments to examine the priority exchange of neighbouring states. As presented in figure 3.7 the primary state in this aspect ratio contained 4-rolls and its neighbouring state was a 6-roll state. The justification for the choice of this aspect ratio is based on the theoretical studies of Schaeffer [61] and Hall [62, 63], which were later detailed by Cliffe [54] as explained in Chapter 1. Briefly, they show that the hysteresis observed in experiments regarding pattern competition in Taylor-Couette flows is highly suppressed for 2 and 4-roll states due to quadratic terms which are included in the model for these states. Thus, in order to avoid the effect of the

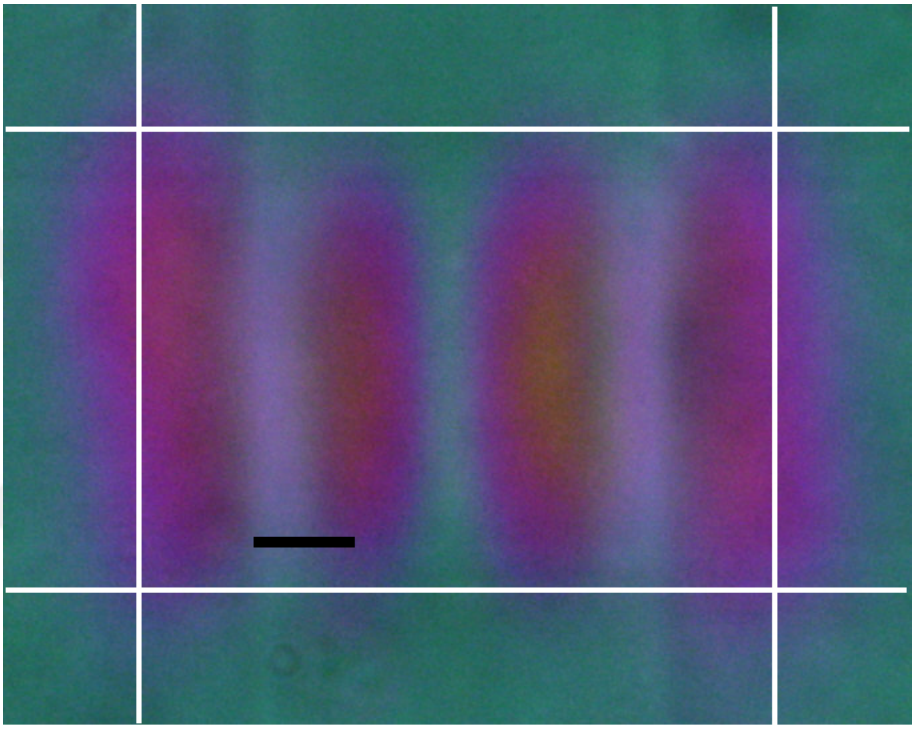

Figure 3.7: Four rolls created in an aspect ratio $2:2:1$. The black solid line indicates $5\mu m$ and the borders of the electrodes are given by the white lines. The picture was taken at voltage and frequency values $20.60V_{rms}$ and $30.10kHz$ respectively, with 80X objective and N.A. number of 0.75.

quadratic terms, aspect ratio 2 : 2 : 1 was used in the experiments so that the priority exchange between 4 and 6-roll states can be studied. In the next section, we will introduce the 6-roll state as well as further instabilities that can develop in EHC. However, prior to this, the Freedericksz Transition(FT) observed in this active area will be presented.

3.3 Observations in Aspect Ratio Two

The general properties of the nematic LC used in our experiments, namely TX2A, was introduced in Chapter 1 and revisited in Chapter 2. In this material, for frequencies below the crossover frequency[5], the dielectric anisotropy has positive values. Consequently, the response of the LC to AC field is a Freedericksz transition. A picture of an FT state observed at frequencies within this range is shown in figure 3.8. Near the centre of the active area, which is the dark region in the photograph, the molecules are aligned approximately perpendicular to the surface of the glass. This is a signature of a nearly complete Freedericksz transition where realignment of the molecules has occurred under the action of the applied field. Elsewhere, the director has a distribution of orientation in accordance with the colour pattern seen in figure 3.8.

When the voltage was further increased above the onset value for FT no motion was found. This is in stark contrast to EHC where temporal oscillation and even turbulence was found near similar voltage ranges as discussed below. The effect of increasing the voltage in an FT state was simply to force the orientation of the director further towards perpendicular alignment to the surfaces as shown in figure 3.9. The photograph presented in this figure was taken at $37.50V_{rms}$, i.e. ~ 5 times greater than the value applied to observe the pattern shown in figure 3.8. The frequency was $20kHz$ as in figure 3.8. It can be clearly seen in the

[5]see Chapter 2 for a definition

photograph that the molecular orientation was distorted and the effect of the AC field extended beyond the borders of the electrodes due to high applied voltage. The black regions near the electrode edges and the centre indicate the areas with complete Freedericksz transition. Interestingly, the middle section of the active area which was darker in figure 3.8 acquired a brighter colour in this case. A similar observation, shown in figure 3.10, was presented in the first Chapter of reference [3] as an example of transient patterns in Freedericksz transition. According to [3] the white regions seen in figure 3.10 are such transient patterns and are observed prior to complete Freedericksz transition due to competitions between the applied and elastic forces. This observation is in accordance with the bright line observed near the centre in figure 3.9. The main difference between the LC cells used in figures 3.9 and 3.10 is that a large aspect ratio cell was used for the case in figure 3.10. Consequently, the number of white regions in figure 3.10 is greater than that of figure 3.9. The test for the evolution of the transient line in figure 3.9 at higher voltages was not performed in order to avoid damaging the LC cell via a short circuit.

When the frequency of the AC field applied to the cell was set at values above the crossover frequency, the dielectric anisotropy of TX2A changed its sign to negative. As a result, the response of the nematic material to AC field is EHC. The primary EHC state observed in aspect ratio $2:2:1$ within this range of frequencies was shown in figure 3.7. In accordance with the explanations given in references [50, 61], for higher frequencies when the voltage was stepped up from the undisturbed state the primary pattern evolved consisted six rolls. A picture of this state is presented in figure 3.11. The experiment regarding the priority exchange of these states is the subject of Chapter 4.

The final pictures presented in figures 3.12 and 3.13 illustrate some of the patterns observed in the same active area as the voltage was increased to values

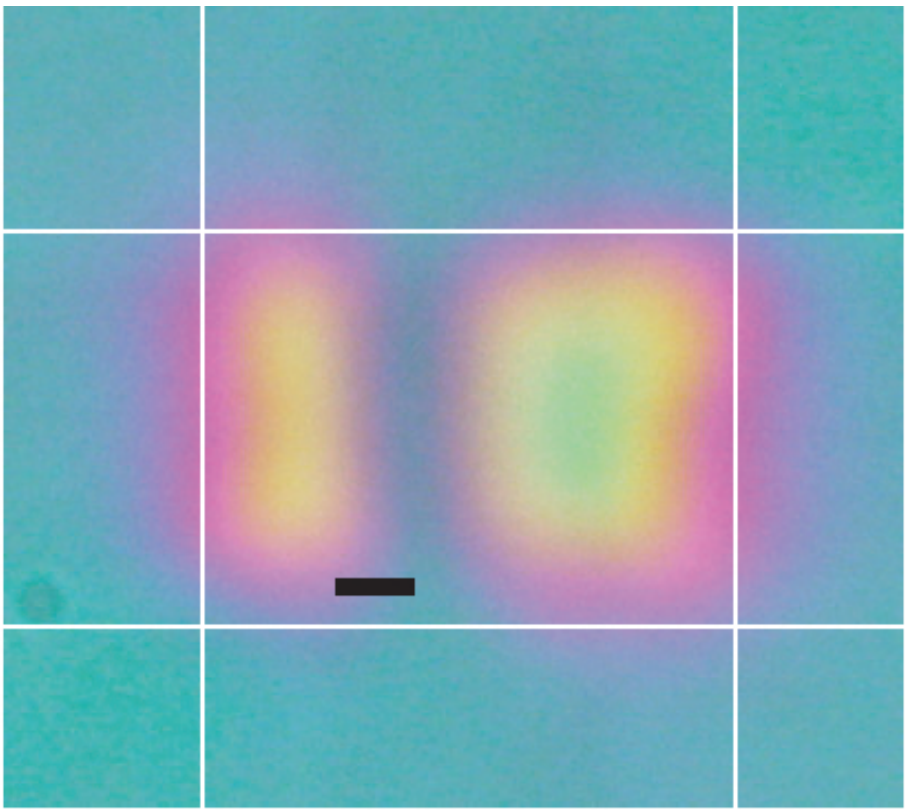

Figure 3.8: A Freedericksz Transition (FT) observed in aspect ratio 2 : 2 : 1. The black solid line indicates $5\mu m$ and the white lines show the borders of the electrodes. The picture was taken at voltage and frequency values $7.42V_{rms}$ and $20kHz$ respectively, with 20X objective and N.A. number of 0.40.

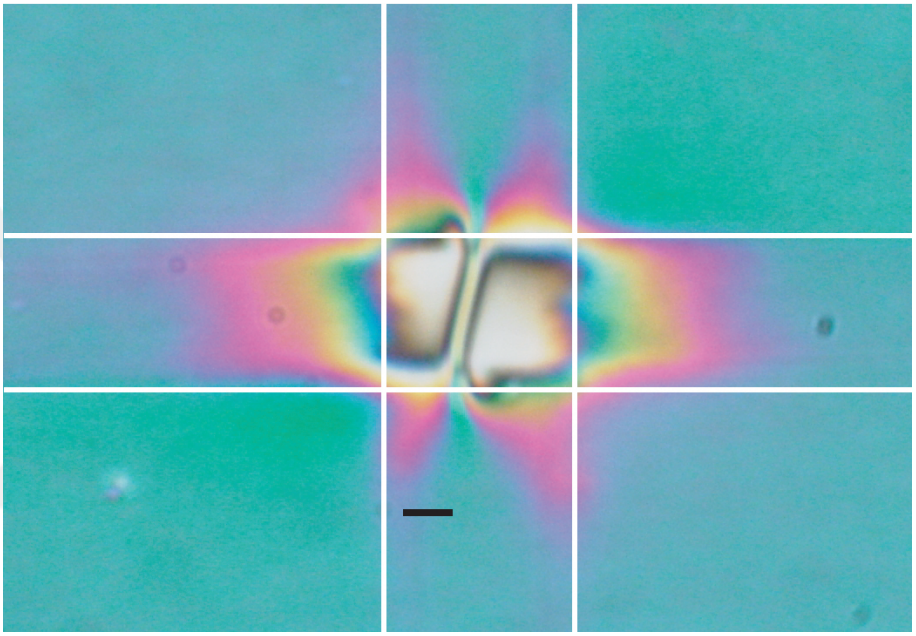

Figure 3.9: A Freedericksz Transition (FT) observed in aspect ratio 2 : 2 : 1. The black solid line indicates $5\mu m$ and the borders of the electrodes are imposed on the photograph by the white lines. The picture was taken at voltage and frequency values $37.50V_{rms}$ and $20kHz$ respectively, with 20X objective and N.A. number of 0.40.

Figure 3.10: A Freedericksz Transition observed in a large aspect ratio cell filled with a nematic LC [3]. The bright lines are transient patterns are observed prior to complete Freedericksz transition due to competition between the applied and elastic forces.

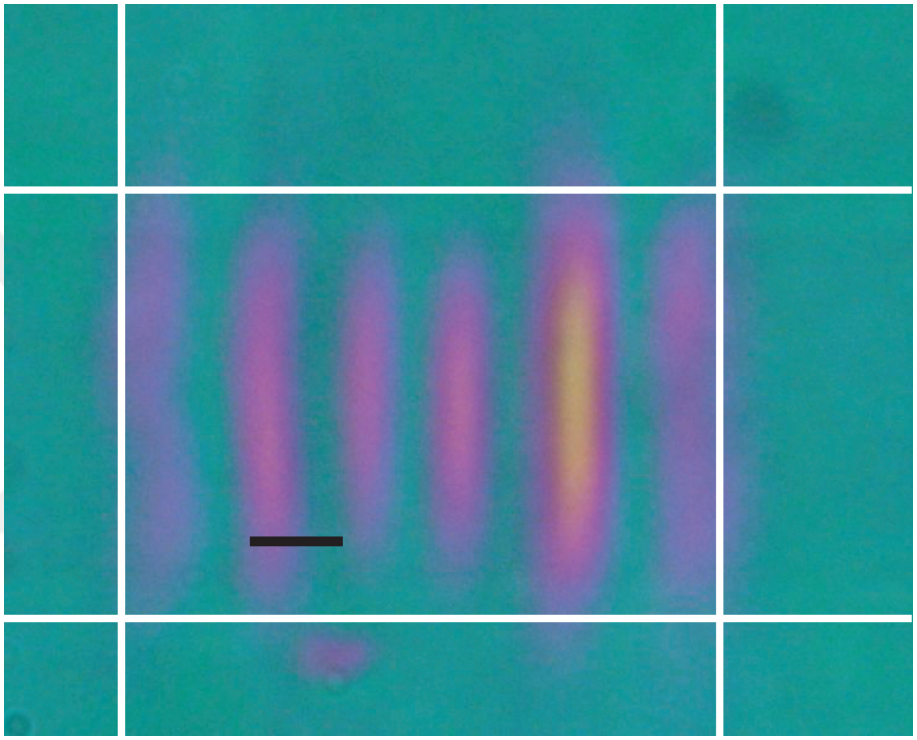

Figure 3.11: Six rolls created in an aspect ratio 2 : 2 : 1. The black solid line indicates $5\mu m$ and the white lines denote the borders of the electrodes. The picture was taken at voltage and frequency values $22.60V_{rms}$ and $32.10kHz$ respectively, with 80X objective and N.A. number of 0.75.

above the one applied for the pattern in figure 3.11. Following the 6-roll state in figure 3.11 an oscillation of the side rolls was activated at $30.00V_{rms}$ as shown in figure 3.12. Contrary to FT states explained above, increasing the voltage further resulted with dynamic states and the loss of the finite wavelength structure, which is given in figure 3.13. The disordered flow at a microscopic scale was pushed outwards from the edges of the active area as seen in the picture. It should be noted that the value of the voltage applied to the cell to obtain this flow pattern was the same value that was applied to observe the pattern in figure 3.9.

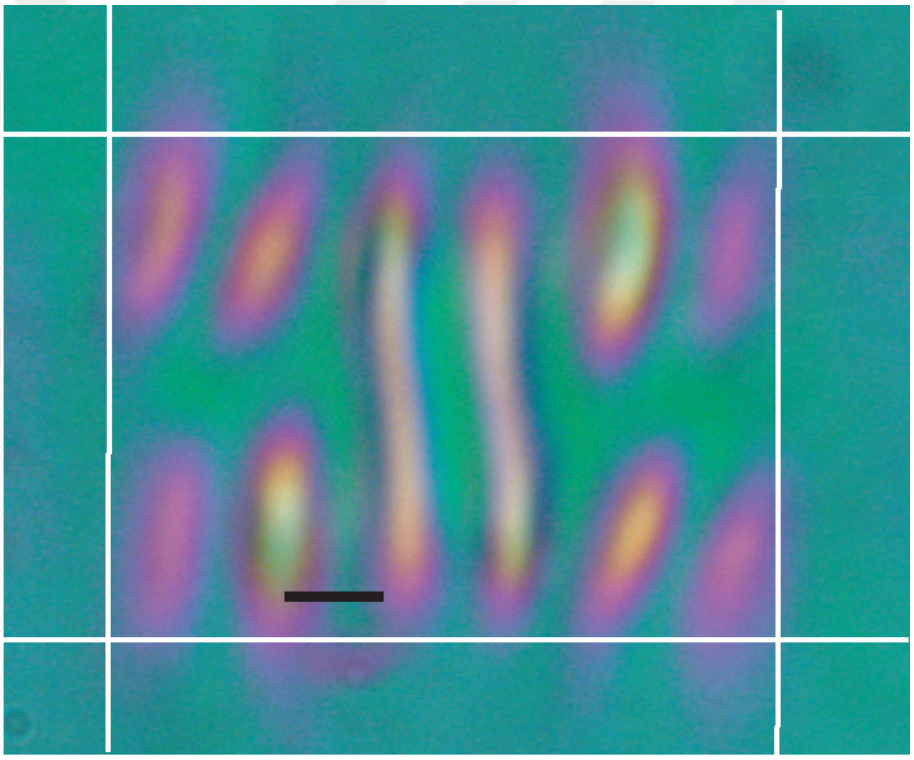

Figure 3.12: Periodic motion of the end rolls observed in an aspect ratio 2 : 2 : 1. The black solid line indicates $5\mu m$ the white lines give the borders of the electrodes. The picture was taken at voltage and frequency values $30.00V_{rms}$ and $32.10kHz$ respectively, with 80X objective and N.A. number of 0.75.

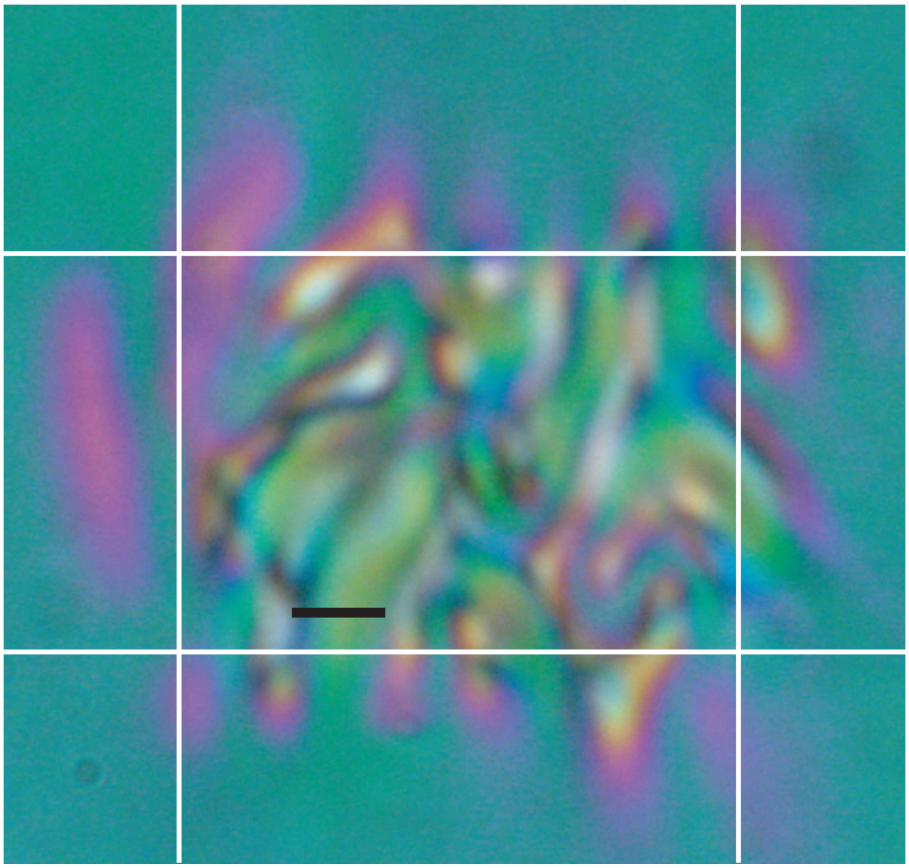

Figure 3.13: Disordered state in an aspect ratio 2 : 2 : 1. The black solid line indicates $5\mu m$ and the white lines show the borders of the electrodes. The picture was taken at voltage and frequency values $37.50V_{rms}$ and $32.10kHz$ respectively, with 80X objective and N.A. number of 0.75.

3.4 Conclusions

In order to carry out a study of the priority exchange between neighbouring states in EHC as well as the competition between EHC and FT, a small aspect ratio system was selected. The main motivation for this was to gain maximum control over the active area by minimising the practical difficulties that arise with the increasing size of LC cells. Hence, the multiplicity of flow states was reduced.

The theoretical predictions relating to the primary roll numbers as a function of aspect ratio in EHC systems was confirmed experimentally by using a specifically constructed LC cell which was designed to include thirty-six different aspect ratios. The relation between the roll numbers and the aspect ratios were in agreement with the theoretical prediction [45] that the convection rolls in EHC are tall and thin in shape. Taking the previous theoretical and experimental studies into consideration, the aspect ratio chosen to conduct the experiments was $2:2:1$. These observations, thus, formed the basis of our studies regarding the priority exchange of different flows. In the next Chapter, the first of these studies, the priority exchange of 4 and 6-roll states in EHC will be presented.

Chapter 4

Priority Exchange of Four and Six-Roll States

The discussion presented in this chapter is concerned with the priority exchange of steady cellular patterns of EHC observed in the liquid crystal flow as the control parameters were varied.

The general topic of pattern competition has been of great interest and importance for hydrodynamic stability theory [80]. For the well known Taylor-Couette system, where a fluid is confined between two concentric cylinders and a flow is set with the rotation of one of them, Benjamin[50] suggested a specific sequence of bifurcations to allow the exchange of stability between two neighbouring states in the flow. The mechanism he proposed was confirmed experimentally by Benjamin [50, 51] and Mullin [52, 53]. Moreover, the numerical calculations by Cliffe [54], Bolstad and Keller [55], Furukawa et al. [56] all agree with the experimental observations. The ideas also received further application by Tavener et al [57] to a connected system of Euler struts under compression and Nandarkumar et al [58, 59] to flows in horizontal and curved ducts.

In EHC, the same bifurcation sequence arises when two nearby states with different number of rolls exchange stability depending on the values of the control

parameter. In other words, the number of rolls in EHC are different for two neighbouring regions of the parameter space. Binks [49] showed that the mechanism proposed by Benjamin is in agreement with the exchange of 6 and 8-roll states of EHC formed in nematic BDH-17886. Here, we report new results regarding the exchange between 4 and 6-roll states for the nematic TX2A which form the basis for an investigation into where the additional effects of material properties on control parameter produce interesting novel outcomes.

In section 4.1, prior to explaining Benjamin's theory on how two states exchange stability, the concept of neighbouring states on the parameter space and the role of secondary bifurcations are considered. Benjamin's theory is then introduced in section 4.2. Following these, the experimental method is detailed and the results presented. In section 4.5 the results are discussed and compared to those of Binks' and Mullin's. Finally, conclusions are given in section 4.6.

4.1 Neigbouring states

In a model nonlinear system which is controlled by two parameters A and B, symmetry breaking of the trivial state will give rise to a pair of new states, N_1 and N_2, as the control parameter, A, is varied and B is held fixed. At other fixed values of B a separate bifurcation can occur where other states K_1 and K_2 can arise above a critical value of A. The associated type of bifurcation in both cases, namely the pitchfork bifurcation, is discussed in greater detail in Appendix A. An illustration of the paths of such bifurcations is given in figure 4.1(i) where the parameter space is spanned by A and B. The two parabolas in the figure, called the neutral stability curves, indicate the loci of bifurcations to N and K states.

Varying A, in the direction given by the dotted arrows in the figure 4.1(i) at various fixed values of B will give rise to distinctly different bifurcation sequences, depicted in figures 4.1(ii-iv), for each of the three different values of B indicated. In figures 4.1(ii-iv) solid lines indicate stable branches, dashed lines represent unstable ones and the evolution of the states are given on the z-axis.

Specifically in the case of $B = p$, varying A will result in the bifurcation set given in figure 4.1(ii) where the stable branches of N develop from the trivial state. A further pitchfork bifurcation to a pair of K solutions can then arise from the trivial branch with further increase in A. At the second bifurcation point the trivial state is unstable and hence the resulting solution branches of the pitchfork will also be unstable. As reviewed and shown in [81], secondary bifurcations will arise to restabilise these secondary states, which are essential features to facilitate the smooth exchange of priority between the states as discussed below.

When A is varied while B is held fixed at r, the stable states that arise from the symmetry breaking of the trivial state are K_1 and K_2 as shown in figure 4.1(iii). Now the state N bifurcates from the trivial when A is increased further and is hence initially unstable. As before, secondary bifurcations restabilise the N

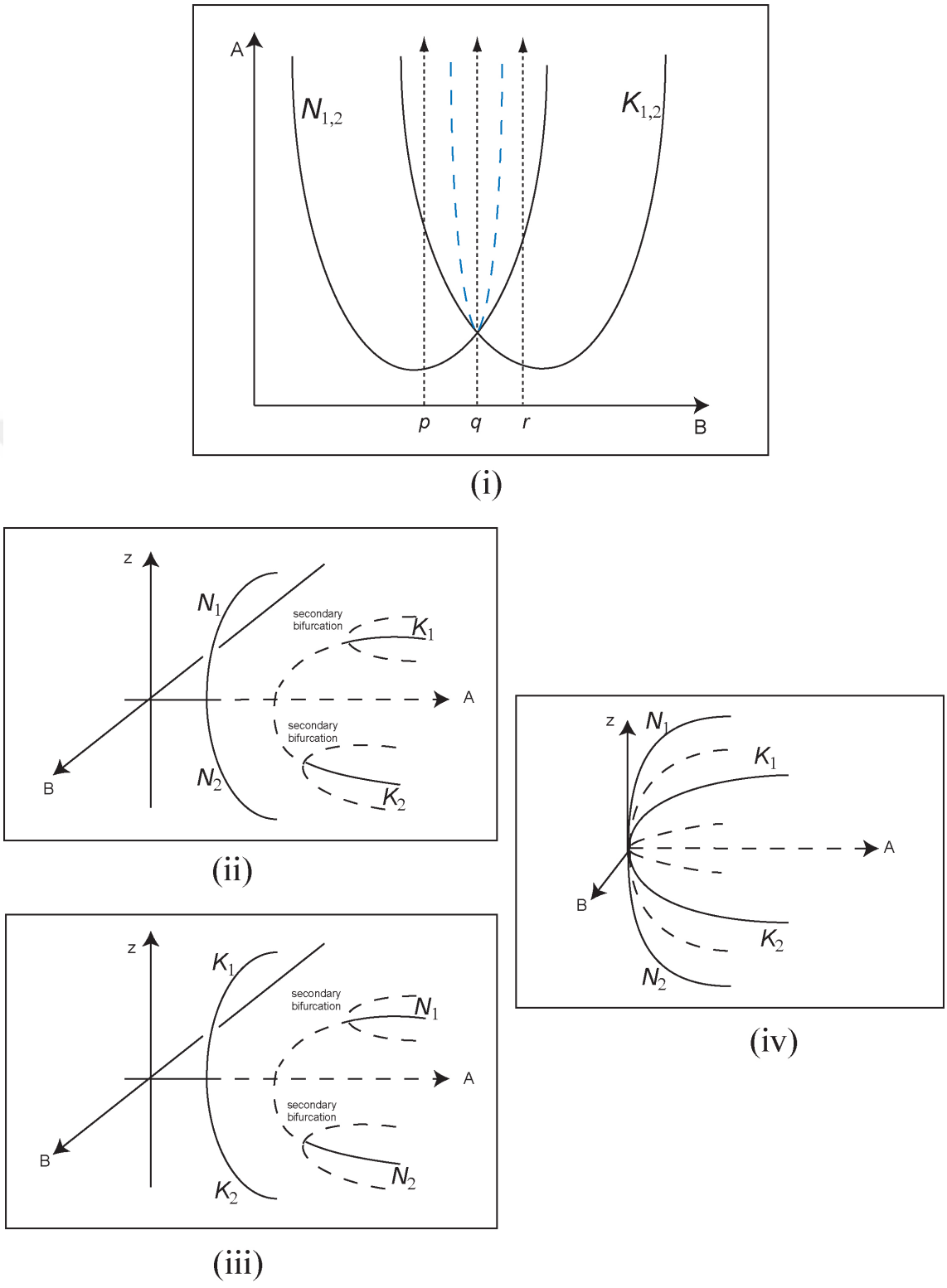

Figure 4.1: Loci of bifurcations are shown in part (i). The effect of varying A for $B = p$, $B = r$ and $B = q$ are given in parts (ii), (iii) and (iv) respectively.

branches.

A special case arises when B equals q which is the point where the two neutral curves intersect. In order to enable a smooth transition between N and K branches, secondary bifurcations indicated as blue dashed lines in figure 4.1(i) and shown in figures 4.1(ii),(iii) are necessary [81]. As the two control parameters are varied sequentially the effect of varying B is to slide the secondary states towards each other. Consequently, all branches will meet at $B = q$ as illustrated in figure 4.1(iv). Thus, states with different number of rolls can approach each other and moreover exchange priority in the parameter space when secondary bifurcations are present. Otherwise, in the absence of secondary bifurcations the exchange of stability would require an entire branch(for instance an N state) to become unstable at a critical value and the other state (K state) to gain stability, which is a highly implausible scenario. Bauer et al. gives a detailed discussion of this argument in [81].

However, in physical systems imperfections that will disconnect the branches must be taken into account. In figure 4.2 the bifurcation diagrams of the ideal case in figures 4.1(ii,iii), shown as black lines, are combined with those which include the effect of experimental imperfections, plotted as blue lines. As before, the solid lines are the stable branches and the unstable ones are plotted as the dashed/dotted lines.

In addition to experimental imperfections, the finite size of physical systems can have an effect on the branches. The symmetry of models of Taylor-Couette and EHC is one of translation and since this cannot be realised easily in an experiment, the bifurcation is effectively destroyed. In figure 4.3 the red frame encloses the branches with an opposite sense of symmetry to the ones outside the frame. Since the enclosed branches can be largely separated from the rest, as in the case of Taylor-Couette flows [82] and EHC [8, 45], they will be omitted here

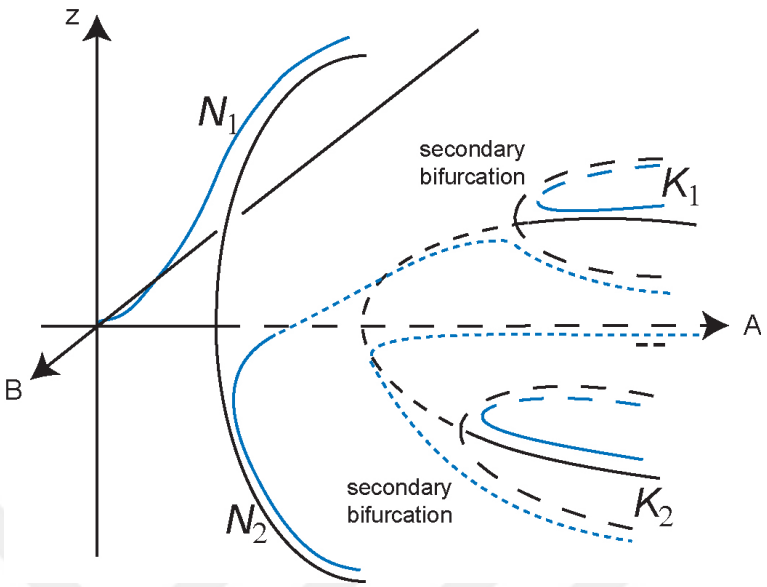

Figure 4.2: Bifurcation diagram including imperfections are shown in blue whereas the black branches indicate the perfect case.

onwards. Hence, in a system with two control parameters, states with different patterns can approach each other in the parameter space, as shown in figure 4.4, and are experimentally observable.

The branch that evolves smoothly in figure 4.4 is referred to as the *primary state* whereas the disconnected branch is called the *secondary state*. In any practical case the trivial state of the perfect system is always a combination of the primary and secondary states. Therefore, the initial state, from which the primary branch evolves smoothly, will be referred to as the *mixed state* henceforward. As a consequence of the smooth evolution of the primary state a well defined bifurcation point will no longer exist. Experimentally, when the system is stable on the secondary state and A is varied towards the mixed state, the system will jump to the primary state instantly at the *limit point* in this representation. The exploitation of limit points as well defined points will be explained in section 4.4.

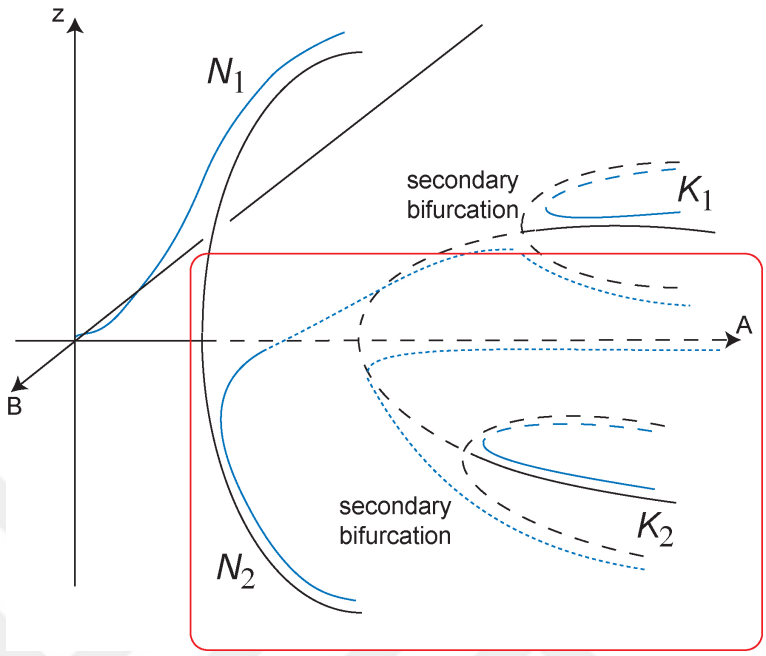

Figure 4.3: Branches framed in the red box possess a counter sense of symmetry to the ones outside the frame. Due to large separation of the enclosed branches they are not observed in EHC and will be omitted.

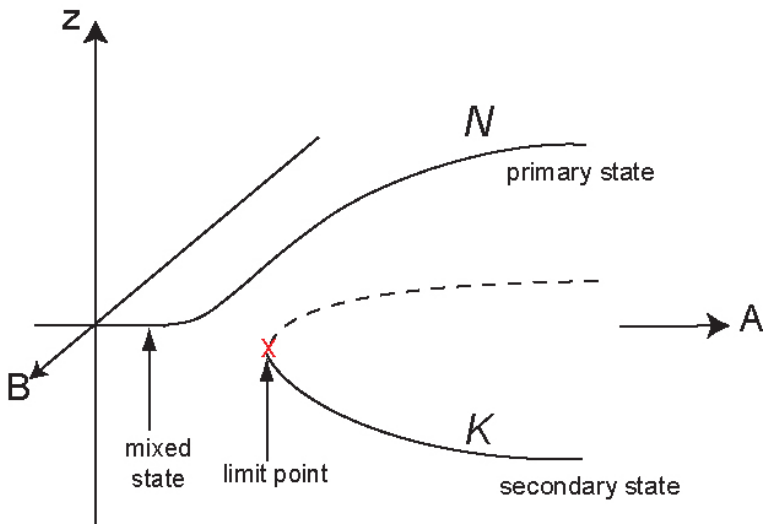

Figure 4.4: The neighbouring states N and K. The primary state N evolves smoothly while the nearby secondary state K stays disconnected.

4.2 Benjamin's Theory

The interaction of a smoothly evolving state with a nearby disconnected branch in a *single mode* system generically involves an unfolding of a transcritical bifurcation. In the presence of perfect symmetry the interaction occurs via a pitchfork bifurcation [83]. A more detailed discussion of the unfolding of pitchfork bifurcation for a single mode system is given in Appendix A.

In [50] Benjamin applies the arguments of unfoldings given above to fluids, specifically to Taylor-Couette flows and predicts a series of bifurcations for the exchange mechanism between two stationary states. The prediction is concerned with the variation of two control parameters so that the system can be regarded as having *two modes*. One of the control parameters is kept fixed at chosen values and selects the primary state while the other control parameter is varied.

Nevertheless, the local bifurcation structure for a two-mode system is qualitatively the same as for the universal unfolding of a pitchfork given in equation A.3, and Benjamin [50] uses the following equation as his model:

$$\frac{dx}{dt} = x^3 - \alpha x^2 - Bx + A \tag{4.1}$$

where A and B are the control parameters for a system with two neighbouring states N and K that exchange priority in accordance with B. The parameter α is set to one here and its role is discussed in detail in [50]. The limit points for this equation as a function of A and B are given in figure 4.5(0) and the series of bifurcations predicted by Benjamin's theory are illustrated in figures 4.5(i-iv) where the evolution of the states in relation to B is given on the z-axis, as A is kept constant at fixed values.

In figure 4.5(0) the set of limit points are divided into three regions which are denoted by region I below the lower dashed line, region II between the dashed lines and region III above the upper dashed line. A typical change in parameter B

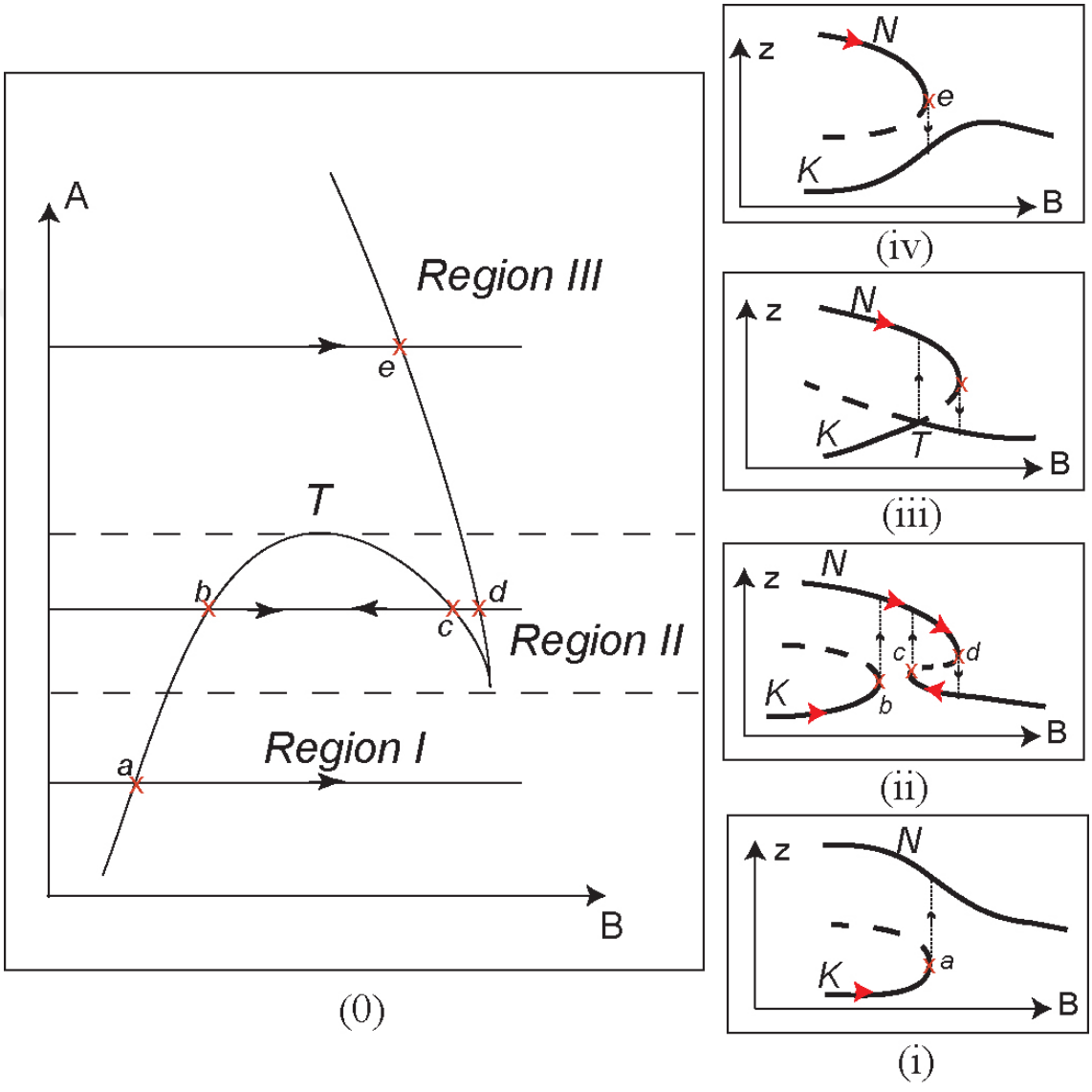

Figure 4.5: The limit points of equation 4.1 and a series of bifurcations predicted by Benjamin's theory for the stability exchange of two neighbouring states.

at fixed A is indicated by the arrow shown in region I. The associated bifurcation diagram is labelled 4.5(i). When the system is in the secondary branch, i.e. in the K state and the control parameter B is varied in the direction shown by the arrow, the secondary branch loses stability at the limit point a followed by a sudden jump to the primary branch N. Hence, the A and B values where this change takes place give the coordinates of the limit point a in figure 4.5(0).

As clearly seen in figure 4.5(i), starting from the mixed state and varying B in the direction opposite to that shown in figure 4.5(0) will result with the smooth evolution of N and no sudden change in the states will be observed. Therefore, in order to find limit points it is necessary to begin the parameter scans from the secondary states. Furthermore, once the system jumps to N at the limit point a, it will stay on the primary branch even when B is varied in the direction opposite to that shown in figure 4.5(0). In other words, there are no limit points on the primary branch in region I that depends on the history of the scans and thus the region is not hysteretic.

In region II of figure 4.5(0), similarly to the previous case, the arrows represent varying B at a fixed value of A and the related bifurcation diagram is given in 4.5(ii). However, here the primary state of figure 4.5(i) has become hysteretic and hence there are two more limit points compared to the previous case due to the dependency of the limit points on the history of the path followed on the parameter space. Changing B in the same direction as indicated by the arrow in region I gives the limit point b where the state K loses stability and jumps to state N. Once the system is in the state N following the arrows shown in figure 4.5(ii) brings the system to another limit point, d, where state N becomes unstable. When the direction of changing B is reversed, as marked by arrows in both figures 4.5(0) and 4.5(ii), the system jumps back to state N at a different value than d and thus a hysteresis loop is created. This third limit point is called

c in both figures. An alternative path to take in the parameter space can be going under and around the cusp. In this case, as A is decreased to go below the cusp, the system will approach the *mixed state*, introduced in figure 4.4. As B is increased to go around the cusp, state K can become the primary state due to non-uniqueness of the mixed state. Hence, through this path states can exchange priority without undergoing a bifurcation.

At point T in figure 4.5(0) and the corresponding bifurcation diagram, 4.5(iii), hysteresis reaches its maximum value and with the merging of limit points b and c a transcritical bifurcation takes place. Thus, the hysteretic region ends for values of A above point T.

The bifurcation diagram given in figure 4.5(iv) for region III and the existence of a single limit point is similar to the case of figure 4.5 (i) with the major difference being the primary state in region I is a secondary state in region III. Hence, starting from state N and varying B in the direction indicated by arrows in both figure 4.5(0) and (iv) will end with a rapid collapse to a K state at point e.

In summary, the series of bifurcations explained in figures 4.5(i-iv) contain a mechanism for the stability exchange of a smoothly evolved primary branch and a disconnected secondary state in a system with two control parameters. This mechanism constitutes Benjamin's Theory.

In practice, the competition between two states have been examined in various physical systems, such as Taylor-Couette, a connected system of Euler struts under compression and horizonal and curved ducts, by both experimental and numerical studies. In the next section the interesting results of the experiment done in EHC are presented.

4.3 Experimental Method

In accordance with the theoretical and physical systems considered above, the two experimental control parameters were the voltage and frequency of the AC field applied to the nematic material. As the control parameters were varied sequentially, the resulting states, which correspond to N and K in the previous sections, were 4-roll and 6-roll states of convection. Frequency was the control parameter used to locate the primary state. Therefore, after reaching the neighbouring state the voltage needed to be kept constant and the frequency was then varied in order to find the limit points and hence trace out the bifurcation set.

During data collection, the states were identified visually since they were easily distinguishable through the microscope. As also mentioned in Chapter 2, data was taken with steps of $0.01kHz$ in frequency and $0.03V_{rms}$ in voltage. The waiting time between successive increments/decrements of the control parameters was set as 10 seconds for the following reasons: The response time of nematics to electric fields is mostly given as a few hundred milliseconds[1]. Nevertheless, preliminary measurements showed that the collapses/jumps from one state to another were completed over $3-4$ seconds on average. Hence, 10 seconds of waiting time was large enough to enable reproducible results.

The measurements were meticulously carried out with special attention paid to the drift of impurity ions and the non-dimensionalizing of the parameters as explained in Chapter 2. The frequency range over which the bifurcation set was measured corresponded to 7.69% of the available range. In order to measure the drift in frequency, the reference point was taken at the lowest frequency value at which the 6-roll state was observed. Consequently, the drift value found for the frequency was 0.20% per hour. As for the voltage, the reference point was chosen to be the value at which the 6-roll state collapses to the 4-roll state, at frequency $30.2kHz$. Thus, 0.85% shift per hour was noted for the amplitude.

Accumulation of the preliminary data over several days showed that the drift in voltage was noticeable whereas the drift in frequency was small compared to the frequency range of the experiment. Therefore, the frequency was kept at its absolute value whilst a reference value for the voltage was determined daily before the measurements began and was checked throughout the experiment every 30 minutes. After finding each limit point, the voltage was converted to its relative value in the way explained in Chapter 2 by taking the ratio of the absolute amplitude value and the reference value.

4.4 Results

The limit points found after careful scans are presented in figure 4.6 together with the associated bifurcation diagrams presented in subfigures (i)-(iv). As explained in section 4.2 the paths taken during the scans are of great importance and they will be described in further detail below along with the figure 4.6.

In figure 4.6 the circles and squares represent the upper and lower limit points of the 4-roll states respectively and the triangles indicate the limit points of the 6-roll state. For simplicity, the parameter space in figure 4.6 can be considered to comprise three regions as illustrated schematically in figure 4.7. The grey region is where the 4-roll state of EHC is the primary state and in the blue region it is the secondary state. More specifically, for a constant frequency value in the grey area increasing the relative amplitude results in 4 rolls. The same procedure for a higher frequency value in the blue region, i.e. above $\sim 31.7kHz$, ends in 6-roll state. The shaded region in between the grey and blue areas corresponds to a narrow range of frequencies of $\sim 0.6\%$ of the total, over which the exchange of stability takes place. The arrows in the figure, which will be detailed shortly, represent the paths taken on the parameter space.

The scans to determine the limit points of the 6-roll state were always started

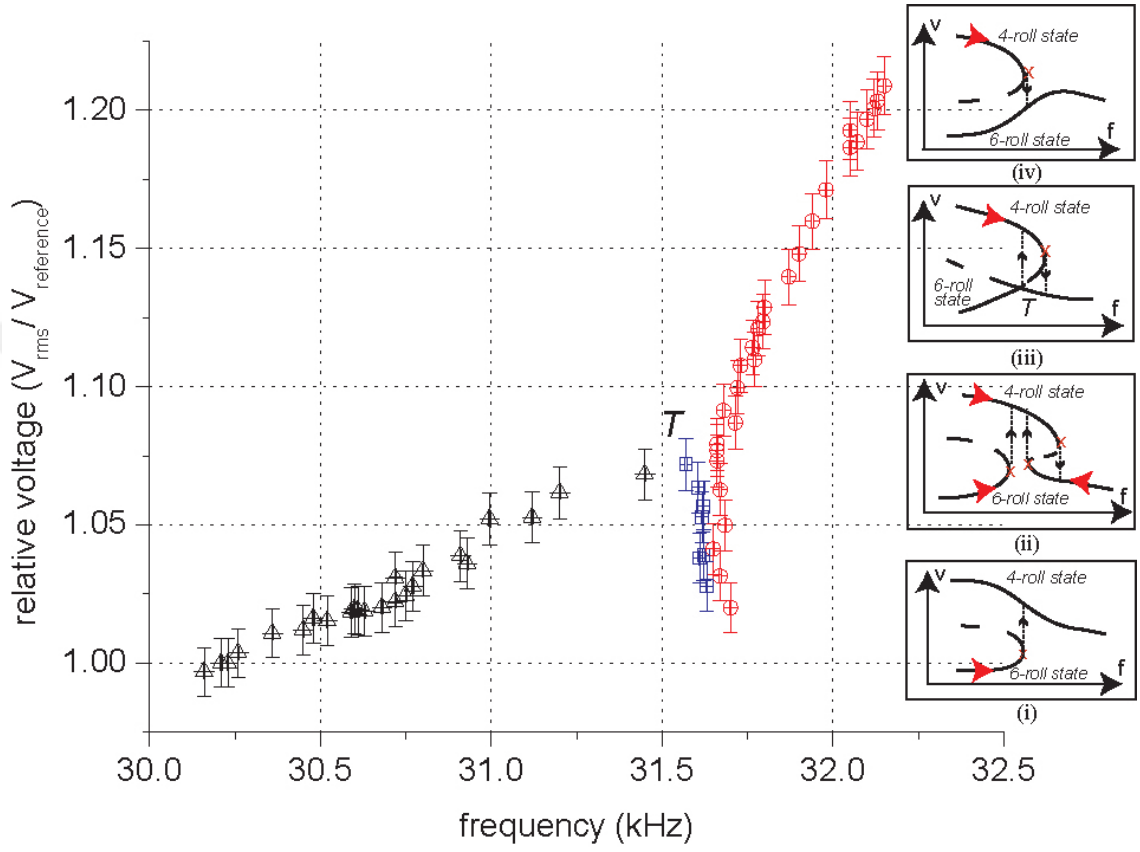

Figure 4.6: The set of limit points found for the stability exchange between the primary (4- and 6-rolls) states in EHC of nematic TX2A. The red circles and blue squares indicate the upper and lower limit points of the 4-roll state whereas the black triangles are the limit points of the 6-roll state. The associated bifurcation diagrams for each set of limit points are given in subfigures (i)-(iv). The arrows have the same meaning as in figure 4.5.

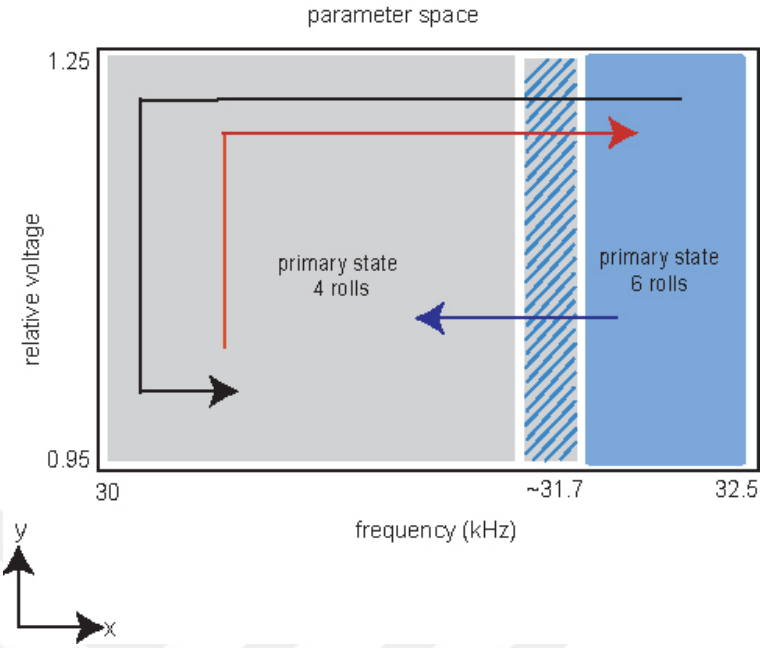

Figure 4.7: The section of the parameter space where the experiment was done and the paths taken on the parameter space.

from values $(1.23, 32.5kHz)$. Once the 6-roll state was reached, the frequency was decreased keeping the relative amplitude value constant as represented by the black arrow in figure 4.7. The variation of the control parameters was carried out systematically with the step sizes indicated above. When the frequency was varied such that the operating point was moved to values below $\sim 31.5kHz$ in figure 4.6, i.e. into the region indicated by the grey area in figure 4.7, the system continued to exhibit 6-rolls. However, the 6-rolls state was the secondary state in this region. Hence, the condition of having the system in a secondary state, which is required to find limit points was established. The search for the limit points continued systematically varying one control parameter at a time until a sudden change was observed in the number of the rolls when viewed through the microscope. The black triangles shown in figure 4.6 are the limit points at which 6-rolls jumped to 4-rolls state instantly. The associated bifurcation diagram is given in figure 4.6(i).

The red circles in figure 4.6 denote the loci of limit points where the 4-roll state collapsed to a 6-roll state. The path followed in the parameter space in order to find these limit points is represented by the red arrow in figure 4.7. Applying an AC field to the LC cell at $30.5kHz$ resulted in a smooth emergence of 4-roll state. Having established a well defined 4-roll state, the frequency was then increased whilst the voltage was kept constant at a desired value. Once the frequency was greater than $\sim 31.7kHz$ the system was in the region where 4-rolls is a neighbouring state. As the frequency was increased further the 4-roll state became unstable and collapsed catastrophically to a 6-roll state at the limit points shown in figure 4.6. The associated bifurcation diagram in this case is figure 4.6(iv). Data above the relative voltage of 1.22 were omitted since above this value time dependence sets in and we are concerned with steady state behaviour.

For the two sets of data described thus far, reversing the direction of the frequency after reaching the primary state did not result in a sudden change to another state. Once the system stabilised itself in the primary state, increasing or decreasing the frequency for a given relative amplitude showed smooth extinction of the primary state and re-emergence of it respectively. However, for relative amplitude values between 1.02 and 1.07 observations confirmed the main prediction of Benjamin's theory, in that, for this range of values hysteresis of the 4-roll state was found. Figures 4.6(ii) and (iii) correspond to this hysteretic region of the parameter space. Following the blue arrow shown in figure 4.7, i.e. reversing the direction of frequency increments, after the collapse of 4-roll to 6-roll state, 4-rolls formed again at the points marked as blue squares in figure 4.6. Therefore, two distinct set of limit points depending on the history of the measurements were found for the 4-roll state. It should be noted that point T in figure 4.6(iii) corresponds to the point where the lower limit points of 4-roll state meet with

the limit points of 6-roll state and is also marked in the bifurcation set.

4.5 Discussion

The limit points presented in figure 4.6, which were collected over a period of 80 days, fall on a smooth curve and are therefore testament to the reproducibility of the experiment. The general form of figure 4.6, including a cusp shaped region, agrees well with Benjamin's predictions given in figure 4.5(0).

At the apex of the cusp, near the relative voltage value of 1.02 and frequency $31.7kHz$, a narrow hysteretic region begins. The quality of the results in this section of figure 4.6 reveal the requirement of a high level of experimental control to uncover the delicate but important features of the cusp. At relative voltage 1.07 the lower limit points of 4-roll state merge with the 6-roll limit points and thus the hysteretic region where the priority exchange of 4 and 6-roll states takes place ends with a transcritical bifurcation. As stated in section 4.2 in a two-mode system, such as EHC, the neighbouring patterns are expected to interact via a transcritical bifurcation according to Benjamin's theory. Indeed, the unfolding in figure 4.6 is that of a transcritical bifurcation in complete agreement with the theory.

The error bars shown in figure 4.6 were determined by taking the accuracy of the electrical devices and the drift values into consideration. The accuracy of the electrical equipment, given in chapter 2 was added to the drift values of the voltage and frequency, which was the dominant source of errors.

In comparison with related experimental studies the results in figure 4.6 are in agreement with those reported by Binks [49], who studied the exchange mechanism between the 6-roll and 8-roll states of EHC [1]. He also found [49] that the exchange of stability occurs via hysteresis and a transcritical bifurcation but the

[1] created in nematic BDH-17886

6-roll state is the primary pattern to form in that case since the aspect ratio of the LC cell was is 4:4:1.

In [52] Mullin presents the set of limit points found for different states, i.e. different number of rolls, in Taylor-Couette system where 4, 6, 8, 10 and 12-rolls states successively take priority as the primary flow when the aspect ratio is varied. The general shape of the limit-points-curve for the two initial flow patterns (4/6 rolls states) is very similar to the ones presented here and by Binks. Nonetheless, as the exchange mechanism between further states is investigated, it is seen that the shape of the limit-points-curve gets more complicated. Therefore, comparing the three experimental cases it can be said that the mechanism proposed by Benjamin for the exchange of stability is in general valid. Nonetheless, the loci of limit points may vary with further details of a system. Considering the physical differences of the EHC and Taylor-Couette systems (EHC system involving visco-elastic fluids and Taylor-Couette system Newtonian fluids) it can be concluded that Benjamin's theory is robust.

One difference between the results regarding the limit-point-curves of Taylor-Couette flows and EHC is the direction of the cusp. The cusp points downwards in both of the EHC experiments whereas it is upwards in the 4/6-rolls states of Taylor-Couette system. As mentioned above, the limit points for the exchange mechanism between further states become more complicated in the case of Taylor-Couette system and in fact the direction of the cusp changes for the 8/10-rolls states [52]. Hence, it is not possible to make a generalisation for the direction of the cusp.

4.6 Conclusions

An experiment was conducted in order to investigate the exchange mechanism between the initial neighbouring states of EHC set in a LC cell with an aspect

ratio 2 : 2 : 1. Determined by the aspect ratio, the initial flow pattern of EHC was a 4-roll state with a nearby 6-roll state, in accordance with [45]. The small aspect ratio cell used in the experiment has enabled the neighbouring patterns to be clearly distinguishable from the large number of interactions between various states observed commonly in large aspect ratio systems. The limit points of the disconnected branches were thus found by taking various paths along the parameter space.

The results were reproducible and the accuracy of the experiment made it possible to resolve the limit points in a narrow range which revealed hysteresis and consequently unfolding of a transcritical bifurcation as predicted by Benjamin's theory. Comparing the results presented here with those of the experiments done in a Taylor-Couette system and in EHC with aspect ratio 4:4:1 it can be concluded that Benjamin's Theory applies to a general class of nonlinear systems since its predictions are proven for both Newtonian and visco-elastic fluids and it is therefore robust.

Next, the investigation of pattern competition will be taken a step further to a more interesting case. The mechanism of exchange between EHC and Freedericksz transition (FT) will be considered in Chapter 5, where the material properties have greater significance in the stability exchange.

Chapter 5

Priority Exchange of Freedericksz Transition and Electroconvection

In the previous chapter, a study of the exchange of priority between flow patterns with different numbers of rolls observed within EHC was given. In the present experiment, the values of the control parameters were chosen such that the primary EHC state contained four rolls as before. Instead, in the work presented here, the competing states arose from two qualitatively different effects which are observed when an AC field is applied to TX2A: These are EHC at frequencies above the crossover frequency and Freedericksz Transition (FT) for lower frequencies.

As detailed in Chapter 1, the conditions under which EHC or FT exist depends on the sign of the dielectric anisotropy. For the dual frequency nematic LC used here, the dielectric anisotropy is a function of the frequency of the AC field applied to the LC material. As a consequence, changing the frequency in very small steps in an experiment permits smooth evolution between these qualitatively different states. Hence, the exchange mechanism to be discussed here reveals a more detailed structure than the one given in Chapter 4. An analogous case was studied experimentally and numerically by Cliffe and Mullin [85] in a Taylor-Couette system, where asymmetric boundary driven motion produced a

qualitatively similar bifurcation set. The details of this experiment are given in section 5.3.

The experimental method is outlined in section 5.1. Since the majority of the method is the same as that used to produce the results in Chapter 4, only new aspects are described in detail. The results are presented in section 5.2 and discussed in section 5.3, which is followed by conclusions in section 5.4.

5.1 Experimental Method

The experimental method was very similar to the one discussed in the previous chapter. Specifically, the control parameters, voltage and frequency of the AC field applied to the LC cell, were varied systematically and sequentially in order to place the system in a secondary state. The parameter space was then scanned to find limit points at which a sudden change of stability took place between the neighbouring states. As before, visual observations were made and critical parameter values were obtained where there was a definite change in the flow field. The size of the increments/decrements of the control parameters were as indicated in Chapter 2 and the waiting time between successive changes was 10 seconds for the same reasons explained in the previous chapter.

The experiment was carried out in the frequency range $26.00 - 27.50kHz$, which covers an interval of 5.45% of the available parameter space. The preliminary observations showed that below $(26.56 \pm 0.02)kHz$ FT was primarily observed and for frequencies above $(26.70 \pm 0.02)kHz$ the smoothly evolved pattern was the 4-roll state of EHC. Hence, the region where FT and EHC coexisted (analogous to the shaded area in figure 4.7) was 0.50% of the available frequency range of the experiment, i.e. approximately 17% smaller than the region of coexistence of the 4 and 6-roll states in EHC. The effect of drift was even more important for the EHC results and this required the frequency to be non-dimensionalised in addition to voltage. A well defined frequency (specified to within 0.07%), which separates the primary FT state from the mixed region was taken as the reference frequency. As for the voltage, the value at which FT collapsed to EHC at the relative frequency value of 1.0100 ± 0.0018 was set to be the reference point. The drift found in the reference frequency and voltage were 0.18% and 0.85% per hour respectively. Given the delicate nature of the experiment the reference values were checked throughout the measurement period every 15 minutes.

5.2 Results

The bifurcation set constructed from critical points taken within the range specified above is presented in figure 5.1. The data was collected with great care over a period of 180 days. It reveals a detailed structure, including two evident cusps. Thus, the plot is a manifestation of the delicate yet reproducible nature of the experiment. The accuracy of the points, which are indicated by the error bars, were calculated in the same way as explained in section 4.5. The dashed horizontal lines on the plot are numbered in correspondence with the bifurcation diagrams in figure 5.2 and discussed in section 5.3.

Analogously to figure 4.7, figure 5.1 can be considered to consist of three regions. Within the first region, which included relative frequency values below 1.0025 ± 0.0018, FT appeared as the primary state when the voltage was increased smoothly. The second region was between this value and relative frequency 1.0075 ± 0.0018 where FT and EHC coexisted as stable observable states. Above the relative frequency 1.0075 ± 0.0018, which is the lower boundary of the third region, EHC was the primary state.

The first set of limit points we will consider in figure 5.1, correspond to loci of critical points where FT lost stability to EHC with increasing frequency and are shown as the open circles between points B and E. The method for obtaining these data was to first set the relative frequency to 0.9700 ± 0.0018. A well defined FT state was then established by increasing the voltage systematically to a preselected value and the frequency was then increased in small specified steps until a sudden change from FT state to 4-roll EHC state was observed. The voltage and frequency values, at which this change occured, were converted to their relative values and marked on the plot shown in figure 5.1.

Another set of limit points was found at which EHC lost stability with decreasing frequency. They are shown as open triangles in figure 5.1 and the locus

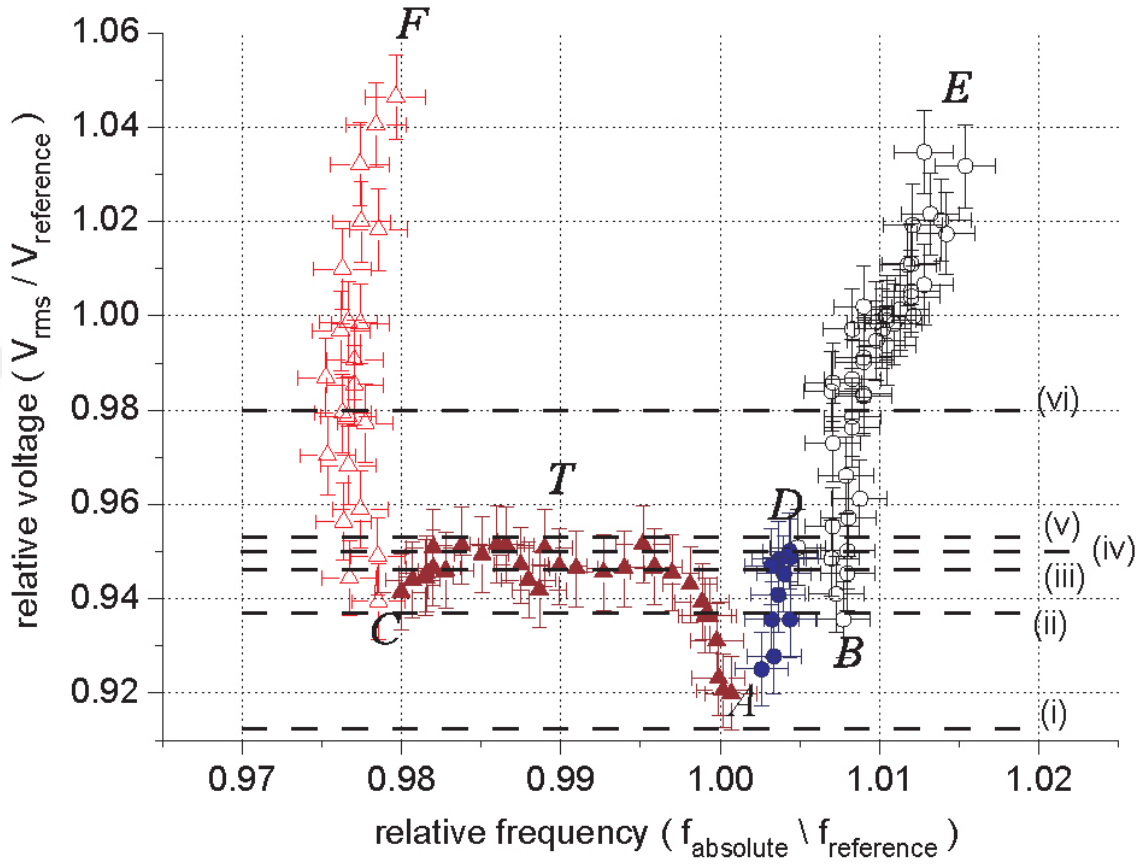

Figure 5.1: The set of limit points found for the stability exchange between the EHC and FT. The limit points between B and E indicate the loci at which FT lost stability to EHC. The rest of the data denote limit points where EHC jumped/collapsed suddenly to FT. However, the limit points between A and D and C and A were found by taking a different route on the parameter space than the one followed to find the open triangles. The plot is divided into six sections by dashed lines where each line corresponds to a bifurcation diagram in figure 5.2 and is numbered accordingly.

is labelled FC. In determining these critical points each measurement was initiated at the equivalent value of relative frequency 1.0200 ± 0.0018 where EHC was the primary state. The frequency was then decreased systematically for various voltage values until the limit points indicated as open triangles between points F and C were crossed and FT became the preferred state.

As a consequence of the measurements described thus far, a gap in the parameter space between curves FC and EB is clear. Investigation of this intervening parameter range required an alternative route to probe the states and their limit points. Accordingly, the following path was taken: scans were initiated at the corresponding frequency and voltage values of 1.0200 ± 0.0018. By decreasing the frequency with the same step size as in the previous cases, the frequency was reduced to a preselected value corresponding to a point in parameter space within the gap. Thus, the system was placed in a stable secondary state. Then, the voltage was decreased until EHC jumped catastrophically to FT. The critical values at which these stability exchanges occurred are shown as filled triangles between points C and A and as filled circles between A and D[1] in figure 5.1. By using this procedure, two cusps, with apexes at points C and A were uncovered. Importantly, when the voltage was decreased keeping the frequency fixed at values within the cusp regions the EHC state remained stable. FT became the preferred state when the limit points on either side of the cusps were crossed, i.e. EHC was stable only inside the cusp shaped region. This provides evidence for the presence of dual cusps as discussed in the next section. In addition, a possible third cusp bordered by points D, B and E is considered in section 5.3 where the bifurcation set in figure 5.1 is examined further.

[1]The reason for marking the filled circles and triangles separately even though they were found by taking the same path in the parameter space is clarified in the next section.

5.3 Discussion

The sequence of bifurcations shown in figure 5.2 is proposed as the exchange mechanism for the bifurcation set given in figure 5.1. The plot in figure 5.1 is divided into six sections by dashed lines where each line corresponds to a bifurcation diagram in figure 5.2 and is numbered accordingly. For each bifurcation diagram there is a corresponding fixed voltage and the evolution of the state is given on vertical z-axis as a function of frequency.

We will discuss the results presented in figure 5.1 by starting from relative voltage values below 0.92. In this section, represented by dashed line (i) in figure 5.1, only the mixed state[2] existed and hence stability exchange from one state to another could not be distinguished. The bifurcation diagram corresponding to the observations in this region is given in subfigure (i) of figure 5.2 where EHC state is doubly unstable and the mixed state is the only one observed.

The dashed line labelled (ii) in figure 5.1 denotes the lower limit of the region between the relative voltage values $\sim 0.935 - 0.945$. As shown in the corresponding bifurcation diagram figure 5.2(ii), the continuous branch given in part (i) became folded and developed hysteresis. In this region of the parameter space FT could be identified more easily. After establishing an FT state when the frequency was increased, the pattern returned to its initial mixed state at limit points indicated as open circles as shown in the bifurcation diagram of figure 5.2(ii). The limit points of the lower state were not found within the narrow region where FT and EHC coexisted. The lower limit points would have served as the link between points D and B in figure 5.1 to form a third cusp defined by points D, B and E.

Also, the unstable secondary state in figure 5.2(ii) developed two folded regions, giving rise to two stable (EHC) states, whose limit points are indicated by

[2]A *mixed state* can present features of both FT and EHC. Also see section 4.1 for the definition of *mixed state*.

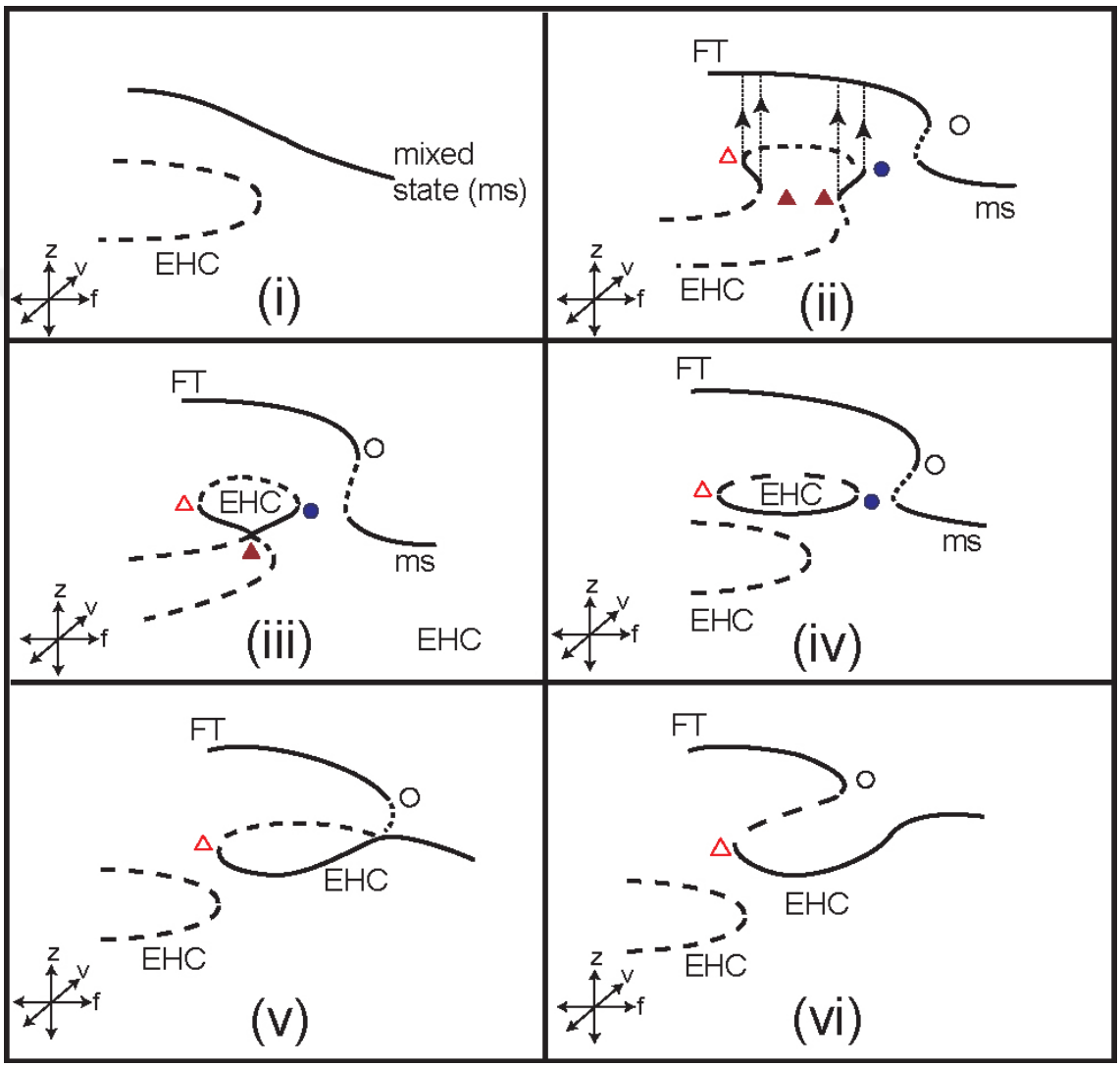

Figure 5.2: The bifurcation sequence suggested for the exchange mechanism of FT and EHC.

the same symbols both in figure 5.1 and 5.2(ii). After the system was placed in one of the two stable secondary states, as described in section 5.2, EHC jumped to FT at two separate frequency values bordered by points FC and CT (in the stable secondary state corresponding to lower frequency values) or TA and AD (in the the secondary state corresponding to higher frequencies) in figure 5.1. The crucial result in this region of the bifurcation set in figure 5.1 was that the limit points formed two cusps at points C and A.

The emergence of a stable state from an unstable branch can occur when the surface becomes folded as shown schematically in figure 5.3. The fold, shown at the top of the figure, is projected on to the parameter space spanned by voltage and frequency, as illustrated at the bottom. The upper and lower layers of the fold correspond to unstable EHC states and the shaded region is where EHC is stable. The solid lines with arrows indicate the paths taken to find the limit points which constructed the cusp on the parameter surface. Consequently, within the cusp region, EHC was stable until the limit points on the edges were reached. Such type of cusps are called *dual cusps*. Further details and a mathematical model of dual cusps can be found in [84].

The dashed line (iii) in figure 5.1 denotes the approximate location where the limit points between C and A approach each other from two dual cusps and meet near point T via a transcritical bifurcation as indicated in figure 5.2(iii). However, the precise position of the transcritical bifurcation could not be resolved in the experiment.

The limit points in the region between the relative voltage values $\sim 0.945 - 0.953$ will be considered next. In this section of figure 5.1 dashed lines (iv) and (v) are situated very close to each other. The corresponding bifurcation diagram of line (iv) in figure 5.2 displays an isola of an EHC state whose limit points are given as open triangles and filled circles. This is followed by a transcritical

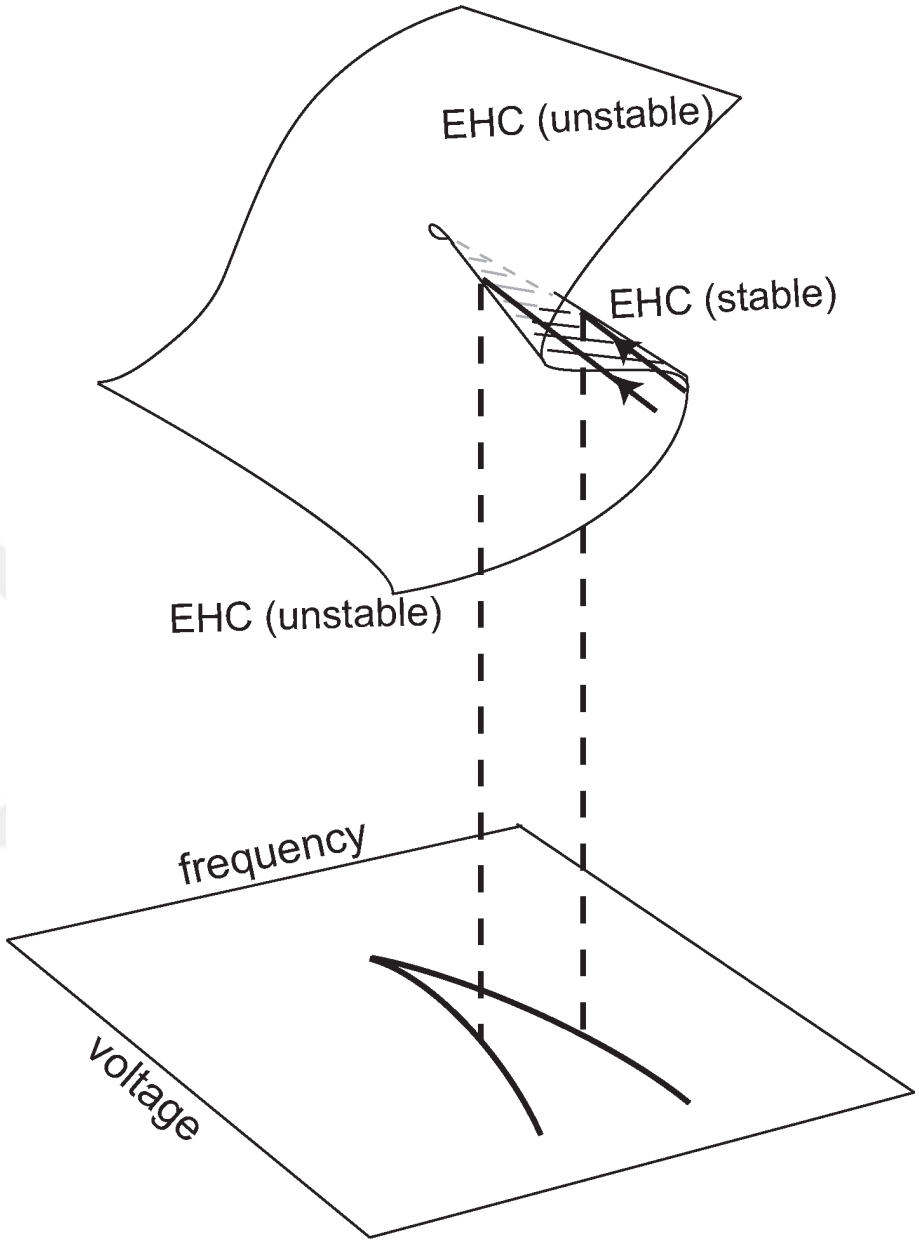

Figure 5.3: An illustration of a dual cusp. In the top figure the shaded region indicates a stable state whereas the upper and lower layers are unstable. The bottom surface demonstrates the parameter space comprised by frequency and voltage. In the experiment the limit points were determined by following the paths represented by the solid lines with arrows in the upper figure. Thus, a dual cusp is the projection of the folded surface on the parameter space.

bifurcation in figure 5.2(v) where filled circles merge with the limit points of the EHC state, which developed out of the mixed state. It is clear in figure 5.1 that at point D the distance between open and filled circles decreased to its minimum value. Therefore, although it was not possible to reveal all the fine structure of the bifurcation diagrams presented in figure 5.2(iv) and (v), the claim is that this is a self consistent bifurcation sequence and is in accord with results obtained in a Taylor-Couette flow [85] which will be discussed below .

For relative voltage values above ~ 0.953, represented by the dashed line (vi), the FT and EHC states were connected to each other via an unstable branch as shown in figure 5.2(vi). Physically, this arises because of the dependence of the dielectric anisotropy on the frequency of the applied field. Explicitly, when the system was in the EHC state, decreasing the frequency for a fixed voltage value resulted with a jump to the FT state as the open triangles were crossed. Increasing the frequency for the same voltage value afterwards, gave a sudden collapse to the EHC state when the open circles were reached.

A bifurcation sequence similar to that given in figure 5.2 was originally proposed by Cliffe and Mullin [85] for the limit points acquired from an experiment regarding the priority exchange of two neighbouring states in a Taylor-Couette system[3] with asymmetric end conditions. The results of this experimental and numerical investigation, shown in figure 5.4, exhibit an astonishing qualitative similarity with the bifurcation set presented in figure 5.1.

In figure 5.4 the symbols represent the experimental data and the solid lines are numerical predictions for the limit points where 3 and 5-roll states of Taylor-Couette system exchange stability. In this work, Cliffe and Mullin [85] study the effect of boundary conditions by allowing one end of the apparatus to rotate with the inner cylinder. For aspect ratio values greater than 4.6 the primary pattern

[3]A brief explanation of the Taylor-Couette problem was given in Chapter 1 and revisited in Chapter 4.

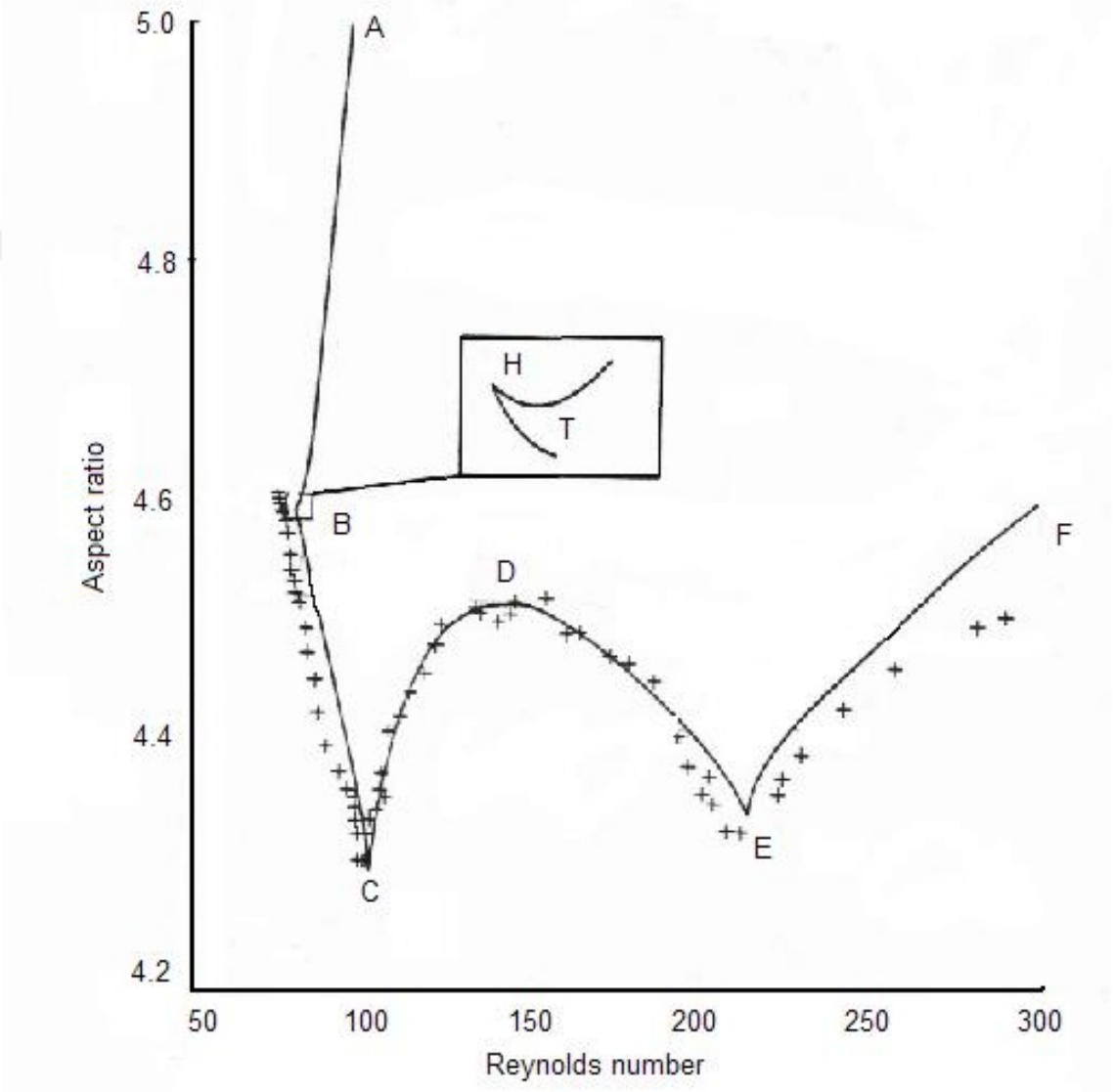

Figure 5.4: Limit points of 3 and 5-roll states in a Taylor-Couette system with asymmetric end conditions [85].

that forms has 5 rolls and for smaller values this state becomes secondary leaving priority to the state with 3 rolls.

As in the case of figure 5.1 two dual cusps are seen in figure 5.4. Within the cusps C and E, shown in the latter figure, the secondary (5-roll) state stays stable but it collapses to the 3-roll state when the Reynolds number is either increased or decreased to the limit point values given in figure 5.4. These observations are compatible with the results of the EHC-FT experiment presented in figure 5.1.

Another common point between the two set of results is the existence of another small cusp near the values where the primary state changes. For the Taylor-Couette system, this cusp is expected near the aspect ratio value of 4.6 according to numerical predictions. However, experimentally it is not realised since time dependence was observed in this region [85]. On the other hand, as already discussed, an analogous cusp is likely to exist in the bifurcation set of FT-EHC exchange between points D and B in figure 5.1.

Yet the main parallelism between the two specific experiments is the coupling of the competing states. In the Taylor-Couette experiment the size of the roll next to the rotating end depends on the Reynolds number[4]. Therefore, the space available for other rolls and hence the stability boundary of the neighbouring state also has a dependency on the Reynolds number. The analogous condition in the EHC-FT system is the dependency of both EHC and FT on the sign of the dielectric anisotropy which is a function of frequency of the AC field applied to the LC cell. Thus, increasing frequency in an EHC-FT system has a qualitatively similar effect to increasing the Reynolds number in a Taylor-Coutte experiment, which moves the border of stability for one state[5] in expense of the other.

As a final note, the striking resemblance between the results of two systems imply that the qualitative features they share play a more important role in the

[4]The size of this roll grows with increasing Reynolds number.

[5]EHC in our case and 3-roll state for the Taylor-Couette system

priority exchange mechanism than their diverse physical properties.

5.4 Conclusions

An experimental study of the priority exchange of EHC and FT has been performed. It was found that, as in the competition of 4 and 6-roll states in EHC, hysteresis and transcritical bifurcations play important roles in the exchange mechanism. Nevertheless, more intermediate steps are involved, such as the creation of an isola. These appear to arise from a parameter coupling between competing states.

An interesting qualitative similarity was noticed between the bifurcation set found for a Taylor-Couette system with asymmetric end conditions and the results presented in this chapter for the EHC-FT exchange. The coupling of neighbouring states generated in both cases (by dependence of the dielectric anisotropy on the frequency of the field applied, in our case, and by forcing from asymmetric end conditions in the Taylor-Couette experiment) enables us to propose a bifurcation sequence for the EHC-FT experiment, which is qualitatively similar to that calculated for the Taylor-Couette problem.

Chapter 6

Conclusions

The work presented in this thesis was an experimental investigation concerning the pattern selection mechanisms of flow states in a dual-frequency nematic liquid crystal. These states were generated in a planarly aligned liquid crystal cell by applying a sinusoidal electric field across the device. The arrangement of the electrodes on the liquid crystal cell was made in a unique way in order to enclose a range of small aspect ratio active areas within the same device. As a result of the finite size aspect ratios the multiplicity of states was reduced in the solution space and patterns which correspond to well separated solutions were obtained. Moreover, the actual dimensions of the active areas, over which the electric field was effective, were of the smallest size constructed to date for pattern formation studies. Hence, the effects of experimental imperfections, such as the unavoidable thickness variations across the cell, were minimised. The novel geometry of the liquid crystal cell also facilitated the examination of the primary flow states as a function of aspect ratio.

The preliminary observations affirmed that the response of the liquid crystal molecules to an electric field gave rise to distinct dynamical effects depending on the frequency of the applied field. The parameter space was therefore divided into two regions by a critical frequency value. Above this value a convective flow

developed at a threshold field amplitude. As the field amplitude was increased further, disordered flow state was observed. At frequencies lower than the critical frequency the liquid crystal molecules re-aligned according to the amplitude of the field applied. High values of field amplitude, in this case, did not induce a flow but increased the tilt of the molecules.

The observations regarding the primary flow states in the convective regime showed a dependency on the aspect ratio values, which was consistent with the numerical results reported by Tavener et al [45]. For aspect ratio values greater than or approximately equal to one, the convection rolls preferred the same rotation direction and no solution rotating counter to these were observed. The absence of a counter rotation direction is an as yet unresolved problem for convection studies in nematic materials which suggests that a pitchfork bifurcation is an inappropriate model of the phenomenon [8, 45].

For aspect ratios smaller than one, a pattern suggesting a single convection roll was observed for the first time. Existence of a single roll will break the left/right symmetry and consequently, the solution with the counter rotating roll can be expected to be nearby in the parameter space. The resolution of the images necessary to make detailed observations could not be achieved in this study. Nevertheless, further investigation on this issue is recommended. It is believed that more efficient results can be obtained from a liquid crystal cell of same aspect ratio built with larger electrode widths and cell thicknesses. This would not only increase the area of observation but would also decrease the effect of fringing electric fields at the electrode edges.

The first experiment carried out to examine the pattern selection in nematic flows was conducted in the convective region of the parameter space. The primary flow that evolved for a range of frequencies within this region consisted either of four or six convection rolls. In the experiment, the loci of limit points

of the secondary states were determined and the reproducibility of the data was confirmed. In accordance with Benjamin's theory hysteretic behaviour and unfolding of a transcritical bifurcation was found. Considering the previous theoretical and experimental success of Benjamin's theory in studies [50, 51, 52, 53] of Taylor-Couette flows and in the experimental work of Binks [49] concerning the six/eight-roll priority exchange in a nematic liquid crystal, the robustness of Benjamin's theory is evident.

Our study was then focussed on the pattern selection between the two discrete effects. The experiment was performed in a frequency range that included the vicinity of the critical frequency that separated the parameter space into two sections. Our results revealed a similarity with those of the numerical and experimental studies [85] on a Taylor-Couette system that bares qualitative analogies with the experiment done here. The bifurcation sequence proposed for both experiments involves hysteresis and transcritical bifurcations, as in the priority exchange of four/six roll convection states of the first experiment. The significant difference here was the coupling of the neighbouring states due to the dependency of the material properties of the liquid crystal on the frequency of the electric field. Consequently, evidence of a dual cusp was found. It is believed that this was the first experimental revelation of a dual cusp in a liquid crystal flow.

Appendix A

Unfolding of a pitchfork bifurcation

A pitchfork bifurcation is locally described by the following ordinary differential equation:

$$\frac{dx}{dt} = \lambda x - x^3 \tag{A.1}$$

where x is a dynamical variable, which defines an equilibrium state, $\frac{dx}{dt}$ gives the evolution of equilibrium states and λ is the bifurcation parameter. The equilibrium states as a function of λ are shown in figure A.1 where solid lines denote stable states and the dotted line indicates an unstable branch.

As it can be seen in figure A.1, at the *bifurcation point*, $\lambda = 0$, the $x = 0$ state(trivial state) loses stability and two new branches, $x = \sqrt{\lambda}$ and $x = -\sqrt{\lambda}$ appear.

However, in any experimental system, imperfections will be present and these can be taken into account by including a constant in the model [86]. Hence, the

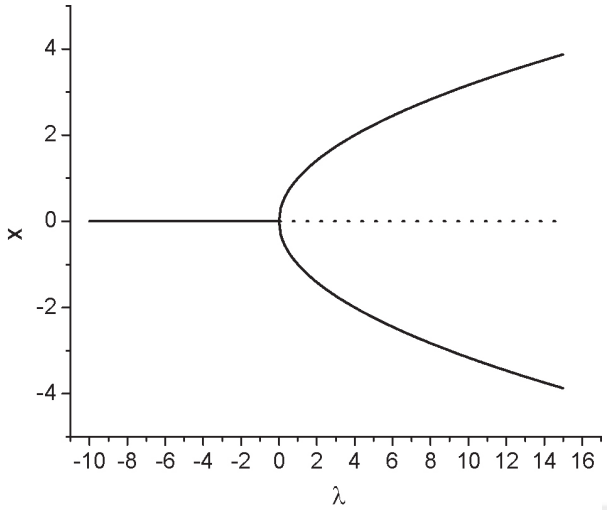

Figure A.1: Bifurcation diagram for an ideal pitchfork bifurcation.

modified version of A.1 will be

$$\frac{dx}{dt} = \lambda x - x^3 + \beta \tag{A.2}$$

where β is called the *imperfection term*. The effect of β is to disconnect one of the branches so that the other becomes continuous as shown in figure A.2. In such a case the disconnected branch has a well defined point called the *saddle node* or *limit point* as indicated in the figure.

The set of limit points for equation A.2 forms a cusp and is given in figure A.3. The line $\beta = 0$, which is parallel to the λ axis, is the case of an ideal system where there are no limit points. For the positive and negative values of β the branches are disconnected and limit points exist.

In a numerical study of a tilted Rayleigh-Bénard system Cliffe and Winters [87] show that the loci of limit points is in the shape of a cusp, as represented in figure A.3. In their study, β corresponds to the tilt angle of the Rayleigh-Bénard cell. Therefore, when the tilt angle is zero, numerically they obtain a symmetrical system, which can be modelled as a pitchfork bifurcation. For non-zero values of the tilt angle, the branches are separated.

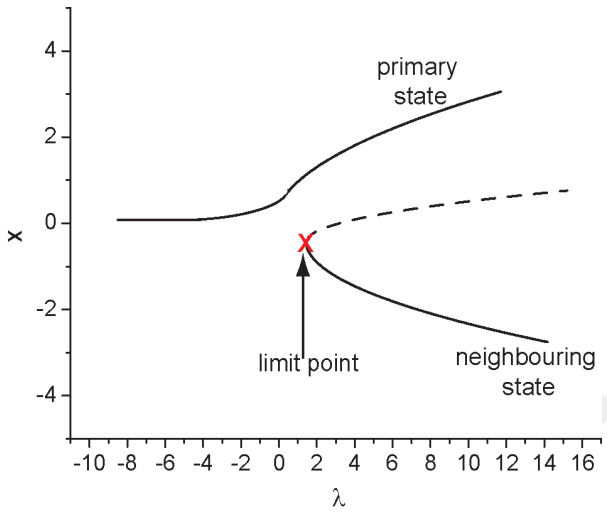

Figure A.2: Pitchfork bifurcation diagram after the imperfection β term is included.

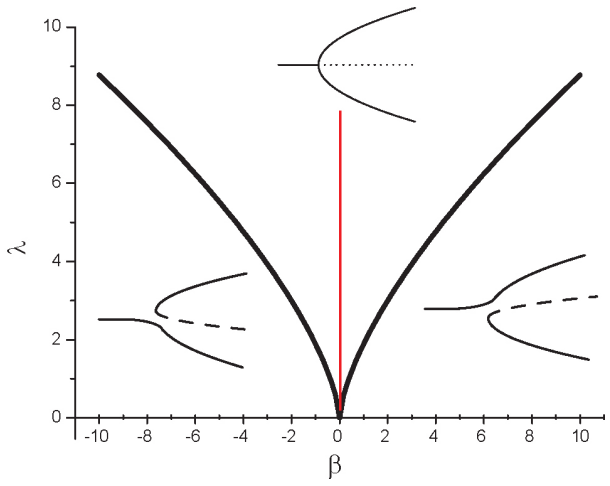

Figure A.3: The cusp formed by the limit points of equation A.2.

Nevertheless, equation A.2 does not include all persistent qualitative dynamics near a pitchfork bifurcation. Golubitsky and Schaeffer[83] show that a fourth variable must be added in order to achieve *the universal unfolding of the pitchfork*. It is given by

$$\frac{dx}{dt} = \lambda x - x^3 + \beta + \alpha x^2 \tag{A.3}$$

where α is a second control parameter after λ. The limit points of equation A.3 are illustrated in figure A.4. It can be seen that the $\beta = 0$ line cutting the cusp into two halves in figure A.3 is no longer parallel to neither of the parameter axis in figure A.4. Hence, it can be concluded that the inclusion of the term αx^2 has broken the symmetry of the cusp.

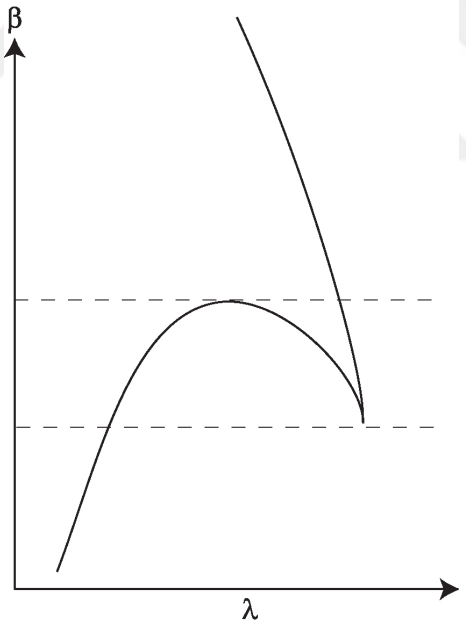

Figure A.4: An illustration of the limit points of equation A.3.

Appendix B

Nematic TX2A

*Clearing point	101^oC
Viscosity (measured at 20^oC)	$98cSt$
Optical anisotropy (measured at 20^oC, $589nm$)	$\Delta n = 0.12$ $n_o = 1.51$ $n_e = 1.63$

*Values obtained from Merck R&D UK (1999)

B.1 Dielectric Anisotropy of TX2A

As described in Chapter 2, TX2A is a so called dual frequency material whose dielectric anisotropy[1], $\Delta\epsilon$, varies as a function of frequency of the AC field applied to it and the sign of $\Delta\epsilon$ changes at a value called the crossover frequency.

The dependence of $\Delta\epsilon$ on frequency was examined for the nematic TX2A and the results are presented in figure B.1, where the dots indicate the experimental data and the solid line is the extrapolation of the results up to $28kHz$.

The data points presented in figure B.1 were found by measuring the dielectric constants $\epsilon_{\|}$ and $\epsilon_{\perp}$ separately and then by taking their difference to find $\Delta\epsilon$.

[1]see Chapter 1 for a definition

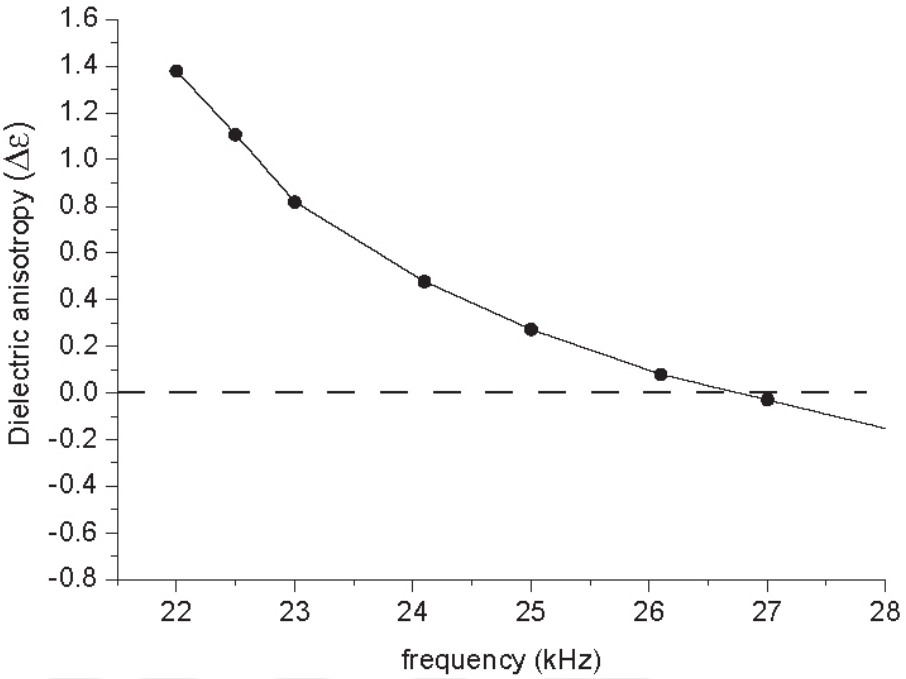

Figure B.1: Dielectric anisotropy as a function of frequency of the AC field.

The method followed for our measurements was introduced by Clark et al[88] and practiced later by Bancroft[89], Allison[90] and Miller[91]. In this method, the LC cell is considered as a parallel plate capacitor. Hence, there is a linear relationship between the capacitance of the cell and the dielectric constant of the material with which it is filled. Consequently, the ratio of the capacitance value of the LC cell when it is empty (C_{empty}) to that when filled (C_{filled}), gives the dielectric constant, ϵ:

$$\epsilon = \frac{C_{filled}}{C_{empty}} \tag{B.1}$$

The capacitance value C_{empty} was measured by a capacitance bridge[2] which was connected to the wires soldered on the electrodes of a large aspect ratio[3] LC

[2]Wayne Kerr Precision Component 6430A

[3]A large aspect ratio (2000:2000:1) cell was used in order to minimise the effects of fringing fields.

cell while it was empty. The device measured the capacitance value by applying an AC probe field across the cell (i.e. in a direction perpendicular to the glass plates), which was generated by the capacitance bridge itself. The stray capacitance of the wires were taken into account and subtracted from the values found from the measurements in order to obtain the capacitance of the LC cell alone.

The LC cell was then filled with nematic TX2A and heated to 33^oC, which was the temperature set in our experiments. The measurements then onwards were taken at this temperature. The dielectric constants $\epsilon_{\|}$ and $\epsilon_{\perp}$ were found by measuring C_{filled} at high and low amplitude values of the probe field respectively in the following way: For a fixed frequency value within the range shown in figure B.1, firstly, the field amplitude was set to values of the order of mV (V_{rms}) and the response of the molecules were observed from a polarising microscope. For such low amplitude values the colour of the image seen from the microscope was the same as the one observed in the absence of the field. This implied that the director retained its original planar alignment, which was perpendicular to the direction of the field. Hence, C_{filled} measured at such probe field amplitudes was proportional to the perpendicular component, $\epsilon_{\perp}$. By taking the ratio of C_{filled} to C_{empty}, the value of $\epsilon_{\perp}$ was calculated for the given frequency value. When the field amplitude was increased for the same frequency value Freedericksz transition was observed. At the field amplitudes where a complete Freedericsz transition was achieved the director was aligned perpendicular to the glass surfaces of the LC cell and parallel to the direction of the field. Hence, C_{filled} value was proportional to $\epsilon_{\|}$. The ratio of C_{filled} to C_{empty} thus, gave the $\epsilon_{\|}$ value at the measured frequency. Similar to the measurement of C_{empty}, the stray capacitance of the wires that connected the capacitance bridge to the LC cell were subtracted from the measured values.

The results presented in figure B.1 reveal that the dielectric anisotropy of

TX2A changes its sign near frequency values of $26kHz$. This is consistent with the observations explained in Chapter 5 where competition between Freedericksz transition and EHC was studied. It is also evident from the extrapolation that the dielectric anisotropy decreases with increasing frequency values. Thus, figure B.1 confirms that in the frequency range of the experiment regarding the priority exchange of 4 and 6-roll states of EHC, the dielectric anisotropy is negative.

Bibliography

[1] PJ Collings. *Liquid Crystals*. Princeton University Press, 2nd edition, 2002.

[2] FH Busse and SC Muller. *Evolution of Spontaneous Structures in Dissipative Continous Systems*, volume m55 of *Lecture notes in Physics*, chapter 8, pages 335–383. Springer, 1998.

[3] A Buka and L Kramer. *Pattern Formation in Liquid Crystals*. Springer, 1996.

[4] S Kumar. *Liquid Crystals, Experimental Study of Physical Properties and Phase Transitions*. C.U.P., 2001.

[5] JL Ericksen. Conservation laws for liquid crystals. *Trans. Soc. Rheol.*, 5:23–24, 1961.

[6] FM Leslie. Some constitutive equations for liquid crystals. *Arch. Rat. Mech. Anal.*, 28:265–283, 1968.

[7] O Parodi. Stress tensor for nematic liquid crystals. *J. Physics (Paris)*, 31:581–584, 1970.

[8] T Peacock. *Global Dynamics in a Liquid Crystal Flow*. PhD thesis, Oxford University, 1997.

[9] PG De Gennes and J Prost. *The Physics of Liquid Crystals*. Oxford University Press, 2nd edition, 1995.

[10] E Hecht. *Optics*. Addison Wesley, 3rd edition, 1998.

[11] V Freedericksz and V Tsvetkov. *Phys. Z. Sov. Union*, 6:490, 1934.

[12] EF Carr. Influence of electric fields on the molecular alignment of the liquid crystal p-(anisalamino)-phenyl acetate. *Mol. Cryst. Liq. Cryst.*, 7:253–269, 1969.

[13] R Williams. Domains in liquid crystals. *J. Chem. Phys.*, 39:384–388, 1963.

[14] W. Helfrich. Conduction-induced alignment of nematic liquid crystals: basic model and stability considerations. *J. Chem. Phys.*, 51:4092–4105, 1969.

[15] LM Blinov. *Electro-optical and Magneto-optical Properties of Liquid Crystals*. Wiley, 1983.

[16] J Guckenheimer and P Holmes. *Nonlinear Oscillations, Dynamical Systems and Bifurcations of Vector Fields*. Springer, 1997.

[17] T Mullin. *The Nature of Chaos*. Oxford Science Publications, 1993.

[18] A Saupe. Die biegungselastizitat der nematischen phase von azoxyanisol. *Zeitschrift fur Naurforschung*, 15a:815–822, 1960.

[19] CM Dafermos. Stability of orientation patterns of liquid crystals subject to magnetic fields. *SIAM Jour. Appl. Math.*, 16(6):1305–1318, 1968.

[20] FM Leslie. Some magneto-hydrostatic effects in nematic liquid crystals. *J. Phys. D: Appl. Phys.*, 3:889–897, 1970.

[21] G Derfel. Field effects in nematic liquid crystals in terms of catastrophe theory. *Liquid Crystals*, 3(10):1411–1424, 1988.

[22] HJ Deuling. Elasticity of nematic liquid crystals. *Mol. Cryst. Liq. Cryst.*, 19:123–131, 1972.

[23] H Gruler and G Meier. Electric field-induced deformations in oriented liquid crystals of the nematic type. *Mol. Cryst. Liq. Cryst.*, 16:299–310, 1972.

[24] GI Blake, T Mullin, and SJ Tavener. The Freedericksz transition as a bifurcation problem. *Dyn. Stab. Syst.*, 14(3):299–331, 1999.

[25] Orsay Liquid Crystal Group. Hydrodynamic instabilities in liquid crystals under a.c. electric field. *Phys. Rev. Lett.*, 25:1642–1643, 1970.

[26] PA Penz and GW Ford. Electromagnetic hydrodynamics of liquid crystals. *Phys. Rev. A*, 6:414–425, 1972.

[27] S. Kai and K Hirakawa. Successive transitions in electrohydrodynamic instabilities of nematics. *Prog. Theor. Phys. Suppl.*, 64:212–243, 1978.

[28] A Joets and R Ribotta. *Cellular Structures in Instabilities*, volume 210 of *Lecture Notes in Physics*. Springer-Verlag, 1983.

[29] A Joets and R Ribotta. Hydrodynamic transitions to chaos in convection of an anisotropic fluid. *J. Phys. (Paris)*, 47:595–606, 1986.

[30] E Bodenschatz, W Zimmerman, and L Kramer. On electrically driven pattern forming instabilities in planar nematics. *J. Phys. (Paris)*, 49:1875–1898, 1988.

[31] T Mullin. Disordered fluid motion in a small scale system. *Physica D*, 62:192–201, 1993.

[32] A Libchaber and J Maurer. *Nonlinear phenomena at phase transitions and instabilities*, pages 259–286. Plenum New York, 1982.

[33] J von Stamm, Th Buzug, and G Pfister. Frequency locking in axisymmetric Taylor-Couette flow. *Phys. Lett. A*, 194:173–178, October 1994.

[34] Th. Buzug, J von Stamm, and G Pfister. Characterisation of period-doubling scenarios in Taylor-Couette flow. *Phys. Rev. E*, 47(2):1054–1065, February 1993.

[35] T Mullin and TJ Price. An experimental observation of chaos arising from the interaction of steady and time-dependent flows. *Nature*, 340:294–296, 1989.

[36] T Mullin. Finite-dimensional dynamics in Taylor-Couette flow. *IMA J. Appl. Math.*, pages 109–119, 1991.

[37] C-Y Yang, H Itakura, S Horie, Y Tsuchiya, and T Kawakubo. Angle deflective oscillation of the stripe pattern in nematic liquid crystals. *J. Phys. Soc. Jap.*, 55:703–706, 1986.

[38] Y Hidaka, H Orihara, and Y Ishibashi. The transition from quasi-periodicity to chaos in the electrohydrodynamic instability of a nematic liquid crystal. *J. Phys. Soc. Jap.*, 61:3950–3959, 1992.

[39] DJ Binks. *Bifurcation Phenomena in Nematodynamics*. PhD thesis, Oxford University, 1995.

[40] T Peacock, DJ Binks, and T Mullin. From low- to high-dimensional dynamics in a microscopic flow. *Phy. Rev. Lett.*, 82(7):1446–1449, February 1999.

[41] T Peacock and T Mullin. Homoclinic bigurcations in a liquid crystal flow. *J. Fluid Mech.*, 432:369–386, 2001.

[42] T Peacock, T Mullin, and DJ Binks. Bifurcation phenomena in flows of a nematic liquid crystal. *Int. Journ. Bifur. Chaos*, 9(2):427–441, 1999.

[43] S Hirata and T Tako. Effect of cell width on the structure of Williams domain. *Jap. J. Appl. Phys.*, 21(10):L607–L609, October 1982.

[44] L Kramer and W Pesch. Convection instabilities in nematic liquid crystals. *Ann. Rev. Fluid Mech.*, 27:515–541, 1995.

[45] SJ Tavener, T Mullin, GI Blake, and KA Cliffe. Numerical bifurcation study of electrohydrodynamic convection in nematic liquid crystals. *Phys. Rev. E*, 63:011708–1–12, December 2000.

[46] K Kirchgassner. Bifurcation in nonlinear hydrodynamic stability. *SIAM Rev.*, 17:652–683, 1975.

[47] PA Warkentkin, HJ Haucke, P Lucas, and J Wheatley. *Proc. Natl. Acad. Sci. U.S.A.*, 77:6983, 1980.

[48] MP Arroyo and JM Saviron. Rayleigh-Bénard convection in a small box: spatial features and thermal dependence of the velocity field. *J. Fluid Mech.*, 235:325, 1992.

[49] DJ Binks and T Mullin. Cell number selection in electrohydrodynamic convection in liquid crystals. *Proc. Math. Phys Eng. Sci.*, 453(1965):2109–2122, October 1997.

[50] TB Benjamin. Bifurcation phenomena in steady flows of a viscous fluid. i. Theory. *Proc. R. Soc. Lond. A*, 359:1–26, 1978.

[51] TB Benjamin. Bifurcation phenomena in steady flows of a viscous fluid. ii. Experiments. *Proc. R. Soc. Lond. A*, 359:27–43, 1978.

[52] T Mullin. Mutations of cellular flows in the Taylor experiment. *J. Fluid Mech.*, 121:207–218, 1982.

[53] TB Benjamin and T Mullin. Notes on multiplicity of flows in the Taylor experiment. *J. Fluid Mech.*, 121:219–230, 1982.

[54] KA Cliffe. Numerical calculations of the primary-flow exchange in the Taylor problem. *J. Fluid Mech.*, 197:57–79, 1988.

[55] JH Bolstad and HB Keller. Computation of anomolous modes in the Taylor experiment. *J. Comput. Phys.*, 69:230–251, 1987.

[56] H Furukawa, T Watanabe, Y Toya, and I Nakamura. Flow pattern exchange in the Taylor-Couette system with a very small aspect ratio. *Phys. Rev. E*, 65(3):036306, March 2002.

[57] SJ Tavener and T Mullin. Buckling of coupled elastic rods. *Physica D*, 30:382–398, 1988.

[58] K Nandakumar and JH Masliyah. Bifurcation in steady laminar flow through curved tubes. *J. Fluid Mech.*, 119:475–490, 1982.

[59] HJ K Nandakumar. A bifurcation study of mixed-convection heat transfer in horizontal ducts. *J. Fluid Mech.*, 231:157–187, 1991.

[60] M Golubitsky and DG Schaeffer. A theory of imperfect bifurcation via singularity theory. *Communs. Pure Appl. Maths*, 32:21–98, 1979.

[61] DG Schaeffer. Analysis of a model in the Taylor problem. *Math. Proc. Camb. Phil. Soc.*, 87:307–337, 1980.

[62] P Hall. Centrifugal instabilities in finite containers: a periodic model. *J. Fluid Mech.*, 99:575–596, 1980.

[63] P Hall. Centrifugal instabilities of circumferential flows in finite cylinders: the wide gap problem. *Proc. R. Soc. Lond. A*, 384:359–379, 1982.

[64] J Cheng, GD Boyd, and FG Storz. A scanning electron microscope study of columnar topography and liquid crystal alignment on obliquely deposited oxide surfaces at low rates. *Appl. Phys. Lett.*, 37(8):716–719, 1980.

[65] J Cognard. Alignment of nematic liquid crystals and their mixtures. *Mol. Cryst. Liq. Cryst.*, S1:1–77, 1982.

[66] JM Geary, JW Goodby, AR Kmetz, and JS Patel. The mechanism of polymer alignment of liquid-crystal materials. *J. Appl. Phys.*, 62:4100, 1987.

[67] K Weiss, C Wöll, and D Johannsmann. Near surface molecular orientation in polymeric alignment layers: a NEXAFS investigation. *SPIE (The international society for optical engineering)*, 104:3800, 1999.

[68] WJ Cassarly and SJ Young. Liquid crystal inversion walls caused by field fringing. *Mol. Cryst. Liq. Cryst.*, 210:1, 1992.

[69] GM Storrow, HF Gleeson, and AJ Murray. An analysis of the optical properties of a single-element liquid crystal device. *Pure Appl. Opt.*, 7:1411–1423, 1998.

[70] Merck Ltd. Data sheet. Merck House, Poole, Dorset, UK.

[71] I Rehberg, S Rasenar, M de la Torre Juarez, W Schopf, F Horner, G Ahlers, and HR Brand. Thermally induced hydrodynamic fluctuations below the onset of electroconvection. *Phys. Rev. Lett.*, 67(5):596–599, December 1991.

[72] S Singh. *Liquid Crystals, Fundamentals.* World Scientific, 2002.

[73] A Buka and L Kramer. *Pattern Formation in Liquid Crystals.* Springer, 1996.

[74] Wim van Saarloos and PH Hohenberg. Fronts, pulses, sources and sinks in generalised complex Ginzburg-Landau equations. *Physica D*, 56(4):303–367, January 1992.

[75] J Abshagen, O Meincke, G Pfister, KA Cliffe, and T Mullin. Transient dynamics at the onset of Taylor vortices. *J. Fluid Mech.*, 476:335 – 343, 2003.

[76] PG Drazin and WH Reid. *Hydrodynamic Stability.* C.U.P., 1981.

[77] B Hof and T Mullin. Critical dynamics in oscillatory convection. *Magnetohydrodynamics*, 37(1-2):3–10, 2001.

[78] S Rasenat, V Steinberg, and I Rehberg. Experimental studies of defect dynamics and interaction in electrohydrodynamic convection. *Phys. Rev. A*, 42(10):5998–6011, November 1990.

[79] T Mullin, Y Toya, and SJ Tavener. Symmetry breaking and multiplicity of states in small aspect ratio Taylor-Couette flow. *Phys. Fluids*, 14(8):2778–2787, August 2002.

[80] MC Cross and PC Hohenberg. Pattern formation outside of equilibrium. *Rev. Mod. Phys.*, 65:851–1112, 1993.

[81] L Bauer, HB Keller, and EL Reiss. Multiple eigenvalues lead to secondary bifurcation. *SIAM Review*, 17(1):101–122, January 1975.

[82] TB Benjamin and T Mullin. Anomalous modes in the Taylor experiment. *Proc. R. Soc. Lond. A*, 377:221–249, 1981.

[83] M Golubitsky and DG Schaeffer. *Singularities and Groups in Bifurcation Theory*, volume 1. Springer, New York, 1985.

[84] PT Saunders. *An Introduction to Catastrophe Theory.* Cambridge University Press, 1980.

[85] KA Cliffe and T Mullin. A numerical and experimental study of the Taylor problem with asymmetric end conditions. *Conference Preecedings: 6th International Symposium of Finite Element Methods in Flow Problems, Antibes, France*, 1986.

[86] SH Strogatz. *Nonlinear Dynamics and Chaos*. Westview Press, 1994.

[87] KA Cliffe and KH Winters. A numerical study of the Cusp Catastrophe for Bénard convection in tilted cavities. *J. Comp. Phys.*, 54:531–534, 1984.

[88] MG Clark, EP Raynes, RA Smith, and RJA Tough. Measurement of the permittivity of nematic liquid crystals in magnetic and electric fields using extrapolation procedures. *J. Phys. D: Appl. Phys.*, 13:2151, 1980.

[89] M Bancroft. PhD thesis, University of Manchester, 1988.

[90] H Allinson. PhD thesis, University of Manchester, 1994.

[91] R Miller. PhD thesis, University of Manchester, 1994.